M 2023

U.PORTO
FEUP FACULDADE DE ENGENHARIA
UNIVERSIDADE DO PORTO

SYNTHESIS OF ZEOLITE ZSM-5 USING NETMIX

FRANCISCA MARIA DA SILVA DUARTE
MASTER THESIS IN CHEMICAL ENGINEERING
PRESENTED TO THE FACULTY OF ENGINEERING
OF THE UNIVERSITY OF PORTO

Master in Chemical Engineering

Synthesis of Zeolite ZSM-5 using NETmix

Master Dissertation

of

Francisca Maria da Silva Duarte

Developed within the course of dissertation

held in

Associate Laboratory LSRE-LCM

Supervisor at FEUP: **Doctor Yaidelin Manrique**

Co-supervisor at FEUP: **Professor Madalena Dias**

August 2023

Acknowledgment

The thesis dissertation represents the finish line for one of the most important stages of my life. It was an opportunity to prove to myself my capabilities and all the knowledge and capacities that I have learned within all the school years, but mostly in these last five ones. Nevertheless, it was an opportunity to learn new subjects, to learn with different people, to work with different equipment, to plan, to face challenges, to create solutions and to put "hands on". This work was only possible due to the support of several people:

Initially, my supervisor, Doctor Yaidelin Manrique. I appreciate the freedom that she gave to me so that I could follow my plans, do all the analysis I thought to be necessary and important, to develop myself and to disagree, sometimes right sometimes wrong. Next, I would like to appreciate the confidence placed in me by my co-supervisor, Professor Madalena, and by LSRE-LCM, to study a new subject in the research group and to perform new characterization techniques.

I would also like to recognize the support and the willingness of CoLAB NET4CO2 to grant several equipment, namely the muffle, the equipment for impregnation and the FTS reactor. More in specifically, Professor José Lopes for being interested in the project and to Dânia, Bruno, Thais and Cláudia to always have guided and helped me.

Furthermore, I would like to appreciate the sympathy of Professor Alexandre to lend the autoclave, Carina to lend the shaking machine and the orientation in some equipment by Luís Carlos, Fátima, Zé Luís, Ana Querido, Joana, Lucília and Liliana. Additionally, since XRD and TPD equipment were not available at FEUP, I would like to acknowledge UTAD and IST for conducting this analysis, respectively. Finally, an eternal thanks to my friends for all recomforting conversations and for the laughs and company during lunch hours.

This work is a result of project Cat4GtL – Continuous Catalytic reactor for the Gas-to-Liquid process using NETmix technology, with reference POCI-01-0247-FEDER-069953, co-funded by the European Regional Development Fund (ERDF), through the Operational Program for Competitiveness and Internationalization (COMPETE 2020) and the Lisbon Regional Operational Program (LISBOA 2020), under the PORTUGAL 2020 Partnership Agreement. This work was also supported by LA/P/0045/2020 (ALiCE), UIDB/50020/2020 and UIDP/50020/2020 (LSRE-LCM), funded by national funds through FCT/MCTES (PIDDAC).

Cofinanciado por:

COMPETE 2020 Lisb@20 20 PORTUGAL 2020 UNIÃO EUROPEIA Fundo Europeu de Desenvolvimento Regional FCT Fundação para a Ciência e a Tecnologia REPÚBLICA PORTUGUESA

Abstract

Zeolite ZSM-5 is an aluminosilicate framework type MFI. It is characterized by having well-defined micropores and being thermally stable, with high crystallinity, surface area and acidic behavior. It is usually produced in batches processes with organic template agents under hydrothermal conditions to favor crystallization.

This dissertation aimed to evaluate a faster route to synthesize the zeolite ZSM-5 using a technology with efficient and reproducible mixing, the NETmix reactor. Two zeolite formulations were produced, template-free and with a template, in batch and with NETmix. Additionally, the formulations were tested with different parameters such as Si/Al ratio, reaction temperature and crystallization time. In the case of NETmix, the influence of Reynolds number was also tested. The produced zeolites were characterized through several techniques: thermogravimetric analysis (TGA) for thermal stability; inductively coupled plasma – atomic emission spectroscopy (ICP-AES) for chemical composition; Fourier transform infrared spectroscopy (FTIR) for chemical bounds; scanning electron microscopy (SEM) for morphology; energy dispersive spectroscopy (EDS) for qualitative chemical composition; dynamic light scattering (DLS) for particle sizes; nitrogen isotherms for porosity and superficial area; X-ray powder diffraction (XRD) for structure and crystallinity; ammonia temperature programmed desorption (NH_3-TPD) for acidity and hydrogen temperature programmed reduction (H_2-TPR) for zeolite reduction temperature. Also, zeolites were evaluated as a support of cobalt and rhenium for Fischer-Tropsch synthesis (FTS).

For both formulations, template-free and with a template, it was possible to transpose the process from batch to NETmix. Regarding template-free formulations, the produced material was an amorphous material, without all the characteristic peaks in FTIR spectrum and with low superficial area and acidity. On the other hand, for template formulations, the produced particles proved to be thermally stable after 500 °C, the FTIR spectra presented all five characteristic peaks, the particles varied between 0.1 and 0.8 μm in size, presented a total superficial area of 446 and 593 $m^2 \cdot g^{-1}$ and a total pore volume of 0.43 to 0.84 $cm^3 \cdot g^{-1}$, the crystallinity for NETmix assay varied from 33 to 70 %, with 13 s and 10 min mixture, and for batch was 93 %, with 24 h mixture, respectively, and a crystal size between 27 and 47 nm. Also, the procedure and the final product was reproducible, and it was verified that 0.3 g of ZSM-5 could be produced with 1 g of Si and Al. FTS was tested with the zeolite as a support impregnated with cobalt and rhenium. The protonated assay produced with NETmix produced a more desirable hydrocarbon chain length and better properties, resulting in a cobalt-time yield (F_{CTY}) and a CO conversion of 13×10^5 $mol_{CO} \cdot g_{Co}^{-1} \cdot s^{-1}$ and 65 %, respectively.

Keywords: Zeolite, ZSM-5, NETmix, synthesis, characterization, Fischer-Tropsch

Resumo

O zeólito ZSM-5 é um aluminossilicato do tipo MFI. É caracterizado por ter microporos bem definidos, ser termicamente estável, possuir alta cristalinidade e área superficial, além de apresentar um comportamento ácido. Geralmente, é produzido em lotes com agentes direcionadores orgânicos em condições hidrotérmicas para favorecer a cristalização.

Esta dissertação teve como objetivo avaliar uma rota mais rápida para sintetizar o zeólito ZSM-5 usando uma tecnologia com mistura eficiente e reprodutível, o reator NETmix. Para isso, foram produzidas duas formulações, sem e com direcionador, em lote e com o uso do NETmix. Além disso, foi avaliado o efeito de parâmetros, como o rácio Si/Al, a temperatura de reação e o tempo de cristalização. O zeólito produzido foi caracterizado por várias técnicas: análise termogravimétrica (TGA) para a estabilidade térmica; espectroscopia de emissão atómica com plasma acoplado indutivamente (ICP-AES) para composição química; espectroscopia de infravermelho por transformada de Fourier (FTIR) para ligações químicas; microscopia eletrónica de varrimento (SEM) para a morfologia; espectroscopia de dispersão de energia (EDS) para a composição química qualitativa; dispersão de luz dinâmico (DLS) para o tamanho das partículas; isotérmicas de nitrogénio para a porosidade e área superficial; difração de raios-X (XRD) para estrutura e cristalinidade; dessorção programada de temperatura com amoníaco (NH_3-TPD) para acidez e redução programada de temperatura com hidrogénio (H_2-TPR) para a temperatura de redução. Além disso, os zeólitos foram avaliados como suporte do cobalto na síntese de Fischer-Tropsch.

Para ambas as formulações, com e sem direcionador, foi possível transpor o processo de produção em lote para o NETmix. No que diz respeito às formulações sem direcionador, o material produzido foi amorfo, sem todos os picos característicos no espectro FTIR e com baixa área superficial e acidez. Por outro lado, para as formulações com direcionador, as partículas produzidas mostraram-se termicamente estáveis após 500 °C, os espectros FTIR apresentaram todos os cinco picos característicos, as partículas variaram de tamanho entre 0,1 e 0,8 µm, apresentaram uma área superficial total de 446 a 593 $m^2 \cdot g^{-1}$ e um volume total de poros de 0,43 a 0,84 $cm^3 \cdot g^{-1}$, a cristalinidade para o ensaio NETmix variou de 33 a 70 %, com uma mistura de 13 s e 10 min, e na produção em lote foi de 93 %, com uma mistura de 24 h, respetivamente, já o tamanho de cristal variou entre 27 e 47 nm. Além disso, o procedimento e o produto final foram reproduzíveis, e verificou-se que 0,3 g de ZSM-5 poderiam ser produzidos com 1 g de Si e Al. Na síntese de Fischer-Tropsch o ensaio protonado produzido com o NETmix apresentou um comprimento de cadeia de hidrocarbonetos mais desejável e com melhores propriedades, resultando num rendimento de cobalto-tempo (F_{CTY}) e uma conversão de CO de $13x10^5$ $mol_{CO} \cdot g_{Co}^{-1} \cdot s^{-1}$ e 65 %, respetivamente.

Palavras-chave: Zeólito, ZSM-5, NETmix, síntese, caracterização, Fischer-Tropsch

Declaration

I hereby declare, under word of honor, that this work is original and that all non-original contributions is indicated and due reference is given to the author and source

Francisca Maria da Silva Duarte

July 2023

Index

List of Figures

List of Tables

Notation and Glossary

A_C	Area under Crystalline Peaks	-
A_{cs}	Area Cross-Section NETmix	mm^2
$\bar{A}_{H_2}$	Mean Area above the H_2 Consumption Curve for Calibration Step	s
a_m	Adsorption Cross Section of the Adsorbate	m^2
A_T	Area under all Peaks	-
C	Crystallinity	%
C_{BET}	Parameter of the Model	-
d	Hydraulic Diameter of the Channels	m
d_c	Channels Depth	mm
F_{CTY}	Cobalt-Time Yield	$mol_{CO} \cdot g_{Co}^{-1} \cdot s^{-1}$
F_{GHSV}	Gas hourly Space Velocity	$m^3 \cdot kg_{cat}^{-1} \cdot h^{-1}$
$F_{\mathrm{in,CO}}$	Initial Quantity of CO	$mol \cdot s^{-1}$
$F_{\mathrm{out,CO}}$	Final Quantity of CO	$mol \cdot s^{-1}$
$\mathrm{H}_{2_{\mathrm{consumption}}}$	H_2 Consumption	$mmol \cdot g^{-1} \cdot s^{-1}$
k	Stoichiometric Number of CO	-
K	Constant Related to Crystallite Shape	-
L	Crystal Size	nm
n	Valence of the Cation	-
N_A	Avogadro Number	mol^{-1}
n_p	Number of Plates	-
n_x	Number of Rows	-
n_y	Number of Columns	-
P	Pressure	Pa
P_0	Maximum Pressure	Pa
q	Total Flowrate	$dm^3 \cdot min^{-1}$
r_c	Ratio between Final and Initial Samples Weight for Calcination	-
Re_d	Reynolds Number	-
$S_{\neq\mathrm{micro}}$	Area of Non-Micropores	$m^2 \cdot g^{-1}$
S_{BET}	BET Surface Area	$m^2 \cdot g^{-1}$
$\mathrm{TCD}_{\mathrm{signal}}$	Signal provided by the Thermal Conductivity Detector	-
t_f	Average Adsorbed Film Thickness	Å
T_{loop}	Loop Temperature for the Calibration Step	K
T_{ref}	Reference Temperature	K
$U_{\mathrm{NH_3}}$	NH_3 Uptake	$\mu mol \cdot g^{-1}$
v	Average Velocity in the Channels	$m \cdot s^{-1}$
V^a	Adsorbed Volume of Nitrogen	dm^3
V_m	Gas Molar Volume in STP Conditions	$dm^3 \cdot mol^{-1}$
V_{micro}	Micropore Volume	$cm^3 \cdot g^{-1}$
$V_{\mathrm{pores\_total}}$	Total Pore Volume	$cm^3 \cdot g^{-1}$
V_s	Analyzed Volume for the Calibration Step	µL
w_a	Initial Mass in the Autoclave	g
w_c	Channels Width	mm
w_{Co}	Cobalt Mass	g
w_s	Samples Mass	g
$w_{\mathrm{Si+Al}}$	Mass of Si and Al in the Initial Mixture	g
w_t	Total Mass of the Initial Mixture	g
w_{w+d}	Samples Mass after Washing and Drying Step	g
x	Number of Al_2O_3 Units	-
X_{CO}	CO Conversion	%
y	Number of SiO2 Units	-
Y	Mass Yield	%
y_i	Metal Loading	%
z	Number of Water Molecules per Unit Cell	-
Z	Zeolite	-

Greek Letters

β	Peak Width of the Diffraction Peak Profile at Half Maximum Height	rad
ξ	Pore Classification	-
θ	Half the Angle between the Incoming and Outgoing Beam	°
λ	X-ray Wavelength	nm
μ	Mixture's Viscosity	Pa·s
ρ	Mixture's Density	$kg \cdot m^{-3}$

Indexes

r	Number in the range from 1 to 8	-
i	Cobalt or Rhenium	-

List of Acronyms

BAS	Brønsted Acid Sites
BET	Brunauer-Emmett-Taylor
CEMUP	Materials Center of the University of Porto
DLS	Dynamic Light Scattering
EDS	Energy Dispersive Spectroscopy
FEUP	Faculty of Engineering from University of Porto
F	Formulations Template-free
F_dil	Template-free Assays with Diluted Concentration Formulation
F_ori	Template-free Assays with Original Concentration Formulation
FTIR	Fourier Transform Infrared Spectroscopy
FTS	Fischer-Tropsch Synthesis
H_2-TPR	Hydrogen Temperature Programmed Reduction
HC	Hydrocarbons
ICP-AES	Inductively Couple Plasma - Atomic Emission Spectrometry
IST	*Instituto Superior Técnico*
IUPAC	International Union of Pure and Applied Chemistry
IWI	Incipient Wetness Impregnation
LPG	Liquefied Petroleum Gas
LSRE-LCM	Laboratory of Separation and Reaction Engineering - Laboratory of Catalysis and Materials
MFI	Mobil Five
MOR	Mordenite
NH_3-TPD	Ammonia Temperature Programmed Desorption
RI	Refractive Index
SEM	Scanning Electron Microscopy
SiC	Silicon Carbide
SP	Spray Dryer
STP	Standard Temperature and Pressure
T	Formulations with Template
TBAOH	Tetrabutylammonium Hydroxide
TEAOH	Tetraethylammonium Hydroxide
TEOS	Tetraethyl Orthosilicate
TGA	Thermogravimetric Analyzes
TMAOH	Tetramethylammonium Hydroxide
TOC	Total Organic Carbon
TPABR	Tetrapropylammonium Bromide
TPAOH	Tetrapropylammonium Hydroxide
UTAD	*Universidade de Trás-os-Montes e Alto Douro*
WGS	Water Gas Shift
XRD	X-ray Power Diffraction

1 Introduction

1.1 Framing and Presentation of the Work

Nowadays, zeolite ZSM-5 holds significant importance in the chemical and petrochemical industries as a valuable catalyst due to its distinct structure and properties. It is typically produced in batches processes under hydrothermal conditions and employing organic templates. The initial mixture takes several hours to be ready for the autoclave's crystallization step. The aim of this work was to develop a continuous process with lower mixing times. For the first time, NETmix was used to produce zeolites. It is a push-forward to the scientific community and the research group.

This dissertation aimed to evaluate a faster route to synthesize the zeolite ZSM-5 using a reactor with a perfect mixture. The specific objectives mapped were:

- Synthesis of ZSM-5 template-free and with template in the formulation;
- Synthesis of ZSM-5 with different Si/Al ratios;
- Physical and chemical characterization of the ZSM-5 synthesized;
- Evaluation of ZSM-5 synthesized as a support for Fischer-Tropsch reaction.

Different conditions in the initial formulation and the process were applied to achieve these goals and to improve the outcomes. Throughout this dissertation, the different assays were evaluated and compared with a commercial reference by different characterization techniques and the results of the Fischer-Tropsch synthesis were analyzed and discussed.

1.2 Associate Laboratory LSRE-LCM Presentation

This work was conducted in the Product Engineering group of the Laboratory of Separation and Reaction Engineering – Laboratory of Catalysis and Materials (LSRE-LCM).

LSRE-LCM is a national R&D Unit and a member of the Associate Laboratory ALiCE, located at the Faculty of Engineering from University of Porto (FEUP). Currently it counts with more than 170 researchers with high levels of outputs, namely published books, papers, book chapters, patents, PhD, theses and spin-off companies.

Its mission is to contribute for the scientific and technological know-how advance, towards the sustainable development of the country, mainly in chemical engineering field.

1.3 Contribution of the Author to the Work

The author performed all assays for the synthesis of Zeolite, both batch and using NETmix. The formulations and procedures were adapted, by the author, from the literature.

The produced materials were characterized through several techniques. For thermogravimetric analysis (TGA), inductively coupled plasma – atomic emission spectroscopy (ICP-AES), Fourier transform infrared spectroscopy (FTIR), dynamic light scattering (DLS), Nitrogen isotherms and hydrogen temperature programmed reduction (H_2-TPR), the author was in a training session and then was autonomous. Regarding X-ray powder diffraction (XRD), ammonia temperature programmed desorption (NH_3-TPD) and high-resolution scanning electron microscopy (SEM) analysis, were performed by other researcher groups, however, the author did the analysis and data processing.

Additionally, Fischer-Tropsch reactions were performed by CoLAB NET4CO2.

1.4 Organization of the Dissertation

This dissertation was organized as follows:

Chapter 1 frames the performed work regarding objectives, the laboratory where this thesis was developed and the author's contribution.

Chapter 2 presents a brief context and state of the art of zeolites. The zeolite ZSM-5 is described in detail, including characteristics, its synthesis methods, parameters and evaluation (both procedure and final product), market perspective and possible applications (Section 2.1). Additionally, Fischer-Tropsch synthesis is detailed in Section 2.2, and the NETmix technology in Section 2.3.

Chapter 3 describes the materials and methods used in this work. Section 3.1 lists all reactants used for each formulation, while Section 3.2 details each formulation, template-free and with template. The procedures for synthesizing ZSM-5, the impregnation with cobalt and rhenium and protonation with ammonium are in Sections 3.3, 3.4 and 3.5, respectively. In Section 3.6, the characterization techniques used in this work are described in detail. The last section of this Chapter describes the Fischer-Tropsch synthesis.

The results were analyzed and discussed in Chapter 4. This Chapter is divided into sections 4.1 and 4.2 for zeolite production template-free and with a template, respectively. Characterization techniques are organized in subsections.

Chapter 5 presents all conclusions for this thesis, and the last Chapter includes the assessment of the work done.

2 Context and State of the Art

Zeolites were discovered a long time ago and described as boiling stones due to their ability to adsorb and release water from micropores when heated. This capacity originated the term Zeolite, as "*Zeo*" and "*Lithos*" are Greek words meaning boil and stone, respectively [1].

Zeolites are crystalline aluminosilicates with tetrahedral arrangement, where oxygen atoms are linked to a central atom of Al or Si. Hence aluminium is a trivalent atom, and the tetrahedral AlO_4^- produces a negative charge in the structure. That is corrected by the presence of cations, M, and water, as shown in Figure A.1 [2, 3].

These cations can be protons, alkaline, alkaline earth metals or organic bases. This last one is often used as a template and can be, for instance: tetrapropylammonium hydroxide (TPAOH), tetramethylammonium hydroxide (TMAOH), tetraethylammonium hydroxide (TEAOH), tetrabutylammonium hydroxide (TBAOH) and tetrapropylammonium bromide (TPABR) [4].

The general formula of zeolites is: $\mathrm{M}\frac{x}{n}[(\mathrm{Al_2O_3})_x(\mathrm{SiO_2})_y \cdot z\mathrm{H_2O}]$, where n is the valence of the cation, z is the number of water molecules per unit cell, x and y are the number of $\mathrm{Al_2O_3}$ and SiO_2 units, respectively [2, 5].

These materials can be either natural or synthetic zeolites. Mordenite, clinoptilolite and chabazite are examples of the first group and are mostly formed from a reaction between saline water and volcanic or sedimentary rocks. This reaction requires more than 50 years and is favored by pH values above 9 and temperatures above 27 °C. These zeolites are usually contaminated with other minerals such as amorphous glass or other zeolites. For this reason, natural zeolites are not widely used in industrial applications, where purity and uniformity are essential. On the other hand, ZSM-5, A and Beta are examples of synthetic zeolites, where different synthetic and/or natural resources can be applied [1, 2, 6].

Regarding the zeolites' synthesis approach, it can be divided into two methodologies: bottom-up or top-down. As the name suggests, the first methodology implies the formation of the structure and its pores during the crystallization, while the second is defined by the partial destruction of zeolite crystals, in order to create hierarchical porosity [2, 7].

Zeolites, with pore diameter sizes of 0.3 – 2.0 nm, are usually called molecular sieves due to their porous structure, which is accountable for their ability to selectively adsorb molecules based on their size, shape and polarity [3].

All zeolites have numerous applications in industrial, biomedical and agricultural processes, mainly due to their catalytic, adsorption and ion exchange properties [2, 8].

Relatively to the global zeolite market, it is expected to increase at an annual rate of 6.2 % from 2022 to 2030, reaching 19.8 billion euros by 2030 [9].

2.1 Zeolite ZSM-5

Zeolites ZSM were first produced industrially by Mobil and Union Carbide in 1972 through the use of organic drivers or, more commonly called, templates [10].

One element of this family is ZSM-5, which refers to Zeolite Socony Mobil – Five, where "five" indicates the average pore space of 5 Å. Relatively to its structure, ZSM-5 is considered as a molecular sieve and classified as Mobil five (MFI), according to the International Union of Pure and Applied Chemistry (IUPAC), using the 3 capital letters code [10], its chemical formula is $\mathrm{M}_r\mathrm{Al}_r\mathrm{Si}_{96-r}\mathrm{O}_{192} \cdot 16\mathrm{H}_2\mathrm{O}$, where r represents a number in the range from 1 to 8 [11].

The ZSM-5 pentasil unit is joined with 9 others to form a unit cell. These rings originate two different pores: one with 5.6 x 5.3 Å on the plane [100] and the other with 5.5 x 5.1 Å on the plane [010] [12-14]. Figure A.2 shows the structural pentasil unit.

In general, ZSM-5 is characterized by having a high Si/Al ratio (>12), which provides unique properties such as high thermic stability, high acidity, high surface area, porous and well-defined crystalline structure [4, 10, 15]. Table 2.1 presents the zeolite's main physical properties.

Table 2.1. ZSM-5 main physical properties [7, 11, 16].

Molar Mass /g·mol^{-1}	Solubility in Water	Density /g·cm^{-3}	Refractive Index (RI) in Water	Surface Area /m^2·g^{-1}	Pore Volume /cm^3·g^{-1}	Crystallinity / %
162.04	Insoluble	1.79	1.48	≈ 300	≈ 0.13	≈ 100

In more detail, some synthetic zeolites show crystallographic alterations around 600 °C and others only at 1200 °C. These alterations may occur since, in that range, the zeolite undergoes a severe dealumination [17]. Nevertheless, the zeolite's high thermal stability is one of the properties that makes it very suitable for high-temperature reactions as a catalyst or support. It is important to note that impurities, low mixing levels, low ambient humidity, and aluminum content drastically decrease the thermal stability of this catalyst [17].

When an AlO_4^- replaces a SiO_4 molecule in the zeolite framework, a cation-exchange center is formed. It produces a charge unbalance that must be neutralized by an additional charge. When protons (H^+) fill that center, the zeolite exhibit a very acidic behavior and form Brønsted acid sites (BAS), as shown in Figure A.3. Furthermore, the acidic capacity is determined by the Si/Al ratio, higher Si/Al originates higher acidity [13].

Equation 2.1 presents the ionic change that can be induced by NH_4^+ [14]:

$$NH_4{}^+ + M^+Z^- \xrightarrow[-M^+]{} NH_4{}^+Z^- \xrightarrow[\approx 300-400\,^\circ C]{-NH_3} H^+Z^- \quad (2.1)$$

where Z stands for the zeolite. All the characteristics mentioned above promote ZSM-5 for adsorption and catalytic properties [8].

Since natural zeolites do not have the best quality and because synthetic zeolite properties can be specifically manufactured, the synthetic route became imperative. Hence it is highly crucial to understand how this can be achieved.

2.1.1 Synthesis

ZSM-5 synthesis is a complex and specific method, as described below. Figure 2.1 shows the main steps to obtain this zeolite. A good mixture of precursors is essential (a), so that ordered subunits are induced to form during the ageing treatment (b). After the nucleation begins (c), the first crystals form from a solution, liquid or vapor, in which a small number of ions, atoms or molecules agglomerates and arrange themselves to establish a characteristic crystalline structure, forming a site where other particles can be deposited. Finally, the deposition of several particles in the sites created is called crystal growth which leads to the zeolite formation (d). Both c) and d) occur during crystallization derived from supersaturation acting as the driving force [2, 13, 18].

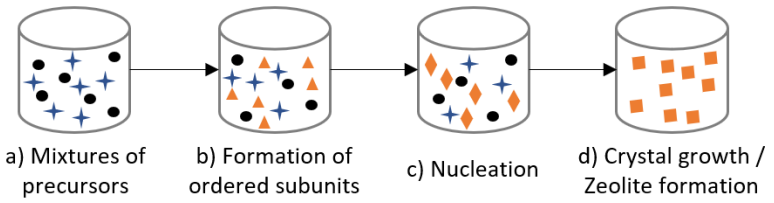

Figure 2.1. Zeolite synthesis steps. Adapted with permission from Derbe, et al. [2]. Copyright 2023 American Chemical Society.

A schematic image of ZSM-5's growth mechanism in the presence of TPA^+ is presented in Figure A.4. Each formulation has it owns precursors, but in general, it is an aluminosilicate gel (mixture of aluminate and silicate) in the presence of alkali hydroxides and water [2].

- **Methods**

ZSM-5 can be produced by two main routes: hydrothermal or green synthesis method [2].

The **hydrothermal treatment** is a process designed to simulate the geological formation of natural zeolites [19], which is characterized by reactions taking place at aqueous solutions in high temperatures, higher than 100 °C and lower than 240 °C [20], and pressures above 1 bar, in a closed system, for instance using a Teflon-lined stainless steel autoclave [21]. However, it has disadvantages, such as using organic bases as templates produce environmental problems

from the thermal decomposition of those species, being a time-consuming process, requiring a large amount of energy mostly for calcination (mainly to remove the organic template), and thus having high operational costs, consuming excessive amount of water and using autoclaves in laboratory experiences that poses some challenges regarding quality control at large-scale manufacturing [20, 22, 23]. It is noteworthy that there have been studies where the close system is a reflux system under stirring at 100 °C but with a much longer duration, minimum 7 days [24].

Therefore, **greener methods** started to be studied, where all the previously stated problems were fixed or improved. For that, researchers studied mostly zeolite production template-free, without solvent, in a continuous-flow and microwave-assisted [2].

For template-free synthesis, the crystalline structure is more difficult to obtain. This occurs since the template acts as the starting point for nucleation and the mold for the crystalline structure. When a template is not applied, the Na^+ ions are used as the specific surface for nucleation [25, 26].

For solvent-free synthesis, solid hydrous precursors such as $Na_2SiO_3 \cdot 9H_2O$ and/or $Al_2(SO_4)_3 \cdot 18H_2O$ are used, in order to maintain the right amount of water required for hydrolysis and condensation reactions during crystallization without the need to add more water [27].

Continuous-flow synthesis uses temperatures around 300 °C and pressures above 70 bar. This method is not commonly found in literature as it requires several safety measures such as pressure valves and equipment for these conditions [20]. Additionally, solid zeolite particles are produced in a high concentration during synthesis, behaving like a slurry. As is commonly known, sedimentation and fouling can occur within different components leading to incorrect residence times and blockages [13].

Regarding microwave-assisted synthesis, Teflon microwave vessels are transferred to a microwave, which substitutes the typical autoclave. This method facilitates a shorter synthesis time, a uniform structure and less energy consumption; however, it presents a considerable limitation for scale-up. Microwaves have a restricted penetration depth, so in a large reaction vessel, the reagents will be heated by convection instead of direct microwave heating [4, 28, 29].

This work applied two synthesis methods: template-free (F) and with template and solvent-free (T). In both methods, poor control of synthetic conditions can lead to amorphous material or other zeolites instead of pure ZSM-5 [23].

- **Parameters**

ZSM-5 production requires several restrictive conditions to produce pure zeolites with high crystallization and small crystals, which offer a higher surface area. Parameters such as

reactants source and quantity, water content, pH, initial solution homogenization and temperature, ageing and crystallization time and temperature, must be controlled [2, 8, 13, 22, 24, 30].

Regarding the reactant's source, the most important ones to consider are Al and Si. According to the literature, the sources which produce more crystalline and with high surface area zeolites are sodium aluminate followed by aluminum sulfate and aluminum hydroxide, for Al, and fumed silica followed by tetraethyl orthosilicate (TEOS) and colloidal silica, for Si [4, 30].

Concerning the reactant's quantity in the initial solution, there are some ratios to consider: for structure composition and acidity, the Si/Al should be around 12-100 [4, 31-33], for crystal size control OH^-/Si should be between 0.1-0.2 [10], for alkalinity regulation in the initial mixture the M/SiO_2 should be among 0.07-0.3 [7, 32] and the M/Al_2O_3 between 5-6 [34].

Another important parameter is the water content since it controls the final particle size. The increase of water leads to larger particles. This occurs because dilution results in alkalinity and cations concentration decrease, causing supersaturation of the solution, which favors the crystal growth in the wrong stage. Nevertheless, a certain amount of water must be available to prevent mordenite (MOR) phase formation instead of MFI [4, 8].

Relating to the pH value, high alkalinity is required to obtain crystalline ZSM-5. However, the crystallization rate decreases for a pH value greater than 14 [35]. To adjust the pH value, more water or sulfuric acid can be added [36].

The initial solution homogenization is also an important parameter since a homogeneous solution is crucial to nucleation. That can be achieved by stirring with a magnetic stir for several hours or by using other equipment such as NETmix, to facilitate the mass transfer, as it will be explained in Section 2.3.

Furthermore, ageing time and temperature affect the size and yield of the zeolites formed. Ageing provides the time to maximize the number of nuclei and increase the crystallization rate. Nevertheless, it is a parameter to be optimized since long times can lead to crystal growth in the wrong stage [26]. On the other hand, ambient temperature is preferred in this step since higher ones maximize crystal growth instead of nuclei formation [37].

Likewise, crystallization time and temperature are parameters which affect the crystal size and the crystallinity obtained. These parameters depend on each other. For instance, the higher the temperature, the less time will require to achieve the same crystallinity. Also, the bigger the time used in this stage, the higher the zeolite crystallinity acquired [4, 22, 23].

- **Yields**

To evaluate the synthesis procedure, Equation 2.2 was applied to calculate the corresponding mass yield (Y), % in mass [13]:

$$Y = \frac{w_{w+d}\, r_c}{\frac{w_{\mathrm{Si+Al}}}{w_t}\, w_a} \cdot 100 \tag{2.2}$$

where w_{w+d} corresponds to the samples mass after washing and drying step, in g, r_c indicates the ratio between final and initial samples mass for calcination step, $w_{\mathrm{Si+Al}}$ corresponds to the mass of Si and Al in the initial mixture, in g, w_t represents the total mass of the initial mixture, in g, and w_a signifies the initial mass in the autoclave, in g. Additionally, to analyze the synthetic zeolite, several techniques can be applied and are described in Chapter 3 [38].

2.1.2 Market and Applications

Zeolyst International, Sigma-Aldrich, ACS Material and Fisher Scientific are examples of companies that sell ZSM-5 with Si/Al ratios between 11.5 and 140 for approximately 1 €·g^{-1}.

MFI structure can be used as an adsorbent, a catalyst or catalyst support for several applications. Its adsorbent capacity for CO_2 and total organic carbon (TOC) molecules allows it to be used for air and water purification [39, 40]. On the other hand, as catalyst, it can be applied in the petrochemical industry for catalytic cracking, dewaxing, isomerization, oligomerization, aromatization, methanol to olefins conversion, methane or aromatics conversion, benzene alkylation and toluene disproportionation and in fine chemical: methyl tert-butyl ether cracking, cyclohexene and acetaldehyde hydration and NH_3 amination [38]. Furthermore, zeolites can be applied as a support for reactions as Fischer-Tropsch synthesis (FTS) [41].

2.2 Fischer-Tropsch Synthesis (FTS)

Fischer-Tropsch Synthesis (FTS) is a polymerization reaction occurring at the catalyst surface [42, 43]. It consists of an initial syngas mixture (CO and H_2) that is converted to a wide spectrum of hydrocarbons (HC): methane, C_1; liquefied petroleum gas (LPG), C_2-C_4; gasoline, C_5-C_{11}; diesel, C_{12}-C_{20} and wax, C_{21+}. It is noteworthy that FTS products are Syncrude and not-ready-to-use synthetic fuels; they need an upgrading stage to meet industry requirements [42, 44, 45]. Also, C_{5+} are the most desirable product, methane is an undesirable low-value product and waxes are only useful if hydrocracked to form gasoline and diesel [42, 46]. Equations 2.3 to 2.6 present the exothermal reactions involved in forming paraffins (or alkanes), olefins (or alkenes), by-products (oxygenated products such as alcohols, aldehydes, acids, ketones and carbonyls, produced but in reduced or non-existent quantities) and the reaction of water gas shift (WGS) [42, 46]:

CO hydrogenation to paraffins: $$(2k+1)H_2 + kCO \rightarrow C_kH_{2k+2} + kH_2O \quad (2.3)$$

CO hydrogenation to olefins: $$2kH_2 + kCO \rightarrow C_kH_{2k} + kH_2O \quad (2.4)$$

CO hydrogenation to by-products $$2kH_2 + kCO \rightarrow C_kH_{2k+1}OH + (k-1)H_2O \quad (2.5)$$

WGS: $$CO + H_2O \rightleftharpoons CO_2 + H_2 \quad (2.6)$$

where k is a stoichiometric number of CO.

Fe-, Ni-, Co- and Ru-based catalysts are the only elements of the group VIII of the periodic table that can act as a catalyst in FTS, due to their sufficient activity to convert CO to HC [42, 43, 47, 48]. Cobalt is considered the best one since: it has high selectivity for long-chain HC; has no water inhibition; has low selectivity for oxygenated products; presents a high activity for CO dissociation; has a low deactivation rate and extended life span, about 5 years [42, 43].

Supported Co catalysts are commonly prepared by incipient wetness impregnation (IWI) with 10-30 % range, in mass, of Co in the catalyst [49], followed by calcination and reduction. According to the literature, cobalt nitrate exhibits the highest reduction degree, resulting in higher C_{5+} selectivity [42, 47].

Calcination is required to break down cobalt salt into cobalt oxide. Although temperatures circa 500 °C appear to increase Co stability, temperatures circa 300 °C enhance CO conversion [50]. Thus, an intermediate calcination temperature must be used.

Reduction is also crucial in catalyst preparation since it reduces inactive cobalt oxide to active metallic cobalt [51]. Reduction equations are presented in Equations 2.7 and 2.8. The reduction temperature should be determined for each specific catalyst, due to the support interaction.

$$H_2 + Co_3O_4 \rightarrow H_2O + 3CoO \quad (2.7)$$

$$3H_2 + 3CoO \rightarrow 3H_2O + 3Co^0 \quad (2.8)$$

Zeolites are good supports for FTS. With Co they form a bifunctional catalyst, since it presents: (i) active sites, which promote chain growth, from the Co; and (ii) acid sites, which promote hydrocracking (converts larger hydrocarbon molecules into smaller, under high hydrogen pressure and temperature) and isomerization (rearrangement for an iso-paraffin), from the zeolite [41]. It is important to notice that iso-paraffins are responsible for high-quality fuel production due to an increase in the octane number [41].

Additionally, a small amount of promoter is typically introduced as it lowers the activation temperature, increases C_{5+} selectivity and promotes catalyst stability [46, 47]. Nevertheless, they do not ensure a better catalyst since it might lead to faster deactivation [52]. The promoters used for Co-based catalysts are usually noble metals, with rhenium being the most applied [47].

FTS is influenced by several factors that can be controlled and adjusted, mainly: H_2/CO ratio; temperature; pressure and gas hourly space velocity (F_{GHSV}) [46]. The H_2/CO ratio should be optimal at circa 2, since a higher value increases the CO conversion but displaces the WGS towards H_2O formation [42, 49]. In this work, other parameters were adjusted based on previous studies, performed by NET4CO2 [53].

The calculation of CO conversion (X_{CO}), in %, and cobalt-time yield (F_{CTY}), in $mol_{CO}{\cdot}g_{Co}^{-1}{\cdot}s^{-1}$, to allow direct comparison between catalysts and selectivity's are presented in Equation B.1 and B.2, respectively.

2.3 MicroNETmix

The NETmix reactor is a static mixer designed, developed and patented by Lopes *et al.* in 2005 at LSRE-LCM [54]. This reactor provides an efficient mixture, intensity and scale control, presents a simple structure, it is easy to implement and adapt based on the project needs, it offers the ability to control residence time and temperature (it has a large area to promote heat exchange) and support the possibility to scale-up since it is possible to associate in series or in parallel [55].

These main characteristics of the NETmix reactor derived from its organization as a 2D network. The network is a repetition of unit cells composed of a chamber interconnected by two inlets and two outlet channels, represented in Figure C.1 [56, 57]. The laboratory set-up used in this work, MicroNETmix, was designed to offer the main characteristics of NETmix but requiring a less quantities of reactants. Hence, relative to the previous NETmix set-ups, it shortens up the experimental time and it allows higher Reynolds number (Re_d) for the same flow rate [57, 58].

The MicroNETmix reactor is composed by 1 plate (n_p), 8 columns (n_y) and 25 rows (n_x). The chambers have a diameter of 3.3 mm, and the channels have a depth (d_c) and width (w_c) of 0.5 mm. The channel cross-section area (A_{cs}) is 0.25 mm^2 and has a hydraulic diameter (d) of 0.5 mm, calculated by Equation b.1. The most important parameter to control when using this technology is the Re_d, which is determined by Equation 2.9:

$$Re_d = \frac{\rho\, v\, d}{\mu} \tag{2.9}$$

where ρ is the mixture's density in $kg{\cdot}m^{-3}$, v the average velocity in the channels in $m{\cdot}s^{-1}$, d in m and μ is the mixture's viscosity in Pa·s.

For simplification in this work MicroNETmix is generally referred as just NETmix. Due to the NETmix high mixture capacity it was used here to study if efficient and controlled mixing can decrease the homogenization time of the initial mixture in ZSM-5 synthesis.

3 Materials and Methods

3.1 Materials

To synthesize the zeolite ZSM-5 template free, a pure powder sodium aluminate ($NaAlO_2$; CAS: 11138-49-1) and a 40 %, in mass, colloidal silica (SiO_2; CAS: 7631-86-9) were used, both from Sigma-Aldrich. Also, pure pellets of sodium hydroxide (NaOH; CAS: 1310-73-2) from VWR Chemicals and deionized water were used.

To synthesize the zeolite ZSM-5 with template, tetrapropylammonium hydroxide (TPAOH; CAS: 4499-86-9) from TCI as a 22.7 % in mass suspension in water was used. Also powder of aluminum sulfate octadecahydrate ($Al_2O_{12}S_3 \cdot 18H_2O$; CAS: 7784-31-8) from Thermo Scientific, tetraethyl orthosilicate (TEOS; CAS: 78-10-4) from Sigma-Aldrich as a 98 % purity solution and distilled water were used. The reactants used for both formulations are presented in Table D.1.

Nano H-ZSM-5 from ACS Material with ratio Si/Al=26 was used as the commercial reference.

Ammonium nitrate (NH_4NO_3; CAS: 6484-52-2) from Sigma-Aldrich with 99.5 % purity and distilled water were used for the protonated zeolite.

For the impregnation method cobalt (II) nitrate hexahydrate ($Co(NO_3)_2 \cdot 6H_2O$; CAS: 10026-22-9) from Labkem with >99 % purity and perrhenic (VII) acid (HO_4Re; CAS: 13768-11-1) from Acros Organics as a 76.5 % in mass suspension in water with 99.99 % purity were used.

3.2 Formulations

Regarding the ZSM-5 production, the formulation used for template-free was, $Na_2O/SiO_2/Al_2O_3/H_2O$, 5/50/1.6/750 and 5/50/1/1875 in moles, for Si/Al ratio of 15 and 25, respectively.

For the ZSM-5 production with template, the formulation used was $TPAOH/SiO_2/Al_2O_3/H_2O$, 24/61/1/42, 24/61/0.5/33 and 24/61/0.34/30, for Si/Al ratio of 30, 60 and 90, respectively, in moles.

For impregnation, 0.5 g of zeolite with metals were prepared, knowing that 15 % of that was Co and 0.75 % was Re, in mass. The quantity of water added was determined based on the total pore volume of each zeolite.

3.3 Synthesis Procedures

The synthesis of the zeolite ZSM-5 was performed by two methods, with and without template. Figure 3.1 presents the production scheme of template-free assays.

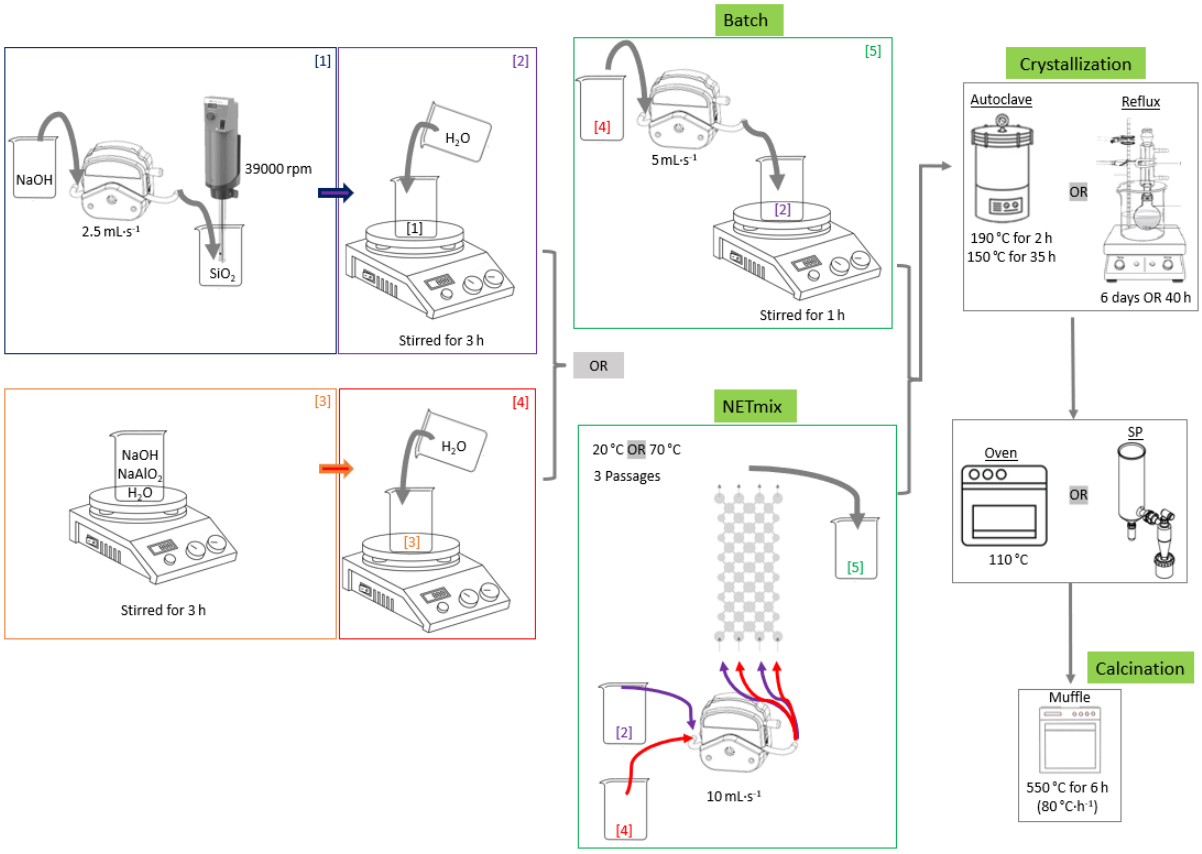

Figure 3.1. Zeolite production scheme for assays with template-free formulations.

For template-free experiments, a protocol was adapted from Mintova and Barrier [59]. Solution (1) was prepared by adding NaOH to SiO_2 through a peristaltic pump (Ismatec MCP) at 2.5 mL·s^{-1}, using a homogenizer (Miccra Mini Batch D-9), with 39 000 rpm (presented in Figure a.1). Afterward the solution (2) was prepared by adding water to solution (1) with stirring with a magnetic stirrer (Agimatic-N from P-select) for 3 h. Solution (3) consisted of simply mixing all the reactants, stirred for 3 h. Then, solution (4) was prepared by adding water to solution (3) with stirring. For the batch experiments solution (4) was added to solution (2) through a peristaltic pump, under stirring, for 1 h, resulting in solution (5). On the other hand, in the NETmix experiments, solution (5) was produced by mixing solution (2) and solution (4) with a peristaltic pump and a bath temperature controller (Viscotherm VT 2 from Paar Physica) and performing 3 passages throughout the NETmix reactor (configuration presented in Figure a.2). After the mixing procedure, for both batch and NETmix experiments, crystallization followed and was achieved by using an autoclave (Paar Instrument Company) placed inside an oven for 190 °C during 2 h and then 150 °C for 35 h or using a reflux installation at 100 °C for the same total time (both reflux configuration, autoclave and a product image after autoclave are showed in Figure a.3). Afterwards, the resulting powder was dried in an oven (P-select from Anatron Instruments) at 110 °C or in a spray drier (SP) from Büchi Mini Spray Dryer B-290 (air pressure of 5 bar; flow 30 mL·min^{-1}; inlet temperature of 190 °C and 10 % pump). Finally, the

samples were calcinated at 550 °C for 6 h, by a ramp of 80 C·h^{-1}, in a muffle (Nabertherm GmbH L15/11).

Figure 3.2 presents the procedure followed for the experiments using a template.

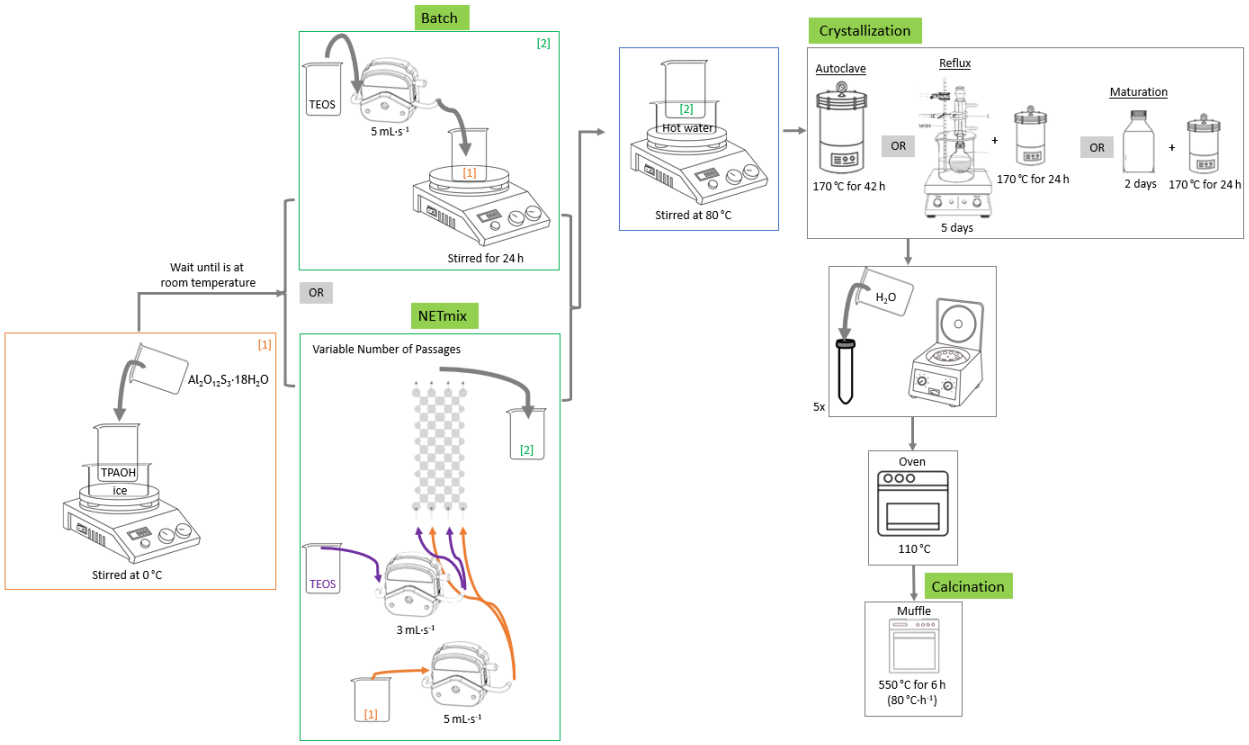

Figure 3.2. Zeolite production scheme for formulations with template.

In this case the Van Grieken, et al. [60] procedure was followed with adaptations. Here, TPAOH was cooled at 0 °C in an iced bath and then $Al_2O_{12}S_3 \cdot 18H_2O$ was added and mixed by a magnetic stir, originating solution (1). After obtaining a clear solution, solution (1) was removed from the bath and allowed to reach room temperature. In the batch experiments, solution (2) was obtained by adding TEOS to solution (1) and mixed it for 24 h, in a magnetic stir. On the other hand, for the NETmix experiments the mixture was performed by the NETmix reactor at room temperature and using two peristaltic pumps to guarantee that both solutions, solution (1) and the TEOS solution, which have different volumes, ended at the same time and a perfect mixture was obtained (configuration presented in Figure a.4). After mixing, for both batch and NETmix experiments, solution (2) was heated at 80 °C to remove the alcohols and water formed; 1/5 of the total volume was evaporated. Next, crystallization followed and was achieved by using an autoclave, inside an oven, for 170 °C during 42 h, or using a reflux installation at 100 °C followed by autoclave, or maturation, at room temperature, and autoclave (product image after autoclave is showed in Figure a.4). The resulting powder was washed with distilled water, centrifugated in a centrifuge for 5 min at 10 000 rpm (Heraeus Multifuge X1R Centrifuge from Thermo Scientific) and decanted and this procedure was repeated 5 times (Figure a.5). Then it

was dried in an oven at 110 °C and finally calcinated at 550 °C for 6 h, by a ramp of 80 °C·h^{-1}, in a muffle.

Table 3.1 and Table 3.2 report all the assays produced and its specifications by template-free and with template formulations, respectively.

Table 3.1. Assays produced without template and its specifications.

Assay	B / N	Si/Al	Concentration	Re_d	Reaction Temperature / °C	Crystallization
F_B_15_dil_20C	B	15	Diluted 2x	-	20	-
F_B_15_ori_20C_mat	B	15	Original	-	20	Maturation in solution (4 months)
F_B_15_ori_20C	B	15	Original	-	20	Autoclave
F_N_15_dil_Re150_20C	N	15	Dilute 2x	150	20	-
F_N_25_dil_Re150_70C	N	25	Dilute 2x	150	70	-
F_N_25_dil_Re360_70C	N	25	Dilute 2x	360	70	Reflux (6 days)
F_N_15_ori_Re360_70C	N	15	Original	360	70	Reflux (40 h) Autoclave
F_N_15_ori_Re400_70C	N	15	Original	400	70	Autoclave

Table 3.2. Assays produced with template and its specifications.

Assay	B / N	Si/Al	Re_d	Crystallization	Crystallization time
T_B_30	B	30	-	Autoclave	42 h
T_N_30	N	30	500 (3 passages)	Autoclave	42 h
T_N_30_rep	N	30	500 (3 passages)	Autoclave Reflux + Autoclave	42 h 5 days + 24 h
T_N_30_24h	N	30	500 (3 passages)	Autoclave Maturation + Autoclave	24 h 2 days + 24 h
T_N_30_recir	N	30	500 (2 min recirculation)	Autoclave Maturation + Autoclave	42 h 2 days + 24 h
T_N_30_10recir	N	30	500 (10 min recirculation)	Autoclave	42 h
T_N_60_recir	N	60	500 (2 min recirculation)	Autoclave	42 h
T_N_90_recir	N	90	500 (2 min recirculation)	Autoclave	42 h

The assays are described as follows: “F” for template-free or “T” for formulations with template, “B” for batch or “N” for NETmix assays, next the Si/Al ratio, and then the synthesis conditions (concentration: “ori” and “dil” for the concentration given by the formulation and diluted two times, respectively, Re_d, reaction temperature and special conditions: “mat” with maturation, “recir” for recirculation). Note that “rep” stands for the repetition of the assay, “Auto” represents autoclave and “Calc” the calcinated sample.

3.4 Impregnation Procedure

The capacity of the produced zeolite to be a good support was studied using FTS. For this, cobalt and rhenium were impregnated in the zeolite using the IWI method [47, 48].

The IWI method consists in sonicate (ULTR-10L-001 from Vevor) the sample at a constant temperature of 23 °C (ice was added to prevent temperature from rising) under vacuum for 15 min with a pump (Buehler Vacuum Impregnation Pump). Afterwards the Co and Re solution, prepared based on the total pore volume, was added dropwise and guaranteeing that all pores were filled, with a peristaltic pump (Ismatec Reglo ICC), 0.3 $mL \cdot min^{-1}$. Given that the sample was then dried with the following program 40 °C for 16 h; 60 °C for 4 h; 80 °C for 4 h and 120 °C for 12 h and calcinated with a ramp of 80 $°C \cdot h^{-1}$ until 400 °C and then 6 h at constant temperature, both in a muffle. Figure a.6 presents a sample image after the procedure and after the drying stage.

Before the metal impregnation it was necessary to measure the wetting volume of each produced zeolite. For this, the same method was applied but water was used instead of the metal solution. Figure a.7 presents the process scheme followed.

3.5 Protonation Procedure

For protonation the methodology presented in Figure a.8 was followed. It consisted of adding 0.8 g of zeolite to 80 mL of a 1 M NH_4NO_3 solution and mix it with a shaker machine (Scansci SI-300R Lab Companion) for 6 h at 25 °C and 150 rpm. The suspension was then centrifugated and decanted. This procedure was repeated 3 times (for logistic reasons, for the second repetition, the solution was left for 15 h instead of the planed 6 h. This change in the procedure did not represent any problem to the protonation efficiency). Afterwards the sample was dried in an oven at 110 °C and calcinated with a ramp of 80 $°C \cdot h^{-1}$ until 550 °C and then 6 h at constant temperature in a muffle [61-63].

3.6 Characterization Techniques

3.6.1 Thermogravimetric Analysis (TGA)

NETZSCH STA 409 PC from LUXX was used to perform TGA from 50 °C until 800 °C with a ramp of 10 $°C \cdot min^{-1}$ and using air. The samples were analyzed with supervision. Around 10 mg were added to a crucible and inserted on the TGA equipment.

TGA is used to determine the sample thermal stability and the fraction of volatile components. That is achieved by heating the sample at a constant rate and monitoring the weight change throughout the increasing of temperature [64].

3.6.2 Inductively Couple Plasma - Atomic Emission Spectrometry (ICP-AES)

ICP analysis of silica and alumina were performed in a ICP spectrometer (iCAP 7000 Series from ThermoScientific). This analysis required that 10 mg of the samples were previously digested in a Microwave Digestion System (Start D from Milestone) for 15 min at 220 °C with 5 mL of phosphoric acid (H_3PO_4; CAS: 7664-38-2), 3 mL of hydrochloric acid (HCl; CAS: 7647-01-0) and 0.5 mL of hydrofluoric acid (HF; CAS: 7664-39-3). Afterwards, the solutions were diluted to guarantee that the concentration of each metal was within the calibration curve, between 0-10 $mg \cdot L^{-1}$ of each metal. This technique was performed to identify and measure several chemical elements presented in the metal sample by detecting the atomic emissions produced as light [65]. The theoretical Si/AL ratio in the final framework was calculated by a correlation between SiO_2/Al_2O_3 ratio in the initial gel and in the final framework provided by Kim, *et al*. [25], presented in *Figure E.1*.

3.6.3 Fourier Transform Infrared Spectroscopy (FTIR)

FTIR analysis were accomplished by a FT-IR spectrometer from Perkim Elmer (UATR Two), in a wavenumber range from 400 to 4000 cm^{-1}, to acquire which compounds bounds are presented in the zeolite. Approximate 10 mg of a solid sample was placed in the platform and then a maniple was rotated until a value of 35 for force was applied. When infrared radiation passed through the sample, some of that radiation is absorbed and the rest is transmitted. An infrared spectrum is obtained by determining the fraction of incident radiation that is absorbed and with a Fourier transformation the data are converted into a sample's spectrum [66].

3.6.4 Scanning Electron Microscopy (SEM) and Energy Dispersive Spectroscopy (EDS)

SEM and EDS analysis were performed by using a Phenom ProX G4 equipment to obtain a surface ampliated imaged of the zeolites produced and a qualitative perspective of the atomic compounds presented. Regarding the sample preparation, approximate 5 mg of zeolite were deposited in a carbon tape, glued to a metallic support. Then the sample passed through compressed N_2 to guarantee that there were no particles poorly fixed, which could damage the equipment. Finally, the sample was analyzed under supervision. Additionally, high-resolution SEM analysis were performed in Materials Center of the University of Porto (CEMUP) by a high-resolution (Schottky) environmental scanning electron microscope with x-ray microanalysis and electron backscattered diffraction analysis (FEI Quanta 400 FEG ESEM / EDAX Genesis X4M).

This technique consisted in obtaining several signals of accelerated electrons that interact with a solid sample and then provide an image of the morphology and topography of the samples. Additionally, an energy dispersive detector is used to separate the characteristic x-rays of different elements into an energy spectrum and, posteriorly, an EDS system software analyses it to determine the abundance of specific elements [67].

3.6.5 Dynamic Light Scattering (DLS)

For the DLS analysis two equipment were used based on their measurement's limitations. Samples after crystallization step were analyzed by a Coulter LS 230, while samples after calcination step were analyzed by a Zetasizer Nano Series from Malvern. Regarding sample preparation, for Coulter analysis only a few drops were added to the equipment. On the contrary, for Zetasizer analysis, 2.5 mg of sample were added to 25 mL of water and after that mixed by a homogenizer (11 000 rpm velocity for 1 min). About 2 mL of prepared solution were set inside a cuvette.

3.6.6 Nitrogen Isotherms

Nitrogen Isotherms were obtained by using a high-speed surface area and pore size analyzer (Nova 4200e, Quantachrome Instruments) at 77 K. Approximate 100 mg of sample were inserted in a cell and kept at 150 °C for 3 h in vacuum before starting the N_2 adsorption [29].

This method evaluates the amount of adsorbed gas into the sample surface, as a function of the relative pressure [68]. This technique allowed the calculation of Brunauer-Emmett-Taylor surface area (S_{BET}), the total pore volume (V_{pores_total}), the area of non-micropores ($S_{\neq micro}$) and the micropore volume (V_{micro}) both by t-method. Where the areas are in $m^2 \cdot g^{-1}$ and the volumes in $cm^3 \cdot g^{-1}$. The BET method should be applied for relative pressures in range of 0.05 and 0.3 (adapted for each obtained isotherm), described in Equation F.1 and F.2, and can be used for isotherms type II and IV (with careful due to the possible presence of micropores) [69]. The t-method represents a linear correlation between the adsorbed volume, in standard temperature and pressure (STP) conditions, with the average adsorbed film thickness, t_f, in Å. This method can be applied for higher pressures and eliminates all deviations caused by capillary condensation [69].

3.6.7 X-Ray Power Diffraction (XRD)

XRD is an efficient technique used for phase identification of a crystalline material. That is achieved by directing a beam of X-rays at the sample and collect the diffracted ones. Both sample and detector rotate in a synchronize motion which allows recording the intensity of the reflected X-rays in each angle [2, 70]. For that 30 mg of zeolite were sent to *Universidade de Trás-os-Montes e Alto Douro* (UTAD). The analysis was performed at room temperature by a PANalytical X'Pert Pro diffractometer, and the data was collected at 2Θ from 5° to 60°, where Θ is the half the angle between the incoming and outgoing beam. Afterwards, crystal size (L), in nm, by Scherrer Equation (Equation G.1) at 8º, and crystallinity (C), in %, by Equation G.2, were calculated [71].

3.6.8 Ammonia Temperature Programmed Desorption (NH_3-TPD)

In the NH_3-TPD technique, the catalyst is submitted to a carrier gas flow of a base, NH_3, while an inert gas flow of helium is flushed into the surface to remove the chemically adsorbed NH_3 fraction. This occurs while increasing linearly the temperature and measuring the desorption of the base. This technique provides the number and the strength of acid sites in the sample by analyzing the thermal conductivity of the output flow during NH_3 desorption [69, 72]. For that 150 mg of zeolite were sent to *Instituto Superior Técnico* (IST) to perform NH_3-TPD analysis with temperature range between 50 °C and 700 °C, and with a 10 °C·min^{-1} ramping rate.

Equation H.1 was used to calculate the NH_3 uptake (U_{NH_3}) in µmol·g^{-1}, which is directly related to the zeolite acidity [69]. Note that it was assumed that each desorbed molecule corresponded to a single acid site. With that, the amount of acid sites is proportional to the peak area.

3.6.9 Hydrogen Temperature Programmed Reduction (H_2-TPR)

The H_2-TPR analysis was accomplished by using Altamira Instruments AMI-200 from 50 °C to 700 °C with a ramp rate of 5 °C·min^{-1} and a flow rate of 1.5 cm^3·min^{-1} of H_2. For this technique, 25 mg of impregnated zeolite were dropped inside a specified cell (U-shaped quartz tube), protected with quartz fused glass wool, to prevent the sample to contaminate de equipment and then placed inside the heating blanket.

This technique provided a correlation for the H_2 consumption with the increasing of temperature, Equation I.1 . That is achieved since the interaction between H_2 and the catalyst leads to the reduction of different species which indicates the catalyst reducibility and the degree of oxidation of the active phase [73].

3.7 Fischer-Tropsch Synthesis (FTS)

The FTS was conducted and analyzed at CoLAB NET4CO2 in a bench-scale fixed-bed down-flow stainless steel SS316 reactor (Microactivity Effi, MAE, from PID Eng&Tech), shown in Figure a.9. Here 250 mg of impregnated zeolite were weighted and silicon carbide (SiC) was added until the sample reached 3 mL, since it reduces the probability of occurring hot spots during the reaction due to its high thermal conductivity [74]. The reaction occurred at 240 °C, 20 bar, $H_2/CO/N_2$ (2/1/0.33) and F_{GHSV} of 7.96 m^3·kg$_{cat}^{-1}$·h^{-1} for 28 h. Before, the reduction step, in-situ, was performed at 400 °C for 10h.

During this process, the gas phase was continuously analyzed using a gas chromatograph YL6500 (YL instrument CO. LTD), the water and the organic phase were condensed, and the waxes were separated. After the reaction, the water and the organic phase produced were separated and the organic phase was analyzed in an offline liquid chromatograph (Supelcowax 10 capillary GC column).

4 Results and Discussion

As previously stated, zeolite ZSM-5 were produced by two formulations, with or without a template. Also, each one was produced in batch and continuous mode (NETmix) for the initial gel mixture (before crystallization step).

For each trial the mass yield was calculated to evaluate the production process. Then, the material produced was characterized through the various techniques described above. For the continuous process (NETmix), rheological tests were performed to obtain the viscosity of the mixture (initial gel mixture), Figure b.1 and Figure b.2, and to determine the Reynolds number, Table b.2.

Finally, the most promising synthesized material was tested for the FTS.

4.1 Zeolite Production Template-Free (F)

4.1.1 Production Mass Yield

The mass yield indicates the percentage of zeolite formed after all the production steps, relatively to the initial amount of Si and Al. Table 4.1 presents the yield for batch and NETmix, considering a Si/Al ratio 15, the concentration of reactant without dilution, and the crystallization step.

Table 4.1. Mass yield for template-free formulations assays, Equation 2.2.

Assays	Y /Mass %
F_B_15_ori_20C_Auto	35.2
F_N_15_ori_Re360_70C_Auto	34.3
F_N_15_ori_Re400_70C_Auto	36.1

For template-free assays, the yield was between 34.3 % and 36.1 %, in the case of the NETmix, the residence time was 57 and 45 s (for Re_d of 360 or 400, respectively) and the result was equivalent to 1 h of the mixture in batch, 35.2 %.

In general, approximately 0.35 g of ZSM-5 are produced with 1 g of both Si and Al. This value derived from all the losses within the processes, namely the passages between the crystallization step to drying and calcination.

4.1.2 Thermogravimetric Analysis (TGA)

TGA was performed to determine the temperature to calcinate the product. Figure 4.1 presents the samples mass loss with temperature as well as its derivative for two products' previous calcination step: (a) product obtained in batch and dried at 110 ºC in an oven (F_B_15_dil_20C)

and (b) material synthesized using NETmix (F_N_15_dil_Re150_20C_washed), this product was washed with ultrapure water and dried at 110 ºC in the oven.

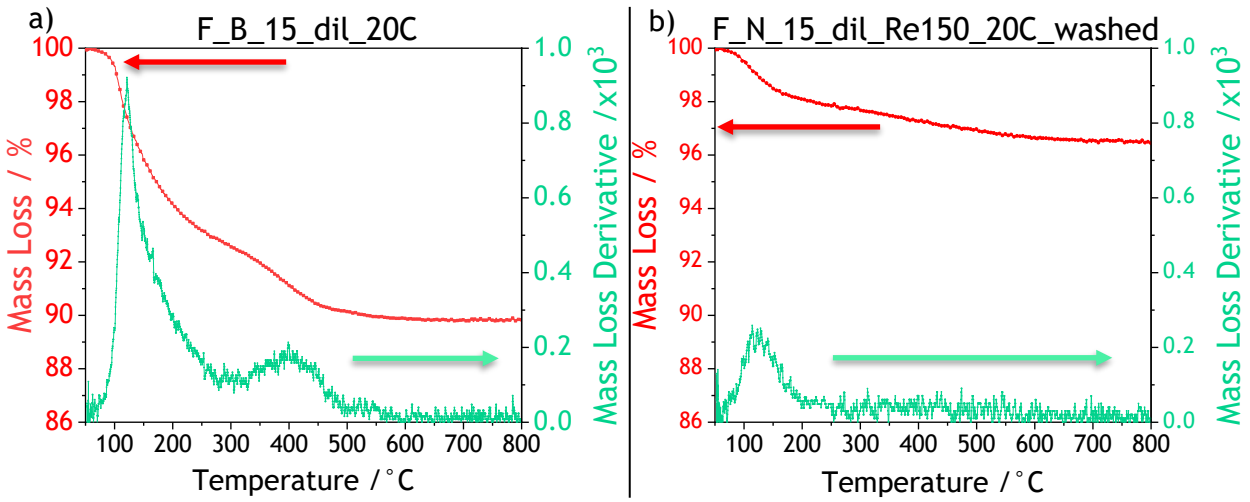

Figure 4.1. TGA curves for template-free assays. (a) F_B_15_dil_20C and (b) F_N_15_dil_Re150_20C_washed.

Around 100 °C, both samples showed a mass loss of 7 % and 3 % for F_B_15_dil_20C and F_N_15_dil_Re150_20C_washed, respectively, due to all adsorbed water. Relatively to the assay in batch mode (F_B_15_dil_20C), it was possible to verify other components present in the sample with a peak of the mass loss derivate around 400 °C. This could be a consequence that other components, presented in the sample were not removed or destroyed preceding the TG analyses.

For temperatures above 500 °C, both samples present a stable thermal behavior, indicating no other mass loss, and that the material is thermally resistant, one important property of zeolites. For temperatures of 800 °C, the F_N_15_dil_Re150_20C_washed assay presented only 3 % loss, derived from water evaporation, while the other, F_B_15_dil_20C assay, presents a total 10 % loss, from water and secondary compounds.

These results show that the washing step was sufficient to remove all extra compounds, visualized in material produced using NETmix analysis, the only mass loss was associated with water. In this case, the protocol of calcination to remove some unreacted organic compounds might not be required in this formulation. However, the literature procedure was followed as previously planned (with calcination step). This conclusion was also observed by Yue, et al. [75].

The calcination temperature must be the minimum to prevent BAS losses but sufficient to guarantee that all extra compounds are degraded [17]. Thus, 550 °C was the calcination temperature chosen for all the assays. This temperature is also verified by literature [17, 24, 76].

4.1.3 Inductively Couple Plasma - Atomic Emission Spectroscopy (ICP-AES)

ICP-AES analyses were executed to obtain the samples' real Si/Al content. Table 4.2 presents the theoretical Si/Al ratio of the calcinated samples in the initial gel, foreseen by the formulation, the theoretical ratio in the final framework and the experimental ratio acquired at 2516 nm and 3092 nm for Si and Al, respectively. The corresponding correlation is presented in *Figure E.1* and the two calibration curves are shown in Figure c.1.

Table 4.2. Experimental and theoretical Si/Al ratio, in the initial gel and in the framework, of samples produced with template-free formulation and for commercial reference.

Assay	Si/Al		
	Theoretical in the gel	Theoretical in the framework [25]	Experimental in the framework
Commercial_26_H	-	-	28
F_B_15_ori_20C	15	9	14
F_N_15_ori_Re360_70C_Auto	15	9	14

Comparing the Si/Al ratios theoretical in the gel and experimental in the framework, it can be observed that both values were similar, and so there was no difference between the initial gel and the final framework composition. This was not expected since the ratio in the framework should have been less than in the gel, as not all Si and Al particles introduced in the gel enter the structure [25]. It indicates, once again, that the produced samples are not following the ZSM-5 usual behavior.

For simplification procedures, the assays continue to be labeled by their theoretical ratio in the gel and not by the real ratio in the framework. Nevertheless, both have a Si/Al ratio of 14 in the final framework.

Note that the commercial reference was evaluated to guarantee that both the digestion procedure and the calibration curves in the ICP-AES were correct.

4.1.4 Fourier Transform Infrared Spectroscopy (FTIR)

FTIR is another crucial analysis, as it exhibits the vibrational bonds between elements in the final material. This technique was one of the first to be performed since it was fast and provided immediate essential information. Figure 4.2 shows the FTIR spectrum obtained to each calcinated final sample as well as the commercial sample with Si/Al ratio of 26.

The zeolite ZSM-5 has five characteristic bands in FTIR, represented by letters "a" to "e": "a" stands for asymmetric stretching of external linkages, around 1220 cm^{-1}; "b" represents the asymmetric stretching of internal linkages, around 1090 cm^{-1}; "c" is for symmetric stretching of the external linkages, around 790 cm^{-1}; "d" is for double ring bonds, around 540 cm^{-1}, and "e" is for T-O bending, where T stands for Si or Al, around 450 cm^{-1}. However, for higher Si/Al ratios the bands tend to be slightly moved for lower wavelengths [77].

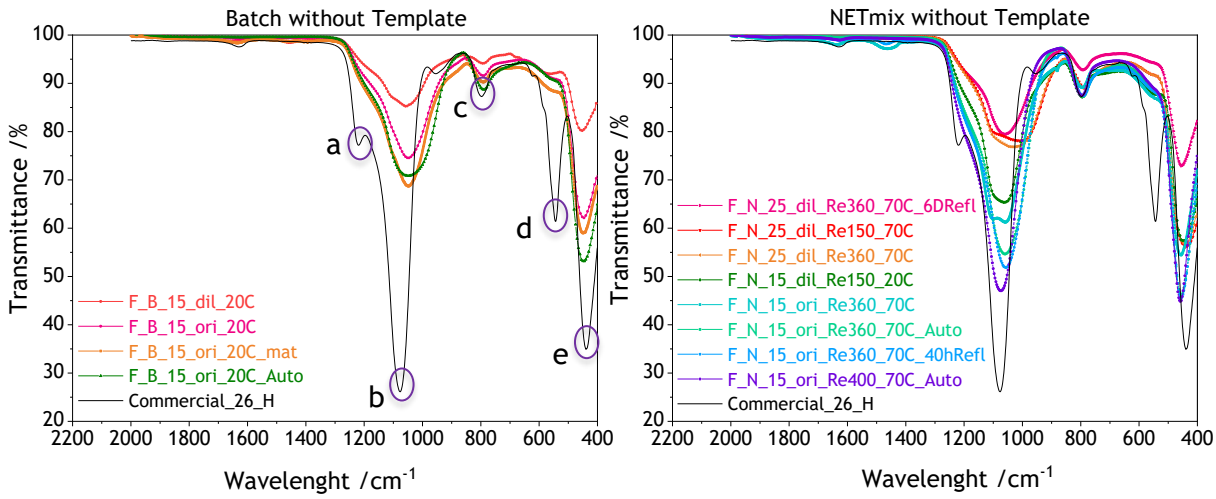

Figure 4.2. FTIR spectra obtained for calcinated assays with template-free formulations. On the left side the assays produced in batch and on the right the assays produced with NETmix.

The bands "a" and "d" were missing for all batch assays, indicating that the zeolite was not correctly formed. Besides that, it is observed that more concentrated initial solutions promote bands with higher intensities. Also, the use of an autoclave appears to promote higher band intensities. In terms of intensity, the 4 months maturation sample in solution seems to have the same behavior of the one with 37 h in the autoclave.

Similarly, for all NETmix assays, bands "a" and "d" were missing indicating that the zeolite was not correctly formed. In this case, Si/Al ratio of 15 appears to favor the bands intensities, probably because that concentration is more favorable to zeolite formation. These spectra indicate that higher Re_d, higher reaction temperature and the use of autoclave or reflux promotes bands with higher intensities, as expected, as all these parameters promote the zeolite formation.

Comparing both methods, the NETmix products have better results in terms of bands intensities. However, all ZSM-5's essential bindings were not shown in any assay. Consequently, only F_B_15_ori_20C_Auto, F_N_15_ori_Re360_70C_Auto and F_N_15_ori_Re400_70C_Auto were further characterized. Note that when choosing only one assay from the NETmix method, F_N_15_ori_Re400_70C_Auto was not chosen as it was performed using different pumps.

Note that initially, the samples were dried by SP and in the oven, however for simplification procedures it was concluded by FTIR analysis that there was no significant difference in the bonds formed by those different methods, as presented in Figure c.2. Thus, the following assays were dried in the oven.

Finally, Figure c.3 presents a comparison between the reactants and the commercial sample.

4.1.5 Scanning Electron Microscopy (SEM) and Energy Dispersive Spectroscopy (EDS)

SEM technique was applied to visualize the zeolites. Figure 4.3 shows the SEM images obtained for ZSM-5: commercial reference (Commercial_26_H), batch (F_B_15_ori_20C_Auto) and NETmix (F_N_15_ori_Re360_70C_Auto), the products obtained in batch and NETmix were crystallized using an autoclave.

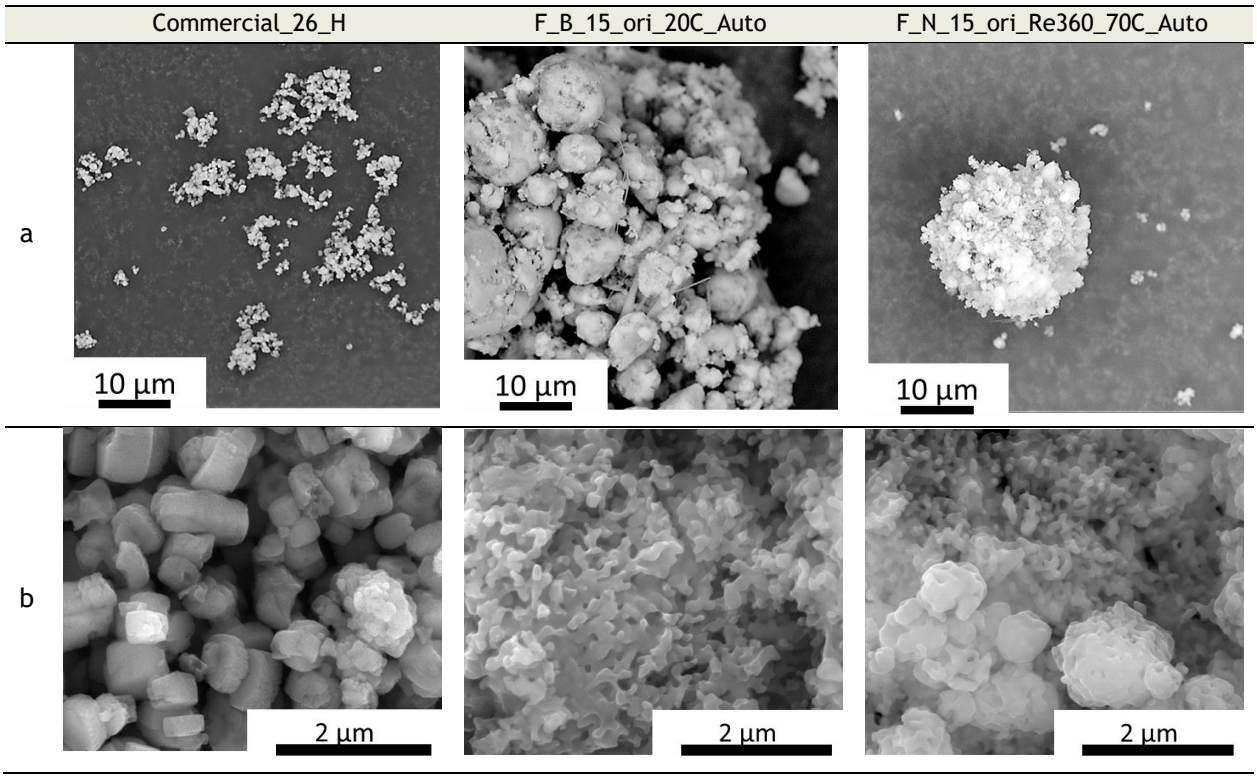

Figure 4.3. SEM images obtained for calcinated samples produced by template-free formulation, for batch and NETmix assays, and for commercial reference, where "a" corresponds to SEM images and "b" to the high-resolution SEM images.

Comparing the commercial reference with the products from batch and NETmix, the commercial sample presented small particles, and individual particles were larger in the batch than the NETmix assays.

Hight resolution SEM was applied to have a clear perspective of the individual particles structure. Both batch and NETmix assays presented a different external structure when compared to the commercial reference. Thus, the particle size was not possible to be estimated and these results indicate that, probably, the product formed is not the desired zeolite.

Furthermore, the qualitative evaluation of different elements present in the sample were analyzed by EDS. The obtained ratio Si/Al was 14 and 12, for F_B_15_ori_20C_Auto and F_N_15_ori_Re360_70C_Auto, respectively and are showed in Figure c.4.

Moreover, Figure c.5 compares drying in the oven or by SP. The results of having particles with defined spherical structure for the SP method and aleatory aggregates for the oven drying method were expected.

4.1.6 Dynamic Light Scattering (DLS)

To obtain the particle size of each sample, the DLS technique was applied. However, this technique required a liquid sample instead of one in the solid state. As previously detected, the zeolite formed aggregates or agglomerates in solution and so the correct method to analyze the particle size had to be tested. The results are presented in Figure 4.4.

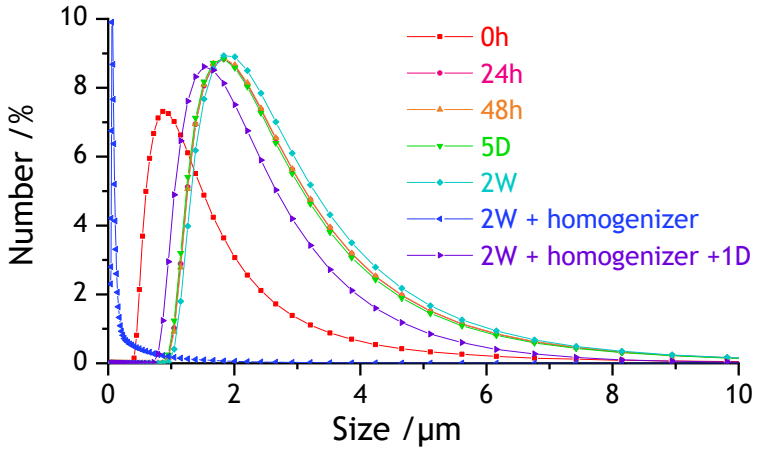

Figure 4.4. Study of aggregation by particle size distribution for template-free formulation, F_N_15_dil_Re150, for different times in solution and after homogenization.

The size measured immediate after NETmix mixture, did not show the real individual particle size but the size of aggregates of 0.9 µm. Additionally, the solution was stored and after 24 h, 48 h, 5 days and 2 weeks the same technique was applied. These tests showed that after 24 h in solution the sample created more aggregates or agglomerates, having a mean size of 1.8 µm. Afterwards that the mean size remained constant, meaning that it became stable in water in terms of size.

To verify that the sample created aggregates or agglomerates, after 2 weeks, the wet sample was homogenized, and the particle size acquired was 0.1 µm. This result shows that aggregates were formed and not agglomerates, meaning that the particle union was not definitive and could be reversed.

Also, it was tested if that separation with the homogenizer was definitive. The previous solution was analyzed after 24 h and the mean size obtained was 1.5 µm, indicating that aggregates were formed again, and the separation was also not definitive.

Because of the above conclusions the real particle sizes were evaluated by submitting the solution to a homogenizer. It was considered that all batch and NETmix assays were similar in

terms of particle size, and only one sample of each method was evaluated. The results are shown in Figure 4.5.

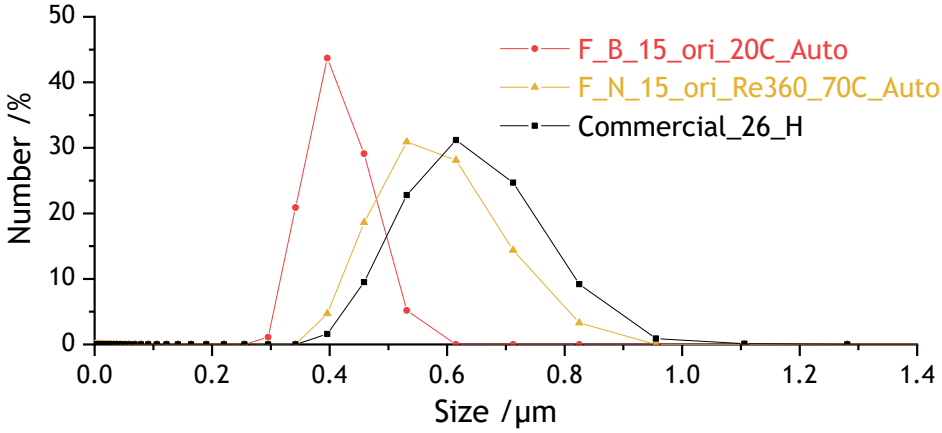

Figure 4.5. Particle size distribution for the commercial reference and for the produced calcinated samples by batch and NETmix with template-free formulation.

The commercial particles, in accordance with the high-resolution SEM, have a mean size between 0.4-1 µm. This indicates that the applied force was sufficient to separate the particles but not enough to crash them.

The particles produced with NETmix and the commercial reference had very similar size. Comparing with the high-resolution SEM images, these particles were different than the commercial, but because of the homogenizer they were probably separated and demonstrated to have the same size.

The batch particles presented a slightly lower particle than commercial and NETmix assays, 0.3-0.6 µm. This occurred in concordance with high-resolution SEM images as they appeared to be smaller but severely aggregated and with the homogenizer they were separated.

The size of the zeolite can vary in a large range due to different synthesis conditions. Nevertheless, the size obtained is within the literature ranges [78].

4.1.7 Nitrogen Isotherms

Nitrogen isotherms were obtained to determine the pore size. Figure 4.6 exhibits an example of the isotherm obtained for template-free formulation. All isotherms are shown in Figure c.6.

According to IUPAC the isotherm corresponds to type IV and hysteresis H4 since absorption and desorption curves did not overlap. All isotherms obtained had the same general behavior, which was expected as they are the same material. This characterization indicates capillary condensation taking place in the mesopores and the presence of aggregates, “assemblage of particles which are loosely coherent” [69], which was expected as visualized by the SEM and DLS techniques. This result is also observed by literature [68].

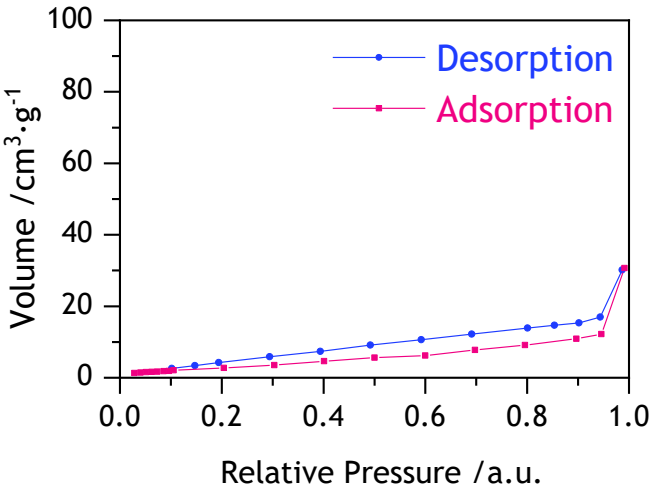

Figure 4.6. F_N_15_ori_Re360_70C_Auto isotherm for adsorption and desorption of nitrogen.

Table 4.3 presents the parameters S_{BET}, $S_{\neq micro}$, V_{pores_total} and V_{micro} of each calcinated sample, which are graphically presented in Figure c.7. The fractional area of micropores, ξ, is also shown, to classify the assays by their pores, based on Equation F.3 and Table F.1 [79].

Table 4.3. Values of S_{BET}, $S_{\neq micro}$, V_{pores_total}, V_{micro} and pore classification, ξ, for calcinated assays produced with template-free formulation and for the commercial reference.

Assay	S_{BET} /$m^2 \cdot g^{-1}$	$S_{\neq micro}$ /$m^2 \cdot g^{-1}$	V_{pores_total} /$cm^3 \cdot g^{-1}$	V_{micro} /$cm^3 \cdot g^{-1}$	ξ
Commercial_26_H	400	40	0.24	0.16	Microporous
F_B_15_ori_20C_Auto	3	3	0.02	0	Mesoporous
F_N_15_ori_Re360_70C_Auto	9	9	0.05	0	Mesoporous
F_N_15_ori_Re400_70C_Auto	26	26	0.08	0	Mesoporous

It was verified that in all template-free assays there were no micropores (S_{BET} equals to $S_{\neq micro}$ and V_{micro} is zero) and thus, the S_{BET} is significantly reduced. Nevertheless, it is noteworthy that NETmix assays had more pores than batch. Also, for the NETmix assay, higher Re_d leads to an increase of the total pore volume.

To summarize, the template-free formulation originates a maximum surface area of only 26 $m^2 \cdot g^{-1}$ and a total pore volume of 0.08 $cm^3 \cdot g^{-1}$, contrary to the commercial 400 $m^2 \cdot g^{-1}$ and 0.24 $cm^3 \cdot g^{-1}$, respectively.

The produced assays were all classified as mesoporous, which distances this formulation to the commercial reference even more.

4.1.8 X-ray Power Diffraction (XRD)

One of the most important characteristics in zeolites is the crystallinity. XRD patterns, of the two chosen assays, were obtained and are shown in Figure 4.7.

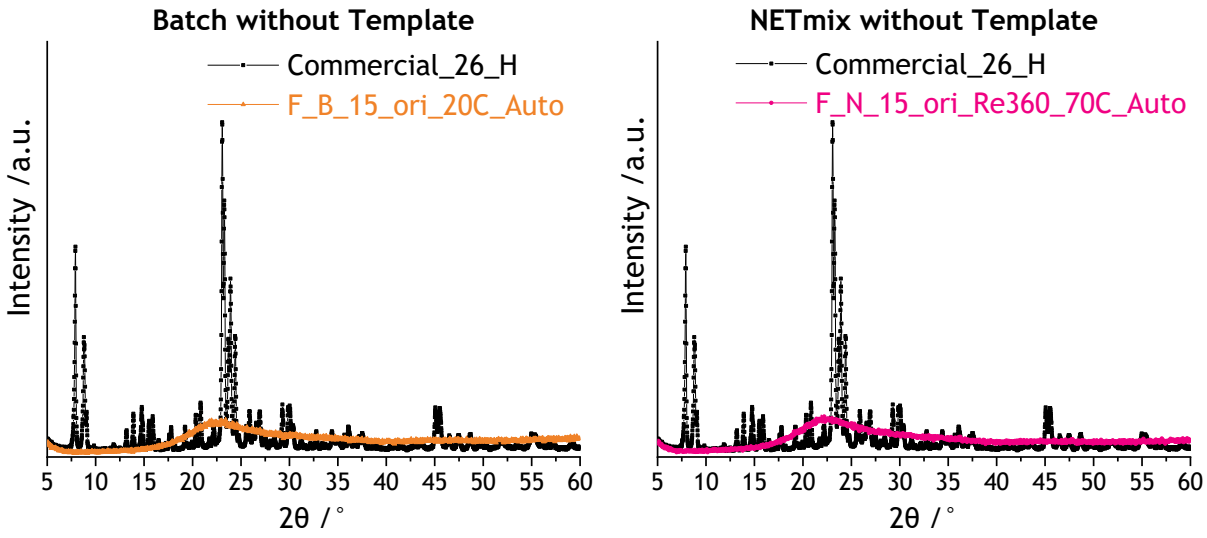

Figure 4.7. XRD patterns of assays produced with template-free formulations. On the left side with batch method and on the right side with NETmix.

Both samples do not presented any defined peak in XRD, meaning that both assays are defined as amorphous, compared to the 98 % crystallinity of the commercial reference. The crystallinity for template-free assays was 2 % and 4 % for batch and NETmix methods, respectively. Crystal sizes were not evaluated.

4.1.9 Ammonia Temperature Programmed Desorption (NH_3-TPD)

The acidic behavior of the produced zeolites was determined by NH_3-TPD.

NH_3 was chosen because it is a small molecule, that enables the access to all surface and all acid sites. Furthermore, NH_3 is a strong base which guarantees its adsorption even in weaker centers, allowing the construction of a good acidity scale based on the chemisorption energy [69].

The strong BAS concentration was also determined by analyzing the second peak of the NH_3-TPD spectra. This was decided to ensure that physisorbed NH_3 and weak acid sites, occurring at lower temperatures, were not being accounted for [69].

The NH_3 uptake from calcinated F_B_15_ori_20C_Auto and F_N_15_ori_Re360_70C_Auto samples at approximately 580 °C were 15.1 and 0.9 $\mu mol \cdot g^{-1}$, respectively, very low values when compared to the commercial reference, 162.2 $\mu mol \cdot g^{-1}$ at 460 °C. The respective spectra are shown in Figure 4.8.

These results show the poor BAS concentration in both template-free produced assays although at higher temperatures than commercial, indicating that the existing acid sites are stronger than in the commercial sample. Once again, the samples with these formulation type distances from the expected behavior of ZSM-5.

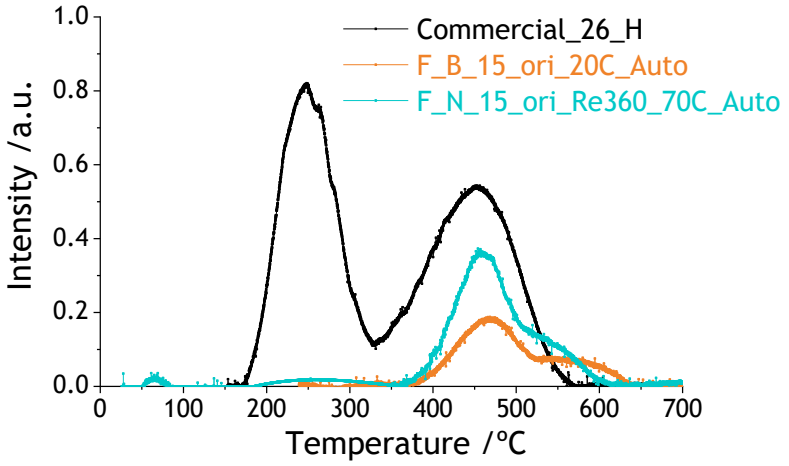

Figure 4.8. NH_3-TPD spectra obtained for template-free formulation assays and for the commercial reference.

4.1.10 Global Assessment

After considering the results obtained for template-free formulations, it was clear that ZSM-5 was not being produced, even with all the changes to the initial procedure. Note that the literature procedure was replicated except the use of a stirring autoclave. Due to these results, the formulation was changed, and a template was used to support the zeolite development. Nevertheless, the batch process was possible to be transferred to NETmix.

4.2 Zeolite Production with Template (T)

4.2.1 Production Mass Yield

For the procedures with template, as well as for template-free formulations, only the assays submitted to the autoclave were analyzed in terms of mass yield, as presented in Table 4.4.

In this case, the batch processes present a slightly higher yield than NETmix, 35.9 % for batch and 28.3, 33.1 and 31.4 % for NETmix with 13 s (3 passages through the NETmix), 2 or 10 min of mixing time.

Regarding the NETmix experiments, T_N_30_Auto and T_N_30_rep_Auto are replicas. Their similar yield confirms the procedure reproducibility. Also, decreasing the time in the autoclave decreases the zeolite mass yield, which is consistent with the crystals having less time to form.

It was also observed that increasing the mixing time (recirculation) increases the mass yield, from 28.3 to 33.1 %, which was expected since longer mixing time results in more particle encounters and consequently more interaction between them. Nevertheless, the 10 min recirculation assay presents a slightly lower mass yield than the 2 min recirculation assay.

And finally, different Si/Al ratios result in similar mass yields.

Table 4.4. Mass yield for assays with autoclave for template formulations.

Assays	Y /Mass %
T_B_30_Auto	35.9
T_N_30_Auto	28.3
T_N_30_rep_Auto	28.7
T_N_30_24hAuto	25.1
T_N_30_recir_Auto	33.1
T_N_30_10recir_Auto	31.4
T_N_60_recir_Auto	32.4
T_N_90_recir_Auto	32.3

In general, approximately 0.3 g of ZSM-5 are produced with 1 g of both Si and Al. The reasons detailed are similar from those for the template-free formulation, namely, losses within the processes.

4.2.2 Thermogravimetric Analysis (TGA)

To verify if the chosen calcination temperature was also applied for template formulations, two assays, one of batch and other of NETmix method, were submitted to TGA. Figure 4.9 presents the samples mass loss with the increase of temperature as well as it derivative to better analyze the curves for (a) T_B_30_Auto_Calc and (b) T_N_30_Auto_Calc assay, both after calcination step.

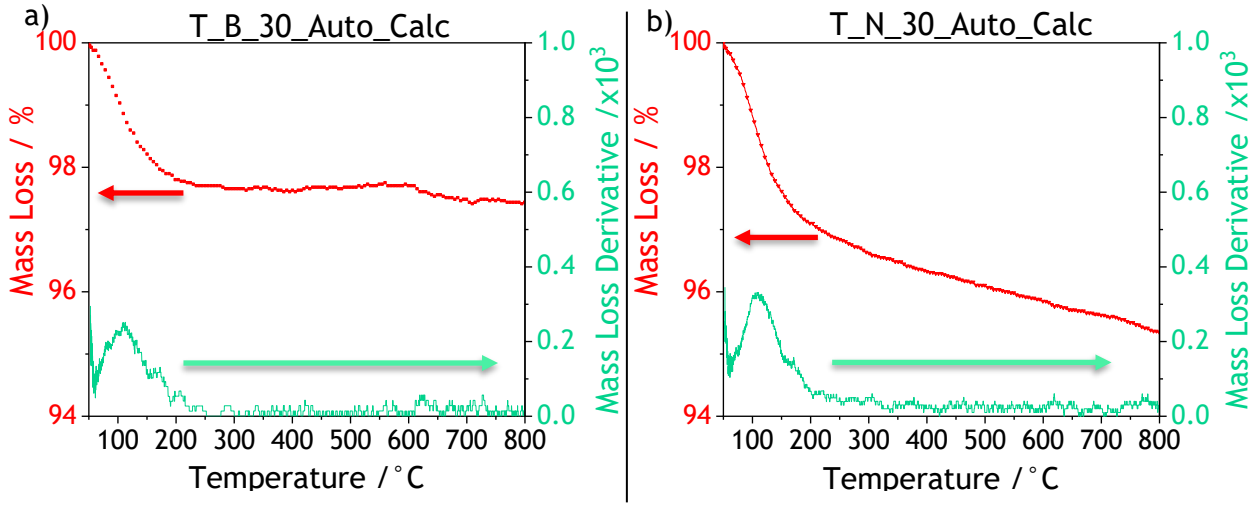

Figure 4.9. TGA curves for template assays. (a) T_B_30_Auto_Calc and (b) T_N_30_Auto_Calc.

Both samples showed, around 100 °C, in the same way as template-free assays, a considerable mass loss due to all adsorbed water. For 800 °C, the NETmix product had a total loss of 3 %, indicating a higher pore volume than batch product, which had a total loss of 2 %.

Additionally, both assays proved that the selected calcination temperature was sufficient to remove all extra compounds and that the produced material is thermal resistant.

The NETmix assay did not present a stable behavior after water evaporation, however, no additional peaks were observed, indicating that there was no further loss of mass. Nevertheless, this behavior does not compromise the material thermal resistant property since it represents less than 2 %. To confirm this result, this analysis should have been repeated, but due to equipment problems it was not possible.

4.2.3 Inductively Couple Plasma - Atomic Emission Spectroscopy (ICP-AES)

Table 4.5 presents the theoretical Si/Al ratio of the calcinated samples in the initial gel, foreseen by the formulation, the theoretical ratio in the final framework, foreseen by a correlation achieved by Kim, *et al.* [25] and the experimental ratio acquired at 2516 nm and 3092 nm for Si and Al, respectively. The corresponding correlation is presented in *Figure E.1* and Figure c.1 shows the two calibration curves.

Table 4.5. Experimental and theoretical Si/Al ratio, in the gel and in the framework, of samples produced with template and for the commercial reference.

Assay	Si/Al		
	Theoretical in the gel	Theoretical in the framework [25]	Experimental in the framework
Commercial_26_H	-	-	28
T_N_30_24hAuto	30	17	25

Due to equipment breakdown only one sample was tested (note that all others should be analyzed relatively to Si, Al and Co concentration).

Nevertheless, T_N_30_24h_Auto was analyzed and in the same way as template-free assay, the Si/Al ratio in the final framework was slightly less than the theoretical ratio in the gel, 25 and 30, respectively. The theoretical ratio in the framework was once again less than the actual ratio, allowing to thought if the correlation obtained by Kim, *et al.* [25] could be utilized in different production procedures.

For simplification, the assays continue to be labeled by their theoretical ratio in the gel and not by the real ratio in the framework. The commercial reference was evaluated to guarantee that both the digestion procedure and the calibration curves in the ICP-AES were correct.

4.2.4 Fourier Transform Infrared Spectroscopy (FTIR)

The FTIR spectra obtained from each calcinated final sample as well as the commercial sample with Si/Al ratio of 26 are presented in Figure 4.10, where the letters “a” to “e” represent the five characteristic peaks and are described in Section 4.1.4.

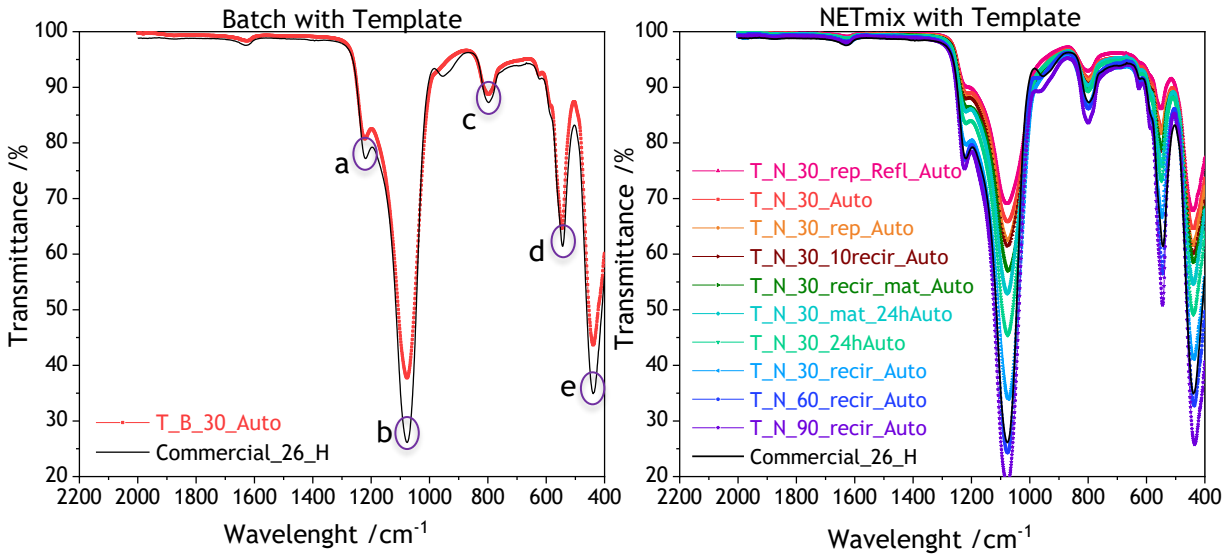

Figure 4.10. FTIR spectra obtained for calcinated assays with template formulations. On the left side the assays produced in batch and on the right the assays produced with NETmix.

It can be observed that all spectra present the zeolite's five characteristic bands, which indicates that the ZSM-5 was correctly formed by the formulation with template, contrary of template-free formulation.

In addition, the batch assay's peaks showed intensities very close to the commercial samples. Furthermore, for the NETmix assays, reflux and maturation steps decrease peak intensities (T_N_30_rep_Refl_Auto and T_N_30_recir_matu_Auto, respectively), opposite to what would be expected as these steps should increase bond strengths. On the contrary, less time in the autoclave and more mixing time favors the commercial behavior (T_N_30_24hAuto and T_N_30_recir_Auto, correspondingly). Nevertheless, the 10 min recirculation spectrum, T_N_30_10recir_Auto, is closer to the commercial's compared to T_N_30_Auto assay, without recirculation, but further distanced than T_N_30_recir_Auto, with 2 min recirculation. These results should be confirmed by XRD analysis.

However, reproducibility is apparently achieved as T_N_30_Auto and T_N_30_rep_Auto spectra are similar. Relatively to different Si/Al ratios, as it increases the peak's intensities also increases.

T_N_30_recir_Auto presents a very similar spectrum with T_B_30_auto, indicating that the 2 min mixture in NETmix is sufficient to form the same bonds intensities as 24 h mixture in batch.

Moreover, the peak intensities for higher Si/Al ratios were also higher. This result should be compared with the ICP-AES and XRD results as the Si/Al of 60 presented a spectrum more similar to the commercial reference.

In this case, all assays were further analyzed since in FTIR technique the most important criteria are the presence of all necessary peaks and not their intensities, which just gives an idea of the resemblance with the comparative reference. Also Figure c.3 presents a comparation between the reactants and the commercial sample.

4.2.5 Scanning Electron Microscopy (SEM) and Energy Dispersive Spectroscopy (EDS)

Figure 4.11 shows the SEM images obtained for the commercial reference and the two synthesis modes, batch and NETmix, after autoclave crystallization.

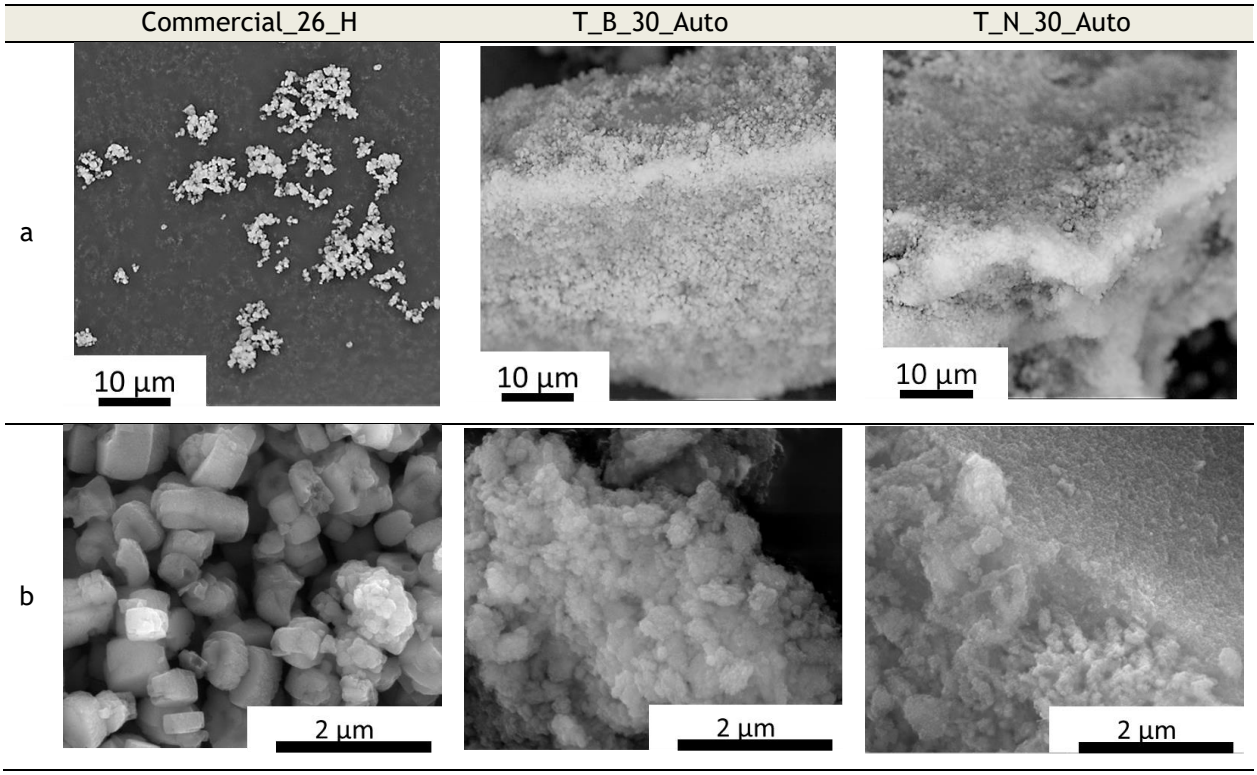

Figure 4.11. SEM images obtained for calcinated samples produced by formulation with template, for batch and NETmix assays, and for the commercial reference, where "a" corresponds to SEM images and "b" to the high-resolution SEM images.

Batch and NETmix samples showed a similar external structure with aggregates, while the commercial reference shows separated particles. High-resolution SEM shows a clear perspective of the individual particles structure of the commercial reference. Batch and NETmix products presented an external structure different from the commercial reference and also, the material produced by template-free formulation.

As mentioned above, a qualitative analysis of different elements present in the sample was done by EDS to know the ratio Si/Al in the material. Those results were Si/Al of 22 and 18 for T_B_30_Auto and T_N_30_Auto, respectively and are shown in Figure c.4.

4.2.6 Dynamic Light Scattering (DLS)

The formation of aggregates was analyzed immediately after by homogenizing the solid sample, T_N_30_mat_24hAuto_Calc, in water and after 3 h. The results are presented in Figure 4.12.

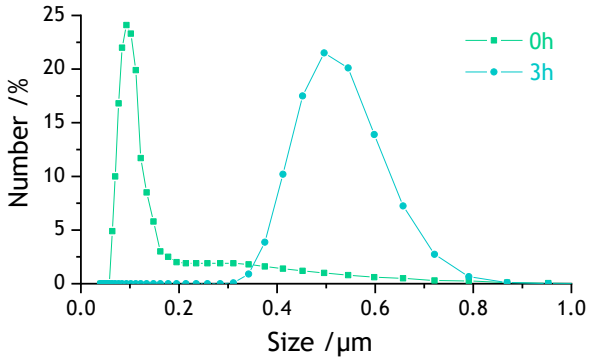

Figure 4.12. Study of aggregation by particle size distribution for formulation with template, T_N_30_mat_24hAuto_Calc, and NETmix for different times in solution.

Initially the mean particle size was around 0.1 µm, while after 3 h was approximately 0.5 µm, indicating that aggregation occurred, and the homogenizer should be used for particle size analysis.

Figure 4.13 shows the particle size distribution obtained for each sample. Once again, one of each method was evaluated, except for different procedures such as reflux and maturation.

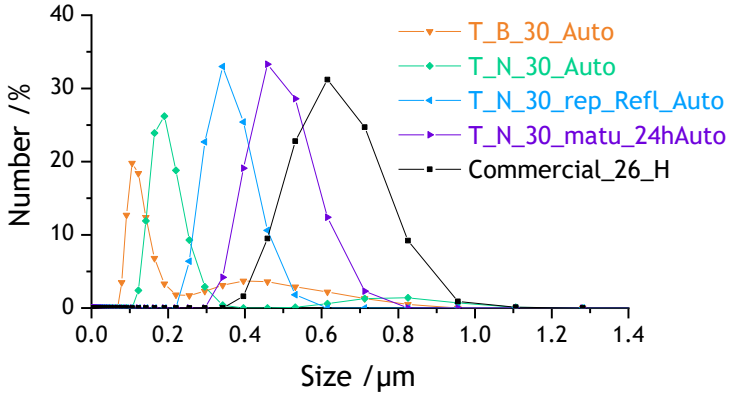

Figure 4.13. Particle size distribution for the commercial reference and for the produced calcinated samples by batch and NETmix with the template formulation.

In this formulation, all assays presented smaller particles than the commercial reference. Nevertheless, the sizes varied from 0.1-0.8 µm. Once again, the obtained size is within the literature range [78].

The batch assay presented the smaller particles, but it showed different size populations, around 0.1 and 0.4 µm, indicating that probably, in this case, the particles were crushed or that the time in the homogenizer was not sufficient. The NETmix assay, also presented two

populations, around 0.2 and 0.8 µm. These results indicate that the analyzes should be repeated with more time, but that would increase the solution temperature and affect the results.

Additionally, it was verified that reflux and maturation increase the particle size to 0.35 and 0.5 µm, respectively. Due to the additional time in these procedures, the result obtained was expected.

4.2.7 Nitrogen Isotherms

An example of the isotherm obtained for template formulations (T_N_30_Auto) is shown in Figure 4.14. All isotherms are presented in Figure c.8 to Figure c.10, divided by each pore classification type.

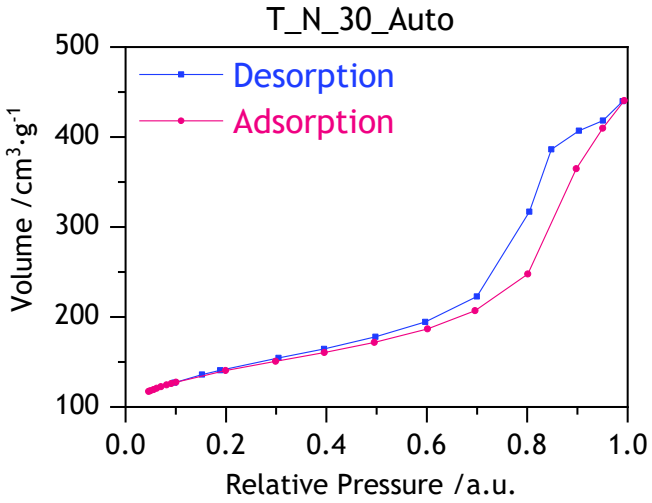

Figure 4.14. Example of an isotherm, for adsorption and desorption of nitrogen, obtained for template formulations: T_N_30_Auto.

According to IUPAC the isotherm corresponds to type IV and hysteresis H4. All isotherms obtained had the same general behavior, which was expected as they are the same material. This characterization indicates capillary condensation taking place in the mesopores and the presence of aggregates [69], which was expected as visualized in SEM and DLS. This result is verified by literature [68].

Table 4.6 presents the parameters S_{BET}, $S_{\neq micro}$, V_{pores_total} and V_{micro} of each calcinated sample, which are graphically shown in Figure c.11, and the corresponding pore classification, ξ.

It can be observed that all produced assays have higher S_{BET} and V_{pores_total} than the commercial sample. In general, NETmix assays presented higher S_{BET} and V_{pores_total} than batch assays, as previously identified in TGA (NETmix assay proved to have more adsorbed water than batch, suggesting more superficial area and pore volume). Both are very important parameters for further zeolite applications, for instance FTS.

Table 4.6. Values of S_{BET}, $S_{\neq micro}$, V_{pores_total}, V_{micro} and pore classification, ξ, for the produced calcinated assays and for the commercial reference.

Assays	S_{BET} /$m^2 \cdot g^{-1}$	$S_{\neq micro}$ /$m^2 \cdot g^{-1}$	V_{pores_total} /$cm^3 \cdot g^{-1}$	V_{micro} /$cm^3 \cdot g^{-1}$	ξ
Commercial_26_H	400	40	0.24	0.16	Microporous
Co/Re_Commercial_26_H	311	33	0.19	0.12	
T_B_30_Auto	469	121	0.44	0.15	MICRO-mesoporous
T_N_30_Auto	510	231	0.68	0.12	micro-mesoporous
Co/Re_T_N_30_Auto	389	194	0.51	0.09	
T_N_30_rep_Auto	511	233	0.67	0.12	micro-mesoporous
T_N_30_24hAuto	526	234	0.68	0.12	micro-mesoporous
T_N_30_rep_refl_Auto	593	336	0.84	0.10	micro-mesoporous
T_N_30_matu_24hAuto	524	307	0.66	0.09	micro-mesoporous
T_N_30_recir_Auto	467	145	0.44	0.14	MICRO-mesoporous
Co/Re_T_N_30_recir_Auto	377	123	0.38	0.11	
T_N_30_recir_mat_Auto	531	289	0.75	0.10	micro-mesoporous
T_N_60_recir_Auto	446	43	0.56	0.18	Microporous
T_N_90_recir_Auto	447	28	0.43	0.19	Microporous

It is important to highlight that the template formulation originates a surface area between 446 and 593 $m^2 \cdot g^{-1}$ and a total pore volume between 0.43 and 0.83 $cm^3 \cdot g^{-1}$, higher than the commercial 400 $m^2 \cdot g^{-1}$ and 0.24 $cm^3 \cdot g^{-1}$, respectively.

Moreover, reproducibility is achieved since all four parameters are similar for T_N_30_Auto and T_N_30_rep_Auto. Additionally, T_N_30_Rep_refl_Auto obtained the higher S_{BET}, $S_{\neq micro}$ and V_{pores_total} values, indicating that more pores were created but with larger sizes (non-microporous), which is expected due to the different crystallization method (with longer time).

Regarding the autoclaving time, the assay with only 24 h in the crystallization step, T_N_30_24hAuto, provided a slightly bigger S_{BET}, 526 $m^2 \cdot g^{-1}$, indicating the formation of more micropores than the one with 42 h, T_N_30_Auto, 510 $m^2 \cdot g^{-1}$.

Furthermore, the recirculation origins lower S_{BET}, $S_{\neq micro}$ and V_{pores_total} but higher V_{micro}, implying the presence of more heterogenous micropores in T_N_30_recir_Auto compared to T_N_30_Auto. Assay T_N_30_10recir_Auto should be analyzed to confirm the expected increase of micropores.

Additionally, maturation results in higher S_{BET} and $S_{\neq micro}$, indicating that it promotes the formation of non-micropores instead of micropores (T_N_30_matu_24hAuto and T_N_30_recir_matu_Auto).

Analyzing the different Si/Al ratios, it can be observed that, for higher ratios, $S_{\neq micro}$ decreases and V_{micro} increases, implying that the number of micropores increases. However, for V_{pores_total}, the effect of higher ratios was not clear, since for Si/Al=60 the V_{pores_total} is higher than the others.

Finally, it is observed, as expected, that the assays with impregnated metals have less S_{BET}, $S_{\neq micro}$, V_{pores_total} and V_{micro} compared to the original assay as expected, since Co and Re occupied several pores.

In general, all assays are characterized by micropores and mesopores, except for higher Si/Al ratios (60 and 90) and commercial reference, which are characterized by being microporous. Nevertheless, T_B_30_Auto and T_N_30_recir_Auto have dominant microporosity. Those results are in accordance with the previous discussion.

4.2.8 X-ray Power Diffraction (XRD)

The XRD patterns obtained for batch and the most relevant NETmix's assays are presented in Figure 4.15.

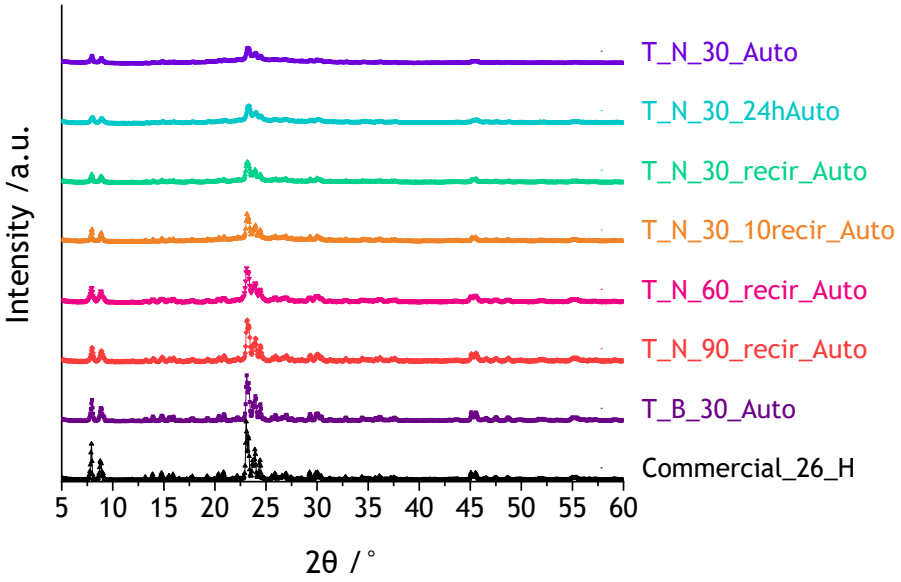

Figure 4.15. XRD patterns of assays produced with template formulations.

For all formulations using a template, the XRD patterns obtained have all the peaks of commercial sample, indicating the correct molecular arrangement leading to reflected X-rays in each right angle [80]. The difference between assays is observed by the peak's intensities, which arise from different crystallinity percentages.

The results show the proximity between the batch and the commercial reference patterns, indicating the correct molecular arrangement and crystallinity higher than 33 %. For NETmix assays, a higher Si/Al ratio and longer recirculation time result in higher crystallinity. It was 33 %, 63 % and 70 % for NETmix products with 0, 2 and 10 min of recirculation (T_N_30_Auto, T_N_30_recir_Auto and T_N_30_10recir_Auto), respectively. The 10 min recirculation assay, T_N_30_10recir_Auto, is more crystalline but provided a smaller mass yield than the 2 min recirculation assay, T_N_30_recir_Auto (yield 31.4 % and 33.1 %, respectively). Table 4.7 shows the percentage of crystallinity, Equation G.2, and the crystal size, Equation G.1.

Table 4.7. Crystallinity (C), in %, and crystal size (L), in nm, values for calcinated assays produced with template formulations.

Assay	C / %	L /nm
Commercial_26_H	98	69.9
T_B_30_Auto	93	39.2
T_N_30_Auto	33	34.0
T_N_30_24hAuto	35	26.9
T_N_30_recir_Auto	63	29.0
T_N_30_10recir_Auto	70	40.0
T_N_60_recir_Auto	79	33.4
T_N_90_recir_Auto	76	47.1

The order of assays according to their crystallinity is the following: Commercial_26 (98 %) > T_B_30Auto (93 %) > T_N_60_recir_Auto (79 %) > T_N_90_recir_Auto (76 %) > T_N_30_10recir_Auto (70 %) > T_N_30_recir_Auto (63 %) > T_N_30_24hAuto (35 %) > T_N_30_Auto (33 %).

The assay produced in batch presents a slightly lower crystallinity than the commercial reference, 93 % and 98 %, respectively, due to the non-optimization of the synthesis parameters (not the focus of this work). The NETmix products have a lower crystallinity, which may be attributed to the lower residence time in NETmix of 13 s (without recirculation), while the process in the batch had 24 h for the initial gel. The best result for NETmix assay for a Si/Al of 30 was considering 10 min of recirculation achieved a 70 % of crystallinity which is 1.11 times higher compared with recirculation of 2 min (T_N_30_recir_Auto) and 2.12 times higher without recirculation (T_N_30_Auto).

Additionally, it was observed that more recirculation time also promoted this parameter. This is expected as higher residence time in the NETmix favors mixture. However, there is an optimum since for higher recirculation time, 10 min, the FTIR peaks intensity and yield decreases.

Regarding the crystallization time, the assay with only 24 h in the autoclave has higher crystallinity than the one with 42 h, concluding that all experiments should have been performed with that crystallization time and that the 42 h postponed the optimal time for this step.

The increase of the Si/Al ratio promoted the increase of crystallinity, which may have occurred due to the higher concentration of Si in the initial gel, leading to more nucleation sites.

This difference in crystallinity between the produced samples and the commercial reference could be one reason for the obtained SEM images.

On the other hand, about the crystal size, the correct order is the following: Commercial_26 > T_N_90_recir_Auto > T_N_30_10recir_Auto > T_B_30Auto > T_N_30_Auto > T_N_60_recir_Auto

> T_N_30_recir_Auto > T_N_30_24hAuto. Note that for assays with lower crystallinity, T_N_30_24hAuto and T_N_30_Auto the error linked to the crystal size calculation increased.

While the commercial reference presented a crystal size of 69.9 nm, the batch assay presented a crystal size of 39.2 nm and the NETmix assays a crystal size of 26.9-47.1 nm. All produced assays formed smaller crystals than the commercial reference.

For the NETmix assays, it was perceptible that higher recirculation and crystallization time promote larger crystals' formation, which may also be the justification for the larger commercial particles.

4.2.9 Ammonia Temperature Programmed Desorption (NH_3-TPD)

The NH_3 uptake from calcinated samples and its respective second peak temperature are presented in Table 4.8 and Figure 4.16 shows the corresponding spectra.

Table 4.8. NH_3 uptake, U_{NH_3}, values from calcinated assays with template and for the commercial reference, as well as the respective second peak temperature.

Assay	U_{NH_3} /μmol·g^{-1}	Second Peak Temperature /°C
Commercial_26_H	162.2	460
T_B_30_Auto	184.5	436
T_N_30_Auto	5.9	438
T_N_30_recir_Auto	182.6	428
T_N_30_recir_Auto_H	108.4	426

The assays were ordered by their NH_3 uptake as following: T_B_30_Auto > T_N_30_recir_Auto > Commercial_26 > T_N_30_recir_Auto_H > T_N_30_Auto.

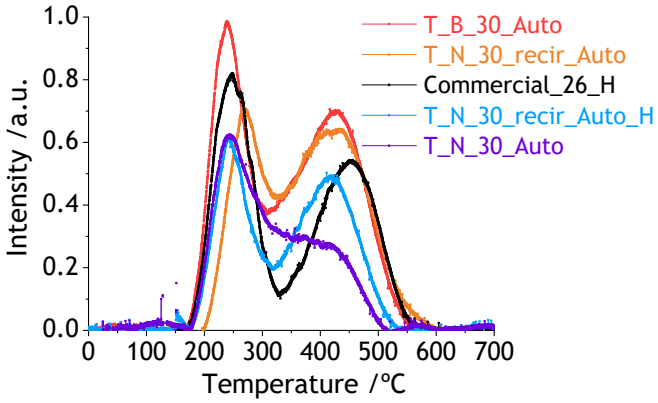

Figure 4.16. NH_3-TPD spectra for assays with template and for the commercial reference.

Both T_N_30_Auto and T_N_30_recir_Auto_H results were not expected and should be repeated. The first should be repeated before any conclusion, as it should have more acid sites as the remaining assays. The second should have obtained an NH_3 uptake greater than the same sample before protonation (T_N_30_recir_Auto), as protonation was performed to produce more acid sites specifically to improve FTS. Nevertheless, as it was a very reactive local, it should have been more carefully manipulated and protected.

Additionally, both T_B_30_Auto and T_N_30_recir_Auto assays presented bigger NH_3 uptake and, consequently, more acid sites than the commercial reference, 184.5 and 182.6 $\mu mol \cdot g^{-1}$, respectively. That is probably justified by the total pore volume and the superficial area being bigger in the produced assays compared to the commercial reference.

Since the peaks' temperatures differ only between 426-438 °C, all samples had BAS with the same strength.

This was an important study to perform as the literature suggests a dependency between rates of isomerization and hydrocracking in the FTS with BAS concentration [41].

4.2.10 Hydrogen Temperature Programmed Reduction (H_2-TPR)

H_2-TPR identify the reduction temperature for FTS. Figure 4.17 presents the obtained results.

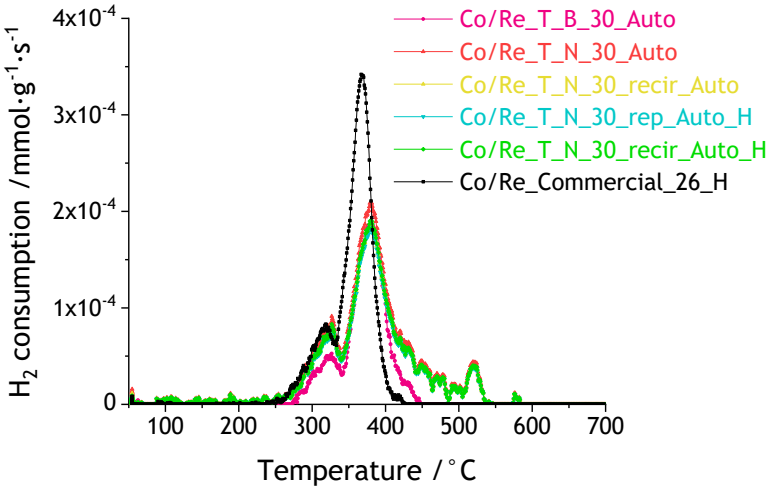

Figure 4.17. TPR spectra for impregnated samples.

All spectra presented two main peaks. The first, around 320 °C, is attributed to the two-step reduction of Co_3O_4 to Co°. The second peak refers to the reduction of Co while interacting with the support, which explains the overlapping curves for the NETmix assays [41].

The commercial sample presents a maximum H_2 consumption at 370 °C while the produced sample is around 380 °C. This indicates a weaker interaction between support and metals in the commercial reference as it reduced itself faster, at lower temperatures.

Additionally, the produced assays presented a slight "tail" in the chart end which could be justified by the heterogeneity of pores and because of that the different interactions forces between support and metals.

The reduction temperature chosen was 400 °C to guarantee that all FTS were executed under same conditions, that all inactive cobalt oxide is reduced to active metallic cobalt and that it is the minimum temperature to reduce the energetic expenses and to avoid nanoparticles sintering. Note that for batch and NETmix assays, at 400 °C, there was still inactive cobalt (H_2

consumption was higher than zero). However, in FTS the reduction step takes 10 h, which was sufficient to activate all cobalt particles.

4.2.11 Global Assessment

Contrary to template-free formulations, this formulation, with template, originated ZSM-5 with characteristics very similar to the commercial sample. Although it presented less crystallinity than commercial, it exhibits a smaller crystal size, had more superficial area and more acidic sites.

4.3 Fischer-Tropsch Synthesis (FTS)

The FTS was executed to compare the performance of zeolites as a support in a bifunctional catalyst. Only commercial, batch and the NETmix most promising samples (T_N_30_Auto, T_N_30_recir_Auto and T_N_30_recir_Auto_H) were tested due to equipment availability. These samples were previously impregnated with 15 % Co and 0.75 % Re, in mass.

Table 4.9 presents the theoretical mass loaded of each metal, in the impregnation method, and the results obtained for F_{CTY}, X_{CO} and the products weight for each tested assay. The values of cobalt and rhenium loading, y_{Co} and y_{Re} , in %, were estimated by their weight in IWI. ICP analysis results were not possible to obtain before the due time of this dissertation, and the conclusions presented below are preliminary. By-products were not analyzed since they were presented in the water phase, and there was no equipment available to quantify it.

Table 4.9. Values of the loaded mass of each metal, in the impregnation method, % in mass, and the results obtained for CTY*, in 10^5 $mol_{CO}{\cdot}g_{Co}^{-1}{\cdot}s^{-1}$, the X_{CO}, in %, and the products weight for each tested assay.*

Assay	Mass Loaded /Mass %		F_{CTY} /10^5 $mol_{CO}{\cdot}g_{Co}^{-1}{\cdot}s^{-1}$	X_{CO} / %	Products Weight /g		
	y_{Co}	y_{Re}			Wax	water	Organic
T_B_30_Auto	0	0	0	0	0	0	0
Co/Re_Commercial_26_H	15.0	0.8	6	27	0.1	4.8	1.1
Co/Re_T_B_30_Auto	15.1	1.0	10	50	0.6	9.2	2.1
Co/Re_T_N_30_Auto	15.0	0.9	13	65	1.2	6.8	3.0
Co/Re_T_N_30_recir_Auto	14.8	0.6	11	54	0.4	7.0	1.9
Co/Re_T_N_30_recir_Auto_H	14.9	1.1	13	65	1.8	5.9	2.3

One first experiment was performed with zeolite without metals to understand whether it had catalytic activity. The presented results showed that, as expected, it did not have catalytic activity, as the catalyst for this reaction is Co. Then, experiments with the produced assays and the commercial reference were executed.

Although y_{Re} are slightly different for each assay, due to the difficult measurement (very small amount), it does not present a large impact on the results as it influences, mainly, the reduction temperature, which was obtained after impregnation and all assays presented the same result.

Regarding F_{CTY} and X_{CO}, all produced assays presented better results when compared to the commercial sample, where Co/Re_T_N_30_recir_Auto_H and Co/Re_T_N_30_Auto presented the best results, suggesting that they are better for this reaction. Nonetheless, products distribution should be analyzed.

In all conducted assays, the predominant products formed were in the order of water phase, followed by the organic phase and then waxes, aligning with expectations. The quantities of each product varied depending on the specific experiment. Co/Re_T_N_30_Auto and Co/Re_T_N_30_recir_Auto_H were the assays with more waxes formed, which is in accordance with TPD results as less BAS concentration corresponds to more waxes formed, since there was poor hydrocracking. In this parameter, the commercial sample was better as it produced less waxes. Co/Re_T_B_30_Auto and Co/Re_T_N_30_Auto formed more water and organic phase, respectively, than the rest. Since the important products for gasoline production are in the organic phase, this was a good result as the produced zeolites delivered more than the commercial reference.

Table 4.10 presents the molar selectivity values obtained for each tested assay, regarding the different carbon length chains and the different structures.

Table 4.10. Molar selectivity values, in %, for the different carbon length chain and for the different structures, obtained for each tested assay.

Assay	Molar Selectivity / %								
	CO_2	CH_4	$C_{2\text{-}4}$	$C_{5\text{-}11}$	$C_{12\text{-}20}$	C_{21}^{+}	Iso-Paraffins	Olefins	Paraffins
T_B_30_Auto	0	0	0	0	0	0	0	0	0
Co/Re_Commercial_26_H	<1	10	2	65	22	<1	15	23	62
Co/Re_T_B_30_Auto	<1	18	6	65	11	<1	13	20	67
Co/Re_T_N_30_Auto	<1	17	6	63	12	1	7	16	77
Co/Re_T_N_30_recir_Auto	<1	19	5	59	14	2	7	19	74
Co/Re_T_N_30_recir_Auto_H	1	21	2	66	9	<1	10	13	77

All assays produced more gasoline followed by diesel and methane, next LPG and CO2 in lower quantity. The Co/Re_T_N_30_recir_Auto_H assay produces the most CO_2 and CH_4, although for CH_4 all produced assays presented similar results, which are bigger than with commercial sample.

Hydrocarbon chain lengths between 2 and 4 are produced in lowers quantities, mainly for Co/Re_T_N_30_recir_Auto_H and commercial reference. Also, for bigger chain length, more than 12 carbons, commercial sample is the one which produces more, indicating lower hydrocracking activity. This result is in concordance with TPD results as commercial presented, in general, less active sites.

The most important chain lengths are between 5 and 11 carbons as it corresponds to gasoline. All assays presented similar results, but because Co/Re_T_N_30_recir_Auto_H and Co/Re_T_N_30_Auto presented bigger F_{CTY} they produce more quantity of gasoline.

Furthermore, the structure is also an important characteristic to be evaluated. As expected, the products were mainly paraffins, followed by olefins and iso-paraffins. However, iso-paraffins are preferable as they improve gasoline properties. In total the commercial reference produces more iso-paraffins and olefins percentage than the rest of the tested assays. On the other hand, Co/Re_T_N_30_recir_Auto_H is the assay which produces fewer olefins and an intermediate amount of iso-paraffins but more paraffins.

Nevertheless, the iso-paraffins should be analyzed for C_5-C_{11} as it corresponds to gasoline. Figure 4.18 represents an example of the product distribution for Co/Re_T_N_30_recir_Auto_H assay to illustrate the numerical results and to attribute the different structures in the different carbon chain length. Figure c.12 presents the product distribution for all assays.

For this assay, 78 % of iso-paraffins are presented in gasoline, while for Co/Re_Commercial_26_H, Co/Re_T_B_30_Auto, Co/Re_T_N_30_Auto and Co/Re_T_N_30_recir_Auto assays the iso-paraffins presented in gasoline corresponds to 64 %, 82 %, 67 % and 51 %, respectively.

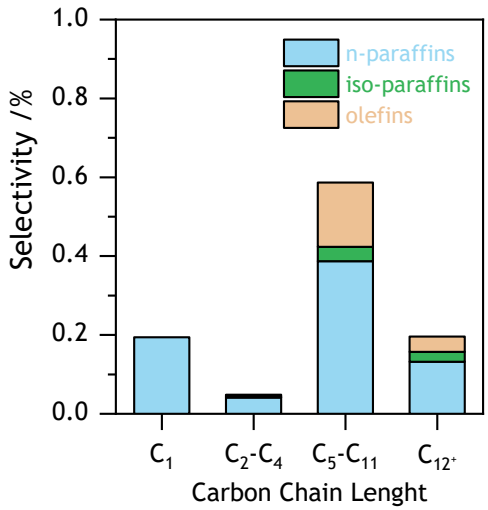

Figure 4.18. Products distribution for the different carbon length chain and for the different structures, obtained for Co/Re_T_N_30_recir_Auto_H assay.

To conclude, Co/Re_T_N_30_recir_Auto_H was probably the best catalyst for FTS as it generates more gasoline with better properties compared to the commercial reference and other catalysts produced.

5 Conclusions

This dissertation was conducted to evaluate a faster route to synthesize the zeolite ZSM-5 using a reactor with efficient mixing, NETmix. These zeolites are usually produced in batch processes which require several hours/days. The NETmix technology was used to reduce the mixture time of the initial gel from hours to seconds or a few minutes.

ZSM-5 was produced with different formulations (template-free and with template) and different Si/Al ratios. Afterwards, the products were physically and chemically characterized by different techniques and the zeolite was tested as a support for the Fischer-Tropsch synthesis. All objectives were achieved, and the main conclusions of this work are presented below.

Regarding the template-free formulation, it was possible to transpose the batch process to NETmix. However, in both cases, FTIR spectra did not present all characteristic peaks, and XRD showed an amorphous material. In addition, the total surface area and the total pore volume were negligible, and the particles were considered mesoporous, in opposition to the commercial sample with higher values of superficial area and pore volume and being microporous. By the NH_3-TPD technique, the produced material presented a low BAS concentration opposite to the commercial reference.

For template formulations, the results were more promising. It was verified that 0.3 g of ZSM-5 could be produced with 1 g of Si and Al.

TGA technique allowed to verify that the chosen calcination temperature, 550 °C for 6 h, was sufficient to remove all extra compounds in the framework and to prove the thermal stability of the produced zeolites above 500 °C.

The real Si/Al content was analyzed for one assay, T_N_30_24hAuto, and the framework content was slightly lower than in the initial gel, 25 and 30, respectively. FTIR spectra presented all five expected peaks and with similar intensities. The evaluation with SEM and high-resolution SEM were not conclusive as the particles were aggregated, and the external delimitation was not clearly visible.

For the particles produced in the solution, they aggregate until 24 h, however, it was possible to separate them using a homogenizer. According to the DLS results, the mean particle size of the produced material was between 0.1 and 0.8 µm, while the commercial sample has a slightly lower size, between 0.4 and 1 µm.

The produced product using NETmix corresponded to particles with a higher surface area and total pore volume, followed by the batch assay and commercial reference. The produced

products presented micropores and mesopores, corresponded to particles with a higher surface area and total pore volume, since 446 to 593 $m^2 \cdot g^{-1}$ and 0.43 to 0.84 $cm^3 \cdot g^{-1}$, compared to the commercial 400 $m^2 \cdot g^{-1}$ and 0.24 $cm^3 \cdot g^{-1}$, respectively.

The XRD patterns showed a 70 % crystallinity for NETmix assay with 10 min recirculation. In contrast, 93 % for batch with 24 h and the commercial reference has 98 % of crystallinity. Although the NETmix presented a lower value than batch and the commercial, it is expected that by increasing the recirculation time and optimizing the synthesis conditions, higher values could be reached. It was observed that higher recirculation time in the NETmix favored crystallinity: crystallinity values of 33, 63 and 70 % were obtained for 13 s, 2 and 10 min of recirculation. Also, the crystal size obtained for the produced zeolites was lower than for the commercial sample, between 27 and 47 nm and 69.9 nm, respectively. It was verified that more mixing and crystallization time favored crystals growth.

The reproducibility of the process and the final product was verified by the nitrogen isotherms and the production yield.

Furthermore, the assays produced with NETmix presented more acid sites, comparing the 183 $\mu mol \cdot g^{-1}$ NH_3 uptake to the 162 $\mu mol \cdot g^{-1}$ from the commercial reference, an important parameter for FTS.

TPR technique was employed to choose the catalyst reduction temperature, 400 °C. The produced material presented higher interaction between the zeolite and metals than the commercial reference.

Considering the FTS, the best support was the protonated assay produced with NETmix, when compared to others produced with NETmix and batch and with the commercial reference, as it produces more gasoline and better properties (iso-paraffins). This assay presented a F_{CTY} and a CO conversion of $13x10^5$ $mol_{CO} \cdot g_{Co}^{-1} \cdot s^{-1}$ and 65 %, respectively. However, these results were just preliminary until the metals' percentage is verified.

To summarize, NETmix proved to be an effective technology to reduce the mixing time in the ZSM-5 synthesis. More studies should be applied but in general, the NETmix assays produce zeolites with better characteristics than the commercial reference but a shorter time in the production of the initial gel is required.

This work demonstrated the potential application of the NETmix technology in industrial ZSM-5 synthesis.

6 Assessment of the Work Done

6.1 Objectives Achieved

This dissertation's main objective consisted of synthesizing zeolite ZSM-5 using NETmix. In order to achieve this objective, assays were carried out in batch mode to reproduce the literature and then the process transposed to semi-continuous mode (NETmix).

The template-free formulation presented environmental advantages. However, the results were unexpected for the different formulations (Si/Al ratios) and procedure conditions (concentration, reaction temperature, crystallization method and time).

To overcome these difficulties, the formulation was changed to one using template to facilitate the correct crystallization process. In the same way, batch assay was firstly analyzed and after presented good results, the NETmix assays were conducted with different formulation (Si/Al ratios) and procedure conditions (Re_d, crystallization method and time).

Postponed, the assays were analyzed regarding physical and chemical characterization: TGA for thermal stability, ICP-AES for chemical composition, FTIR for chemical bounds, SEM for morphology, EDS for qualitative chemical composition, DLS for particle sizes, nitrogen isotherms for porosity and superficial area, XRD for structure, crystallinity and crystal size, NH_3-TPD for acidity and H_2-TPR) for catalyst reduction temperature.

Finally, ZSM-5 was tested as a support for the FTS, where commercial, batch and NETmix assays were compared. NETmix products were very promising.

It is important to highlight that both the topic, zeolites, as several characterization techniques were executed for the first time in the research group where this thesis was developed. Consequently, this thesis holds significance as it initiates a new avenue of research.

6.2 Limitations

Considering that crystallinity is a crucial characteristic in zeolites, it should have been prioritized as the initial assessment for all experiments. However, due to the unavailability of XRD equipment on-site and limited access only at UTAD, the analysis became expensive and time-consuming, taking several weeks to receive the results. Consequently, not all samples could be evaluated, and decisions had to be made without a comprehensive understanding of this vital parameter.

Moreover, even though literature procedure was followed for template-free formulation assays, the zeolite was never achieved. It could be due to not using a stirred autoclave (equipment not available) or due to information omission in papers.

Besides that, some equipment presented issues, resulting in delays in the progress of the work. Nevertheless, such occurrences were out of the author's control and are to be expected in research endeavors.

6.3 Future Work

In the Discussion Section, it was acknowledged that certain analyses should have been repeated. However, due to time constraints and limitations with the available equipment it was not possible: repeat the synthesis of the zeolite with template and using NETmix with more recirculation time and of the T_N_30_10recir_Auto assay; repeat the TGA analysis of T_N_30_Auto_Calc assay, the NH_3-TPD analysis for T_N_30_Auto and for T_N_30_recir_Auto_H assays and the FTIR analysis for T_N_30_10recir_Auto assay; perform the XRD and ICP-AES analysis for the remaining assays, regarding to Si, Al and Co concentrations and the nitrogen isotherm analysis for the T_N_30_10recir_Auto assay.

Furthermore, a parametric study could be conducted on the template formulation with NETmix assays, by optimizing, mainly, the following parameters: ratios, pH, temperature and time of mixture and crystallization.

Finally, to better improve the time consumed in ZSM-5 synthesis, a continuous system could be studied. This idea consists of the reactants entering the NETmix at high temperatures, while this is heated by water at 300 ºC as verified by Liu, *et al.* [20]. The resulting formed zeolite would exit the NETmix in its finalized state. Subsequently, it would undergo thesteps of washing, drying, and calcination. For that the current materials needed to be changed for ones with more pressure and temperature resistance. This involved substituting the pipes, incorporating pressure valves, and potentially increasing the depth of chambers and channels in the NETmix to prevent the slurry from clogging. This idea was not studied in this dissertation as it would require a large investment and could only be justified after completing the study of this dissertation.

7 References

[1] M. N. Moshoeshoe, M. S. Nadiye-Tabbiruka, and V. C. Obuseng, "A Review of the Chemistry, Structure, Properties and Applications of Zeolites", *American Journal of Materials Science,* vol. 7, no. 5, pp. 196-221, 2017, doi: 10.5923/j.materials.20170705.12.

[2] T. Derbe, S. Temesgen, and M. Bitew, "A Short Review on Synthesis, Characterization, and Applications of Zeolites", *Advances in Materials Science and Engineering,* vol. 2021, p. 17, 2021, doi: 10.1155/2021/6637898.

[3] E. M. Flanigen, R. W. Broach, and S. T. Wilson, *Zeolites in Industrial Separation and Catalysis*: Wiley-VCH, 2010, p. 618, ISBN: 978-3-527-32505-4.

[4] S. M. Alipour, R. Halladj, and S. Askari, "Effects of the different synthetic parameters on the crystallinity and crystal size of nanosized ZSM-5 zeolite", vol. 30, no. 3, pp. 289-322, 2014, doi: 10.1515/revce-2014-0008.

[5] C. Brechignac, P. Houdy, and M. Lahmani, *Nanomaterials and Nanochemistry*, 2008, ISBN: 978-3-540-72992-1.

[6] P. Jacobs and J. Martens, *Synthesis of High-Silica Aluminosilicate Zeolites* (Studies in Surface Science and Catalysis): Elsevier, 1987, p. 407, ISBN: 0-444-42814-3.

[7] D. O. Shestakova, K. A. Sashkina, and E. V. Parkhomchuk, "Template-Free Synthesis of Hierarchical Zeolite ZSM-5", *Petroleum Chemistry,* vol. 59, no. 8, pp. 838-844, 2019, doi: 10.1134/S0965544119080188.

[8] K. Motazedi, "Template-free synthesis and modification of LTY, ZSM-5 and LTL zeolite catalysts and investigation of the catalytic pyrolysis of Saskatchewan boundary dam coal", Master of Science, Chemical and Petroleum Engineering, University of Calgary, Faculty of Graduate Studies, 2013.

[9] "Zeolite Market Size, Share & Trends Analysis Report By Application (Catalyst, Adsorbent, Detergent Builder), By Product (Natural, Synthetic), By Region (North America, Europe, APAC, CSA, MEA), And Segment Forecasts, 2022 - 2030". Grand View Research. https://www.grandviewresearch.com/industry-analysis/zeolites-market (accessed May 2023).

[10] T. S. Frantz, "Síntese e Caracterização de Zeólitas do Tipo ZSM-5 para a Adsorção de CO2", Mestrado em Engenharia Química, Escola de Química e Alimentos, Universidade Federal do Rio Grande, 2015.

[11] ACS. "ZSM-5 - Zeolite Socony Mobil–5". ACS Material. https://www.acsmaterial.com/blog-detail/zsm-5-molecular-seive.html (accessed January 2023).

[12] A. Braga and N. Morgon, "Descrições estruturais cristalinas de zeólitos", *Quimica Nova,* vol. 30, 2007, doi: 10.1590/S0100-40422007000100030.

[13] J. Li, "Continuous Flow Hydrothermal Synthesis of ZSM-5 Zeolite", Master of Science in Chemical Engineering, Graduate Faculty of the Swanson School of Engineering, University of Pittsburgh, 2022.

[14] J. Weitkamp, "Zeolites and catalysis", *Solid State Ionics,* vol. 131, no. 1, pp. 175-188, 2000, doi: 10.1016/S0167-2738(00)00632-9.

[15] M. H. Nada, E. G. Gillan, and S. C. Larsen, "Mechanochemical reaction pathways in solvent-free synthesis of ZSM-5", *Microporous and Mesoporous Materials,* vol. 276, pp. 23-28, 2019, doi: 10.1016/j.micromeso.2018.09.009.

[16] D. H. Olson, W. O. Haag, and R. M. Lago, "Chemical and physical properties of the ZSM-5 substitutional series", *Journal of Catalysis,* vol. 61, no. 2, pp. 390-396, 1980, doi: 10.1016/0021-9517(80)90386-3.

[17] T. C. Hoff, R. Thilakaratne, D. W. Gardner, R. C. Brown, and J. P. Tessonnier, "Thermal Stability of Aluminum-Rich ZSM-5 Zeolites and Consequences on Aromatization Reactions", *The Journal of Physical Chemistry C,* vol. 120, no. 36, 2016, doi: 10.1021/acs.jpcc.6b04671.

[18] "Nucleation". Encyclopaedia Britannica. https://www.britannica.com/science/nucleation (accessed March 2023).

[19] C. S. Cundy and P. A. Cox, "The hydrothermal synthesis of zeolites: Precursors, intermediates and reaction mechanism", *Microporous and Mesoporous Materials,* vol. 82, no. 1, pp. 1-78, 2005, doi: 10.1016/j.micromeso.2005.02.016.

[20] Z. Liu, K. Okabe, C. Anand, Y. Yonezawa, J. Zhu, H. Yamada, A. Endo, Y. Yanaba, T. Yoshikawa, K. Ohara, T. Okubo, and T. Wakihara, "Continuous flow synthesis of ZSM-5 zeolite on the order of seconds", *Proceedings of the National Academy of Sciences,* vol. 113, no. 50, pp. 14267-14271, 2016, doi: 10.1073/pnas.1615872113.

[21] A. Rabenau, "The Role of Hydrothermal Synthesis in Preparative Chemistry", *Angewandte Chemie International Edition in English,* vol. 24, no. 12, pp. 1026-1040, 1985, doi: 10.1002/anie.198510261.

[22] X. Huang and Z. Wang, "Synthesis of Zeolite ZSM-5 Small Particle Aggregates by a Two-Step Method in the Absence of an Organic Template", *Chinese Journal of Catalysis,* vol. 32, no. 11, pp. 1702-1711, 2011, doi: 10.1016/S1872-2067(10)60275-6.

[23] X. Huang, R. Zhang, and Z. Wang, "Controlling Crystal Transformation between Zeolite ZSM-5 and Mordenite without Organic Structure-Directing Agent", *Chinese Journal of Catalysis,* vol. 33, no. 7, pp. 1290-1298, 2012, doi: 10.1016/S1872-2067(11)60400-2.

[24] H. Belarbi, Z. Lounis, R. Hamacha, A. Bengueddach, and P. Trens, "Textural properties of ZSM-5 nanocrystals prepared in alkaline potassium fluoride medium", *Colloids and Surfaces A: Physicochemical and Engineering Aspects,* vol. 453, pp. 86–93, 2014, doi: 10.1016/j.colsurfa.2014.03.098.

[25] S. D. Kim, S.-H. Noh, K. Seong, and W. Kim, "Compositional and Kinetic Study on the Rapid Crystallization of ZSM-5 in the Absence of Organic Template Under Stirring", *Microporous and Mesoporous Materials,* vol. 72, pp. 185-192, 2004, doi: 10.1016/j.micromeso.2004.04.024.

[26] Y. Cheng, R. Liao, J. Li, X. Sun, and L. Wang, "Synthesis research of nanosized ZSM-5 zeolites in the absence of organic template", *Journal of Materials Processing Technology - J Mater Process Technol,* vol. 206, pp. 445-452, 2008, doi: 10.1016/j.jmatprotec.2007.12.054.

[27] G. Kadja, M. Rukmana, R. M. Mukti, M. Haris, A. Saputro, and T. Wungu, "Solvent-free, small organic lactam-assisted synthesis of ZSM-5 zeolites", *Materials Letters,* vol. 290, p. 129501, 2021, doi: 10.1016/j.matlet.2021.129501.

[28] H. Antonio De La, A. Jesús, C. José, A. H. María, M. M. Juan De, P. Pilar, C. Abel De, and D.-O. Angel, "Reproducibility and Scalability of Microwave-Assisted Reactions", in *Microwave Heating*, C. Usha Ed. Rijeka: IntechOpen, 2011, ch. 7.

[29] S. Kim and J. Lauterbach, "Synthesis of ZSM-5 catalysts via microwave-assisted heating method for military jet fuel cracking into petroleum gas", *Microporous and Mesoporous Materials,* vol. 328, p. 111446, 2021, doi: 10.1016/j.micromeso.2021.111446.

[30] A. Ismail, R. Mohamed, O. Fouad, and I. Ibrahim, "Synthesis of nanosized ZSM-5 using different alumina sources", *Crystal Research and Technology,* vol. 41, no. 2, pp. 145-149, 2006, doi: 10.1002/crat.200510546.

[31] L. Zhang, S. Liu, S. Xie, and L. Xu, "Organic template-free synthesis of ZSM-5/ZSM-11 co-crystalline zeolite", *Microporous and Mesoporous Materials,* vol. 147, no. 1, pp. 117-126, 2012, doi: 10.1016/j.micromeso.2011.05.033.

[32] S. D. Kim, S. H. Noh, K. H. Seong, and W. J. Kim, "Compositional and kinetic study on the rapid crystallization of ZSM-5 in the absence of organic template under stirring", *Microporous and Mesoporous Materials,* vol. 72, no. 1, pp. 185-192, 2004, doi: 10.1016/j.micromeso.2004.04.024.

[33] R. Peguin, "Synthesis and Characterization of Cu and CoZSM-5 Catalysts – Catalytic Evaluation in the Reduction of NO by Propane and Methane", Master's Thesis, Centro de Ciências Exatas e de Tecnologia, Universidade Federal de São Carlos, 2002.

[34] M. H. Nada, S. C. Larsen, and E. G. Gillan, "Mechanochemically-assisted solvent-free and template-free synthesis of zeolites ZSM-5 and mordenite", *Nanoscale Advances,* vol. 1, no. 10, pp. 3918-3928, 2019, doi: 10.1039/C9NA00399A.

[35] R. Van Grieken, J. L. Sotelo, J. M. Menéndez, and J. A. Melero, "Anomalous crystallization mechanism in the synthesis of nanocrystalline ZSM-5", *Microporous and Mesoporous Materials,* vol. 39, no. 1, pp. 135-147, 2000, doi: 10.1016/S1387-1811(00)00190-6.

[36] S. Baradaran, M. Sohrabi, P. Bijani, and S. Royaee, "Effect of pH on the synthesis of ZSM-5 zeolite using TEOS and performance of H-ZSM-5 catalyst in propane aromatization," presented at the The 15th Iranian National Congress of Chemical Engineering (IChEC 2015), University of Tehran, 2015.

[37] R. Selvin, H.-L. Hsu, L. Selva Roselin, and M. Bououdina, "Effect of Aging on the Precursor Sol for the Synthesis of Nanocrystalline ZSM-5", *Synthesis and Reactivity in Inorganic, Metal-Organic, and Nano-Metal Chemistry,* vol. 41, pp. 1028-1032, 2011, doi: 10.1080/15533174.2011.591339.

[38] V. P. d. S. Caldeira, "Avaliação da Síntese e Caracterização de Zeólita ZSM-5 Ausente de Direcionador Orgânico Estrutural", Mestre em Química, Programa de Pós-Graduação em Química, Universidade Federal do Rio Grande do Norte, 2011.

[39] Y. Xu, Q. Wang, B. A. Yoza, Q. X. Li, Y. Kou, Y. Tang, H. Ye, Y. Li, and C. Chen, "Catalytic Ozonation of Recalcitrant Organic Chemicals in Water Using Vanadium Oxides Loaded ZSM-5 Zeolites", *Frontiers in Chemistry,* vol. 7, 2019, doi: 10.3389/fchem.2019.00384.

[40] H. Jia, T. Du, X. Fang, H. Gong, Z. Qiu, Y. Li, and Y. Wang, "Synthesis of Template-Free ZSM-5 from Rice Husk Ash at Low Temperatures and Its CO2 Adsorption Performance", *ACS Omega,* vol. 6, no. 5, pp. 3961-3972, 2021, doi: 10.1021/acsomega.0c05842.

[41] D. X. Martínez-Vargas, L. Sandoval-Rangel, O. Campuzano-Calderon, M. Romero-Flores, F. J. Lozano, K. D. P. Nigam, A. Mendoza, and A. Montesinos-Castellanos, "Recent Advances in Bifunctional Catalysts for the Fischer–Tropsch Process: One-Stage Production of Liquid Hydrocarbons from Syngas", *Industrial & Engineering Chemistry Research,* vol. 58, no. 35, pp. 15872-15901, 2019, doi: 10.1021/acs.iecr.9b01141.

[42] H. Mahmoudi, M. Mahmoudi, O. Doustdar, H. Jahangiri, A. Tsolakis, S. Gu, and M. LechWyszynski, "A review of Fischer Tropsch synthesis process, mechanism, surface chemistry and catalyst formulation", *Biofuels Engineering,* vol. 2, 2017, doi: 10.1515/bfuel-2017-0002.

[43] H. Schulz, "Short history and present trends of Fischer–Tropsch synthesis", *Applied Catalysis A: General,* vol. 186, no. 1, pp. 3-12, 1999, doi: 10.1016/S0926-860X(99)00160-X.

[44] R. W. Mitchell, D. C. Lloyd, L. G. A. van de Water, P. R. Ellis, K. A. Metcalfe, C. Sibbald, L. H. Davies, D. I. Enache, G. J. Kelly, E. D. Boyes, and P. L. Gai, "Effect of Pretreatment Method on the

Nanostructure and Performance of Supported Co Catalysts in Fischer–Tropsch Synthesis", *ACS Catalysis*, vol. 8, no. 9, pp. 8816-8829, 2018, doi: 10.1021/acscatal.8b02320.

[45] Z. Teimouri, N. Abatzoglou, and A. K. Dalai, "Kinetics and Selectivity Study of Fischer–Tropsch Synthesis to C5+ Hydrocarbons: A Review", *Catalysts*, vol. 11, no. 3, doi: 10.3390/catal11030330.

[46] J. Horáček, "Fischer–Tropsch synthesis, the effect of promoters, catalyst support, and reaction conditions selection", *Monatshefte für Chemie - Chemical Monthly*, vol. 151, no. 5, pp. 649-675, 2020, doi: 10.1007/s00706-020-02590-w.

[47] Z. Gholami, Z. Tišler, and V. Rubáš, "Recent advances in Fischer-Tropsch synthesis using cobalt-based catalysts: a review on supports, promoters, and reactors", *Catalysis Reviews*, vol. 63, no. 3, pp. 512-595, 2021, doi: 10.1080/01614940.2020.1762367.

[48] M. E. Dry, "High quality diesel via the Fischer–Tropsch process – a review", *Journal of Chemical Technology & Biotechnology*, vol. 77, no. 1, pp. 43-50, 2002, doi: 10.1002/jctb.527.

[49] M. E. Dry, "The Fischer–Tropsch process: 1950–2000", *Catalysis Today*, vol. 71, no. 3, pp. 227-241, 2002, doi: 10.1016/S0920-5861(01)00453-9.

[50] H. Karaca, J. Hong, P. Fongarland, P. Roussel, A. Griboval-Constant, M. Lacroix, K. Hortmann, O. V. Safonova, and A. Y. Khodakov, "In situ XRD investigation of the evolution of alumina-supported cobalt catalysts under realistic conditions of Fischer-Tropsch synthesis", *Chemical Communications*, vol. 46, no. 5, pp. 788-790, 2010, doi: 10.1039/B920110F.

[51] M. Amin, B. Farzad, S. Laleh, and Z. Yahya, "Fischer-Tropsch synthesis: Variation of Co/γ-Al2O3 catalyst performance due to changing dispersion, reducibility, acidity and strong metal-support interaction by Ru, Zr and Ce promoters", vol. 16, no. 2, 2018, doi: 10.1515/ijcre-2017-0070.

[52] J. Barrientos, V. Garcilaso, B. Venezia, A. Aho, J. A. Odriozola, M. Boutonnet, and S. Järås, "Fischer–Tropsch Synthesis Over Zr-Promoted Co/γ-Al2O3 Catalysts", *Topics in Catalysis*, vol. 60, no. 17, pp. 1285-1298, 2017, doi: 10.1007/s11244-017-0813-1.

[53] C. Magalhães, "Catalyst development to produce synthetic fuels using the Fischer-Tropsch reaction", Master in Chemical Engineering, CoLAB Net4CO2 unit, Faculdade de Engenharia da Universidade do Porto, Departamento de Engenharia Química, 2022.

[54] J. C. B. Lopes, P. E. L. Laranjeira, M. M. Q. Dias, and A. A. Martins, "Network Mixer and Related Mixing Process", International Application PCT/IB2005/000647, 2005. US Patent 8 434 933 B2, granted May 2013. European Patent EP172643 B1, granted October 2008.

[55] P. E. Laranjeira, A. A. Martins, J. C. B. Lopes, and M. M. Dias, "NETmix®, a new type of static mixer: Modeling, simulation, macromixing, and micromixing characterization", *AIChE Journal*, vol. 55, no. 9, pp. 2226-2243, 2009, doi: 10.1002/aic.11815.

[56] P. Laranjeira, A. Martins, M. Nunes, J. C. Lopes, and M. Dias, "NETmix®, a new type of static mixer: Experimental characterization and model validation", *AIChE Journal*, vol. 57, pp. 1020-1032, 2011, doi: 10.1002/aic.12316.

[57] C. Fonte, M. E. Leblebici, M. Dias, and J. C. Lopes, "The NETmix reactor: Pressure drop measurements and 3D CFD modeling", *Chemical Engineering Research and Design*, vol. 91, pp. 2250–2258, 2013, doi: 10.1016/j.cherd.2013.07.014.

[58] M. F. Costa, C. M. Fonte, M. M. Dias, and J. C. B. Lopes, "Heat transfer performance of NETmix—A novel micro-meso structured mixer and reactor", *AIChE Journal*, vol. 63, no. 6, pp. 2496-2508, 2017, doi: 10.1002/aic.15728.

[59] S. Mintova and N. Barrier, *Verified Synthesis of Zeolitic Materials*, 3ª ed: Synthesis Commission of the International Zeolite Association, 2016, p. 410, ISBN: 978-0-692-68539-6.

[60] R. Van Grieken, J. Sotelo, J. Menéndez, and J. Melero, "Anomalous crystallization mechanism in the synthesis of nanocrystalline ZSM-5", *Microporous and Mesoporous Materials*, vol. 39, no. 1, pp. 135-147, 2000, doi: 10.1016/S1387-1811(00)00190-6.

[61] T. Yokoi, H. Mochizuki, S. Namba, J. N. Kondo, and T. Tatsumi, "Control of the Al Distribution in the Framework of ZSM-5 Zeolite and Its Evaluation by Solid-State NMR Technique and Catalytic Properties", *The Journal of Physical Chemistry C*, vol. 119, no. 27, pp. 15303-15315, 2015, doi: 10.1021/acs.jpcc.5b03289.

[62] J. Kim, E. Jang, Y. Jeong, H. Baik, S. J. Cho, C. Y. Kang, C. H. Kim, and J. Choi, "A Cu-impregnated ZSM-5 zeolite for active cold start hydrocarbon removal: Cation-type-dependent Cu species and their synergetic HC adsorption/oxidation functions", *Chemical Engineering Journal*, vol. 430, p. 132552, 2022, doi: 10.1016/j.cej.2021.132552.

[63] C. Liu, Y. Chen, Y. Zhao, S. Lyu, L. Wei, X. Li, Y. Zhang, and J. Li, "Nano-ZSM-5-supported cobalt for the production of liquid fuel in Fischer-Tropsch synthesis: Effect of preparation method and reaction temperature", *Fuel*, vol. 263, p. 116619, 2020, doi: 10.1016/j.fuel.2019.116619.

[64] K. R. Rajisha, B. Deepa, L. A. Pothan, and S. Thomas, *9 - Thermomechanical and spectroscopic characterization of natural fibre composites* (Interface Engineering of Natural Fibre Composites for Maximum Performance): Woodhead Publishing, 2011, pp. 241-274, ISBN: 978-1-84569-742-6.

[65] "ICP ANALYSIS". Laboratory Testing Inc. https://labtesting.com/services/materials-testing/chemical-analysis/icp-analysis/ (accessed April 2023).

[66] B. Stuart, *Infrared Spectroscopy: Fundamentals and Applications* (Analytical Techniques in the Sciences): John Wiley & Sons, Ltd, 2004, ISBN: 9780470854273.
[67] J. Goodge. "Energy-Dispersive X-Ray Spectroscopy (EDS)". University of Minnesota-Duluth. https://serc.carleton.edu/research_education/geochemsheets/eds.html (accessed March 2023).
[68] J. C. Groen, L. A. A. Peffer, and J. Pérez-Ramírez, "Pore size determination in modified micro- and mesoporous materials. Pitfalls and limitations in gas adsorption data analysis", *Microporous and Mesoporous Materials,* vol. 60, no. 1, pp. 1-17, 2003, doi: 10.1016/S1387-1811(03)00339-1.
[69] J. L. Figueiredo and F. R. Ribeiro, *Catálise heterogénea*, Lisboa: Fundação Calouste Gulbenkian, 2015, ISBN: 978-972-31-1204-7.
[70] B. Dutrow and C. Clark. "X-ray Powder Diffraction (XRD)". Louisiana State University. https://serc.carleton.edu/research_education/geochemsheets/techniques/XRD.html (accessed March 2023).
[71] M. Mahoney. "Percent Crystallinity by the XRD Integration Method". Materials Characterization LAB. https://mcl.mse.utah.edu/xrd-crystallinity-by-integration/ (accessed May 2023).
[72] T. Ishii and T. Kyotani, *Chapter 14 - Temperature Programmed Desorption* (Materials Science and Engineering of Carbon): Butterworth-Heinemann, 2016, pp. 287-305, ISBN: 978-0-12-805256-3.
[73] "What is TPR?". Hiden Analytical. https://www.hidenanalytical.com/blog/what-is-tpr/ (accessed March 2023).
[74] C. Duong-Viet, L. Nguyen-Dinh, Y. Liu, G. Tuci, G. Giambastiani, and C. Pham-Huu, "Nickel Sulfides Decorated SiC Foam for the Low Temperature Conversion of H2S into Elemental Sulfur", *Molecules*, vol. 23, no. 7, doi: 10.3390/molecules23071528.
[75] Y. Yue, Y. Kang, Y. Bai, L. Gu, H. Liu, J. Bao, T. Wang, P. Yuan, H. Zhu, Z. Bai, and X. Bao, "Seed-assisted, template-free synthesis of ZSM-5 zeolite from natural aluminosilicate minerals", *Applied Clay Science,* vol. 158, pp. 177-185, 2018, doi: 10.1016/j.clay.2018.03.025.
[76] M. H. Nada, S. C. Larsen, and E. G. Gillan, "Solvent-free synthesis of crystalline ZSM-5 zeolite: Investigation of mechanochemical pre-reaction impact on growth of thermally stable zeolite structures", *Solid State Sciences,* vol. 94, pp. 15-22, 2019, doi: 10.1016/j.solidstatesciences.2019.05.009.
[77] M. A. Ali, B. Brisdon, and W. J. Thomas, "Synthesis, characterization and catalytic activity of ZSM-5 zeolites having variable silicon-to-aluminum ratios", *Applied Catalysis A: General,* vol. 252, no. 1, pp. 149-162, 2003, doi: 10.1016/S0926-860X(03)00413-7.
[78] A. Čižmek, B. Subotić, R. Aiello, F. Crea, A. Nastro, and C. Tuoto, "Dissolution of high-silica zeolites in alkaline solutions I. Dissolution of silicalite-1 and ZSM-5 with different aluminum content", *Microporous Materials,* vol. 4, no. 2, pp. 159-168, 1995, doi: 10.1016/0927-6513(94)00096-E.
[79] V. Medrano, V. Celis, and R. Giraldo, "Systematic analysis of the nitrogen adsorption-desorption isotherms recorded for a series of microporous – mesoporous amorphous aluminosilicates using classical methods", *ChemRxiv: Cambridge Open Engage,* 2022, doi: 10.26434/chemrxiv-2022-8v4h3.
[80] M. M. J. Treacy and J. B. Higgins, *Powder pattern identification table*, 5 ed, (Collection of Simulated XRD Powder Patterns for Zeolites), Amsterdam: Elsevier Science B.V., 2007, pp. 10-16, ISBN: 978-0-444-53067-7.
[81] C. S. Cundy and P. A. Cox, "The Hydrothermal Synthesis of Zeolites: History and Development from the Earliest Days to the Present Time", *Chemical Reviews,* vol. 103, no. 3, pp. 663-702, 2003, doi: 10.1021/cr020060i.
[82] S. L. Burkett and M. E. Davis, "Mechanism of Structure Direction in the Synthesis of Si-ZSM-5: An Investigation by Intermolecular 1H-29Si CP MAS NMR", *The Journal of Physical Chemistry,* vol. 98, no. 17, pp. 4647-4653, 1994, doi: 10.1021/j100068a027.
[83] R. J. Lewis, *Hawley's Condensed Chemical Dictionary*, 15 ed, New York: John Wiley & Sons, Inc., 2007, ISBN: 9780470114735.
[84] N. A. Kartikawati, R. Safdar, B. Lal, M. I. B. A. Mutalib, and A. M. Shariff, "Measurement and correlation of the physical properties of aqueous solutions of ammonium based ionic liquids", *Journal of Molecular Liquids,* vol. 253, pp. 250-258, 2018, doi: 10.1016/j.molliq.2018.01.040.

Annex A - Zeolite

Figure A.1 presents the zeolite unit bases and the arrangement with cations.

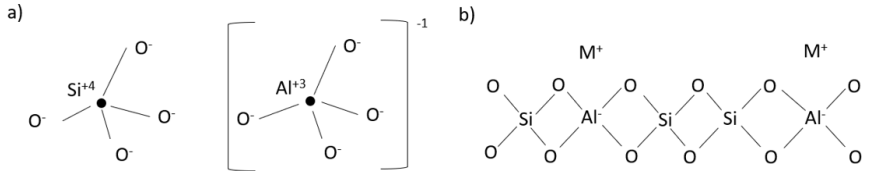

Figure A.1. Representation of zeolite unit bases (a), and zeolite arrangement with cations (b). Adapted with permission from Peguin [33]. Copyright 2023 American Chemical Society.

Figure A.2 represents the pentasil unit of ZSM-5 and the size of its pores.

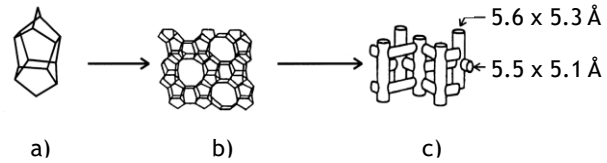

Figure A.2. ZSM-5 structural representation of pentasil unit (a), unit cell (b) and pore size (c). Adapted with permission from Weitkamp [14]. Copyright 2023 American Chemical Society.

Figure A.3 shows the BAS in ZSM-5.

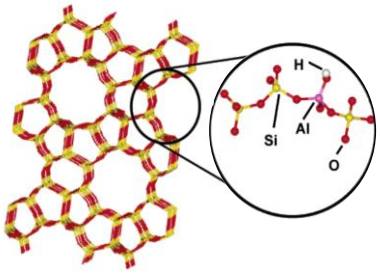

Figure A.3. BAS in ZSM-5. Reprinted with permission from Cundy and Cox [81]. Copyright 2023 American Chemical Society.

Figure A.4 presents a schematic image of ZSM-5's growth mechanism in the presence of TPA^+.

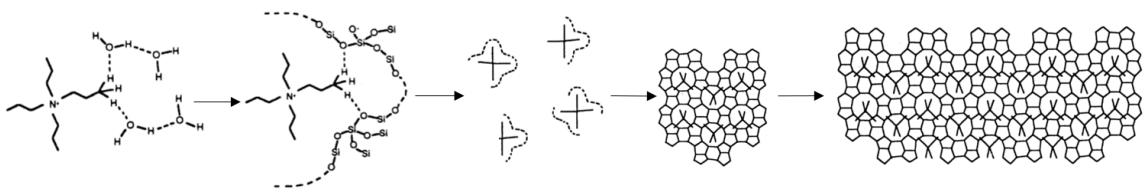

Figure A.4. ZSM-5's growth mechanism in the presence of TPA^+. Reprinted with permission from Burkett and Davis [82]. Copyright 2023 American Chemical Society.

Annex B - FTS

Equation B.1 presents the CO conversion calculation, in %, and Equation B.2 the F_{CTY}:

$$X_{\mathrm{CO}} = \frac{F_{\mathrm{in,CO}} - F_{\mathrm{out,CO}}}{F_{\mathrm{in,CO}}} \times 100 \tag{B.1}$$

$$F_{\mathrm{CTY}} = \frac{F_{\mathrm{in,CO}}\, X_{\mathrm{CO}}}{w_{\mathrm{Co}}\, y_{\mathrm{Co}}} \tag{B.2}$$

where, $F_{\mathrm{in,CO}}$ and $F_{\mathrm{out,CO}}$ corresponds to the initial and final quantity of CO, in mol·s^{-1}, respectively. The variable w_{Co} to the cobalt mass, in g.

Annex C - NETmix Configuration

The schematic representation of a MicroNETmix network and its 2D unit cell are presented in Figure C.1.

(a) (b)

Figure C.1. Schematic representation of a MicroNETmix network, a), and a 2D unit cell, b). Reutilized with permission from Lopes, et al. [54]. Copyright 2023 American Chemical Society.

Annex D - Reactants Structure

Table D.1 present the reactants' structure for template-free formulations and formulations with template, respectively.

Table D.1. Reactants used to produce ZSM-5.

Reactant	Name	CAS	Formulation	Structure
$NaAlO_2$	sodium aluminate	11138-49-1	F	
SiO_2	colloidal silica	7631-86-9	F	
NaOH	sodium hydroxide	1310-73-2	F	
TPA^+	tetrapropylammonium	4499-86-9	T	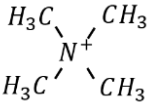
TEOS	tetraethyl orthosilicate	78-10-4	T	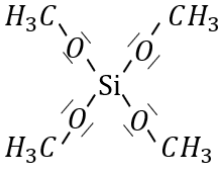
$Al_2O_{12}S_3$	aluminum sulfate	7784-31-8	T	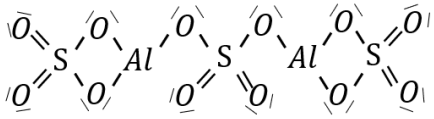

Annex E - SiO_2/Al_2O_3 in the Gel vs. in the Framework

Figure E.1 presents a correlation between SiO_2/Al_2O_3 ratio in the initial gel and in the final framework provided by Kim, *et al*. [25].

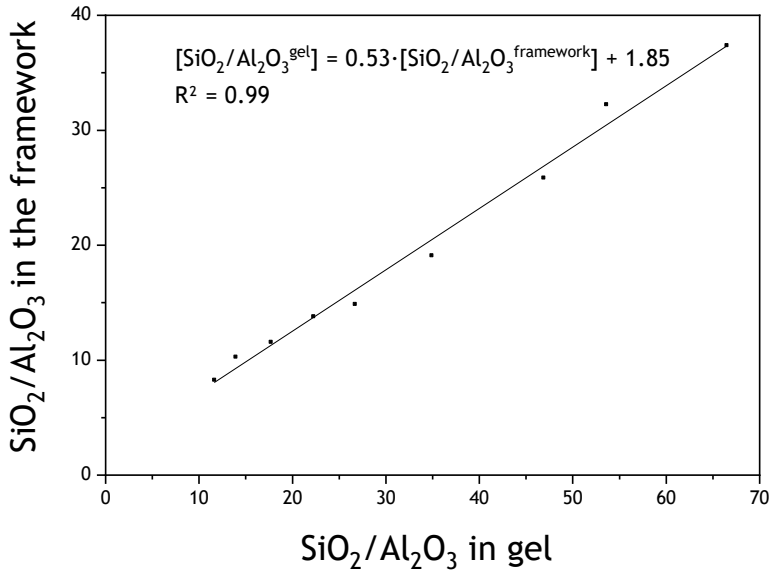

Figure E.1. Correlation between SiO_2/Al_2O_3 ratio in the gel and in the framework. *Adapted with permission from Kim, et al. [25]. Copyright 2023 American Chemical Society.*

Note that to apply the correlation shown in *Figure E.1*, the Si/Al ratio in the gel was converted to SiO_2/Al_2O_3 ratio in the gel.

Annex F - Pore Methods and Classification

The volumetric capacity of the monolayer, V_m^a, was calculated by the linear Equation F.1 and S_{BET} by Equation F.2 [69]:

$$\frac{\frac{P}{P_0}}{V^a\left(1-\frac{P}{P_0}\right)} = \frac{1}{V_m^a\, C_{\mathrm{BET}}} + \frac{C_{\mathrm{BET}}-1}{V_m^a\, C_{\mathrm{BET}}}\,\frac{P}{P_0} \tag{F.1}$$

$$S_{\mathrm{BET}} = \frac{V_m^a\, N_A\, a_m}{V_m\, w_s} \tag{F.2}$$

where P is the pressure, in Pa, P_0 the maximum pressure used, in Pa, V^a the adsorbed volume of nitrogen, in dm^3, C_{BET} a parameter of the model, N_A is the Avogadro number, 6.02×10^{23} mol^{-1}, a_m is the adsorption cross-section of the adsorbate, which for nitrogen at 77 K this parameter takes the value of 0.162×10^{-9} m^2 and w_s is the samples mass, in g.

Based on the literature, the zeolites can be classified by their pores with the division presented in Table F.1 [79] and Equation F.3 presents the calculation of the fractional area of micropores, ξ.

Table F.1. Zeolites classification by their pore size distribution.

ξ / %	Classification	Abbreviation
≤10	mesoporous	Mesoporous
10-40	microporous-mesoporous with mesoporosity being prevalent	Micro-MESOporous
40-60	micro-mesoporous	micro-mesoporous
60-90	microporous-mesoporous with microporosity being dominant	MICRO-mesoporous
>90	microporous	Microporous

$$\xi = \frac{S_{BET} - S_{\neq \mathrm{micro}}}{S_{BET}} \tag{F.3}$$

Annex G - Crystal Size and Crystallinity

Crystal size (L), in nm, was calculated by Scherrer Equation (Equation G.1) at 8º, and crystallinity (C), in %, by Equation G.2 [71]:

$$L = \frac{K\,\lambda}{\beta\,cos\theta} \tag{G.1}$$

$$C = \frac{A_C}{A_T} \times 100 \tag{G.2}$$

where K is a constant related to crystallite shape, normally taken as 0.9; λ is the X-ray wavelength used, 0.154 nm; β is the peak width of the diffraction peak profile at half maximum height in rad. Also, A_C and A_T refer to area under crystalline peaks and area under all peaks, respectively. Note that A_T was obtained by using trapezoidal rule and A_C by using Fityk software.

Annex H - NH_3 Uptake for NH_3-TPD

Equation H.1 was used to calculate the NH_3 uptake (U_{NH_3}), in μmol·g^{-1} [69]:

$$U_{NH_3} = 3.68 \times 10^{-2} \frac{PA}{w_s} \quad \text{(H.1)}$$

where PA to the second peak area (to guarantee that only strong acid sites were being accounted).

Annex I - H_2 Consumption for H_2-TPR

The calculation of $\mathrm{H_2}_{\mathrm{consumption}}$, in mmol·g^{-1}·s^{-1}, is in Equation I.1.

$$\mathrm{H_2}_{\mathrm{consumption}} = \frac{\mathrm{TCD}_{\mathrm{signal}}\, V_s\, T_{\mathrm{ref}}}{1000\, w_s\, V_m\, \bar{A}_{H_2}\, T_{\mathrm{loop}}} \tag{I.1}$$

That is calculated based on the signal provided by the thermal conductivity detector, $\mathrm{TCD}_{\mathrm{signal}}$, dimensionless. Where T_{ref} is the reference temperature, 273.15 K, T_{loop} is the loop temperature for calibration step, 308.15 K, V_s is the analyzed volume for calibration step, corresponding to 58 µL, V_m is the molar volume do H_2 in STP conditions, 22.4 dm^3·mol^{-1} and $\bar{A}_{H_2}$ represents the mean area above the H_2 consumption curve for the calibration step, in s, (integration between time and TCD_{signal} for calibration step).

Appendix a - Experimental Set-up and Procedure

Figure a.1 shows the experimental configuration used to prepare solution (1) for template-free formulation assays.

Figure a.1. Experimental configuration used to prepare solution (1) for template-free formulations assays.

Figure a.2 presents the NETmix configuration used for template-free formulations with different Re_d.

NETmix Configuration for Re_d = 150 and 360 (F)	NETmix Configuration for Re_d = 400 (F)

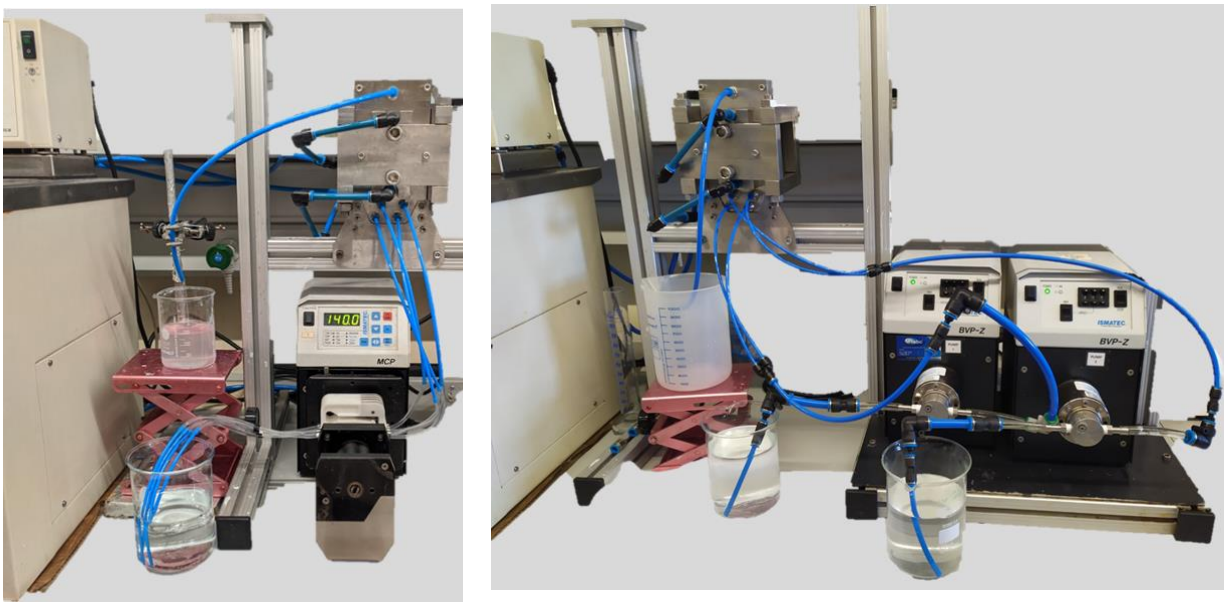

Figure a.2. Image from NETmix configuration for template-free formulations for experiments with different Re_d.

Figure a.3 presents the reflux configuration used in both formulations, an image of the utilized autoclave and a product image after autoclave treatment for template-free formulation.

Reflux Configuration (F and T)	Autoclave	Product after Autoclave (F)

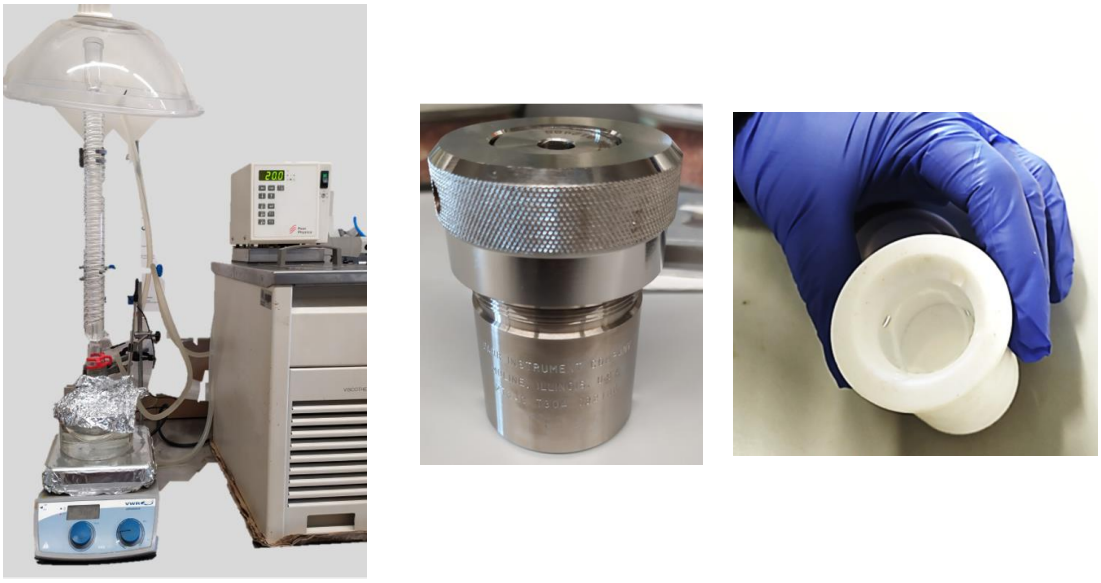

Figure a.3. Reflux configuration used in both formulations (left), an image of the utilized autoclave (center) and a product image after autoclave treatment for template-free formulation (right).

Additionally, Figure a.4 presents the NETmix configuration used and an image of the product after hydrothermal treatment in the autoclave for formulations with template.

NETmix Configuration (T)	Product after Autoclave (T)

Figure a.4. NETmix configuration used (left) and a product image after autoclave treatment (right), for formulation with template.

While for template-free formulations, the final product had two different phases, the product from template formulation was solid, with two different particle types (probably the zeolite and the other components to be removed in washing and calcination steps).

Figure a.5 presents the Falcon tubes before and after centrifuge.

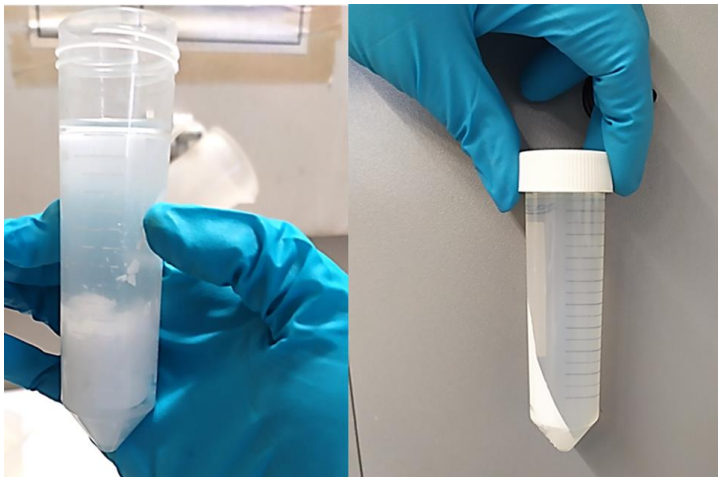

Figure a.5. Washing process for template formulations before (left) and after (right) centrifuge.

Figure a.6 presents an IWI closed image, an image of the samples after IWI procedure and after IWI drying stage.

Sample after IWI	Sample after IWI Drying Stage

Figure a.6. Sample image after IWI procedure (left) and sample image after IWI drying stage (right).

Figure a.7 shows a scheme of the IWI procedure and Figure a.8 of the protonation procedure.

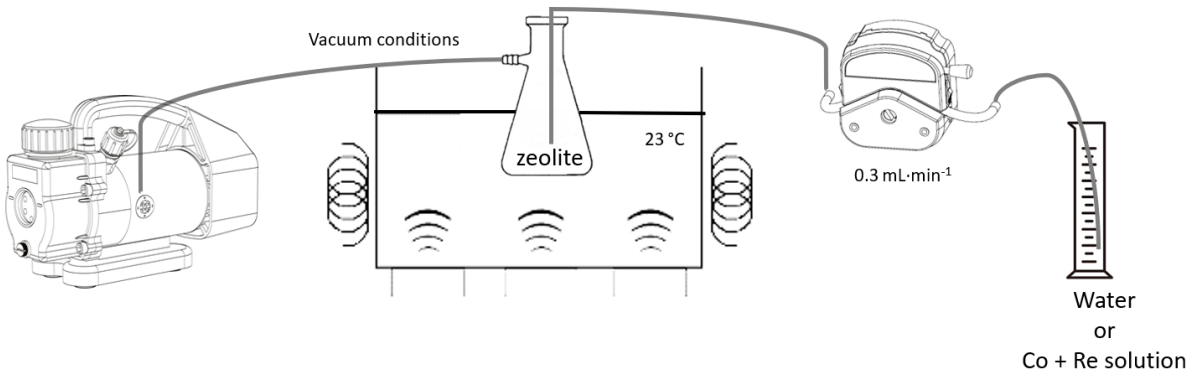

Figure a.7. IWI method procedure scheme.

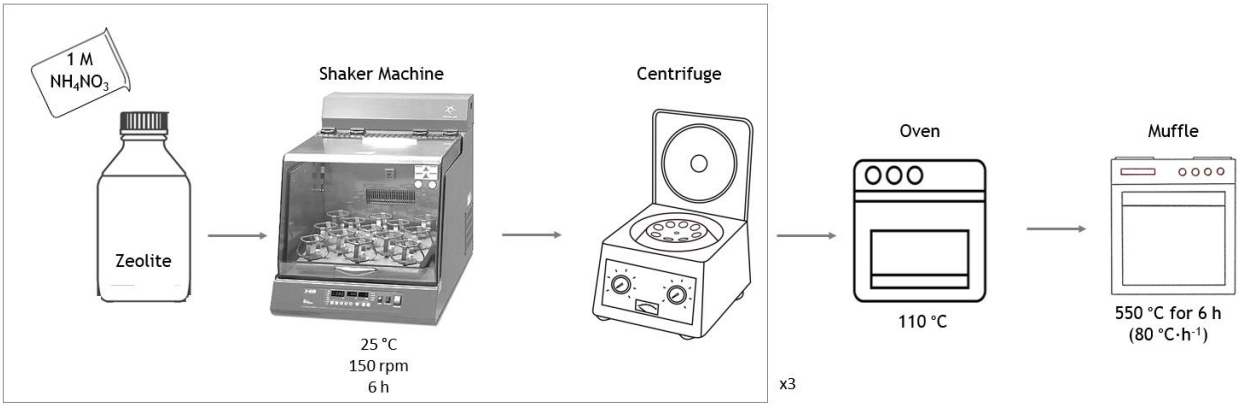

Note: For logistic reasons, the solution was mixed for 6 h, 15 h and 6 h.

Figure a.8. Protonation procedure scheme.

Figure a.9 shows the FTS reactor used.

Figure a.9. FTS reactor. External view on the left side and internal on the right.

Appendix b - Reynolds Number

To calculate the Re_d four parameters needed to be obtained: ρ, d, v and μ.

The density of the three final types of products: template-free assays with original concentration (F_ori); template-free assays with diluted concentration (F_dil); formulations with template (T), were acquired by a pycnometer and are shown in Table b.1. Note that the original concentration is in accordance with the procedure from Mintova and Barrier [59].

Table b.1. Density obtained for the F_ori, F_dil and T formulations.

Assay Type	ρ /g·mL^{-1}
F_ori	1.024
F_dil	1.045
T	1.017

Additionally, the hydraulic diameter, d, was obtained by Equation b.1:

$$d = \frac{2\, d_c\, w_c}{d_c + w_c} = 0.5\, mm \tag{b.1}$$

Regarding to the average velocity in the channels, v, in m·s^{-1}, was calculated by Equation b.2:

$$v = \frac{0.001\, q}{60\, A_{cs}\, (2\, n_y - 2)} \tag{b.2}$$

where q corresponds to the total flowrate, in dm^3·min^{-1}.

Finally, the viscosity of the template-free experiments was obtained by rheological tests, while for template was by mass-weighted average of the reactant's viscosity.

Rheological measurements were performed by a modular compact rheometer from Anton Paar, model MCR 92 with a shear rate from 0 to 300 s^{-1} and a shear gap of 0.5 mm. Circa 2 mL of a liquid sample was dropped into the measuring platform for these analyses. A rheometer records the shear stress caused by a rotational speed and converts it to viscosity values at each measuring point.

For F_ori formulation, Figure b.1 exhibits the curves obtained for assays analyzed at 21 °C or 70 °C.

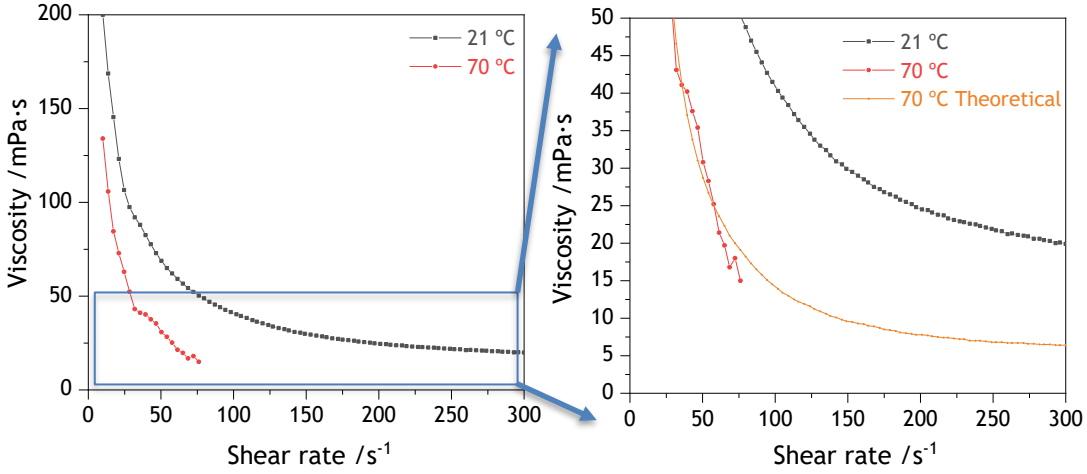

Figure b.1. Viscosity curves for F_ori formulation at 21 ºC and 70 ºC, on the left. The viscosity curves zoomed up to 50 mPa s, with the theoretical curve for 70 ºC, on the right.

It was observed that when performing the rheological test at 70 °C the sample dried and the experiment was interrupted. Nevertheless, it was visible that higher temperatures originate solutions less viscous, as expected. Because of that the viscosity of F_ori_70C was established as 6 mPa·s.

Figure b.2 shows the rheological test results for template-free (F_dil), where the initial solution (NaOH and SiO_2 20 % in mass) present a non-Newtonian behavior, and for the higher shear rate, the viscosity is circa 2 mPa·s. Their mixture originated a fluid (solution (2) from Figure 3.1) with a higher viscosity for a lower shear rate. For a shear rate of 250 s^{-1}, the viscosity is circa 6 mPa·s. The final product originated from the mixture of solution (2) and (4) from Figure 3.1, has a viscosity circa 2.8 mPa·s.

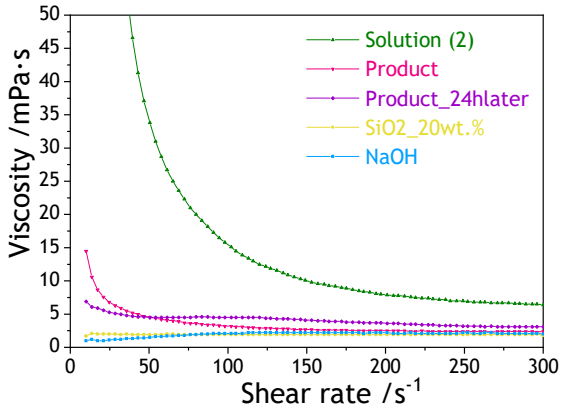

Figure b.2. Viscosity curves for F_dil formulation: reactants (NaOH and SiO_2 20 %), Solution (2), NETmix product after 0 and 24 h in solution.

For template formulations, TEOS viscosity is 0.6 mPa.s [83] and TPAOH 20 % is 2.66 mPa.s [84], at 20 °C.

Considering the viscosity constant and the value obtained for the highest shear rate, Table b.2 shows the Reynolds number, Re_d, calculated by Equation 2.9.

Table b.2. Reynolds numbers for NETmix assays considering the total flowrate, q.

Assay	q /L·min^{-1}	v /m·s^{-1}	Re_d
F_dil_Re150_20C	0.17	0.8	149
F_dil_Re150_70C	0.18	0.9	160
F_dil_Re360_70C	0.41	1.9	363
F_ori_Re360_70C	0.88	4.2	358
F_ori_Re400_70C	0.99	4.7	402
T_Re500	0.40	1.9	505

Appendix c - Characterization Techniques

c.1. ICP-AES

A calibration curve for each element was generated to determine the metals' concentration. Figure c.1 shows the calibration curves obtained for Si and Al metals.

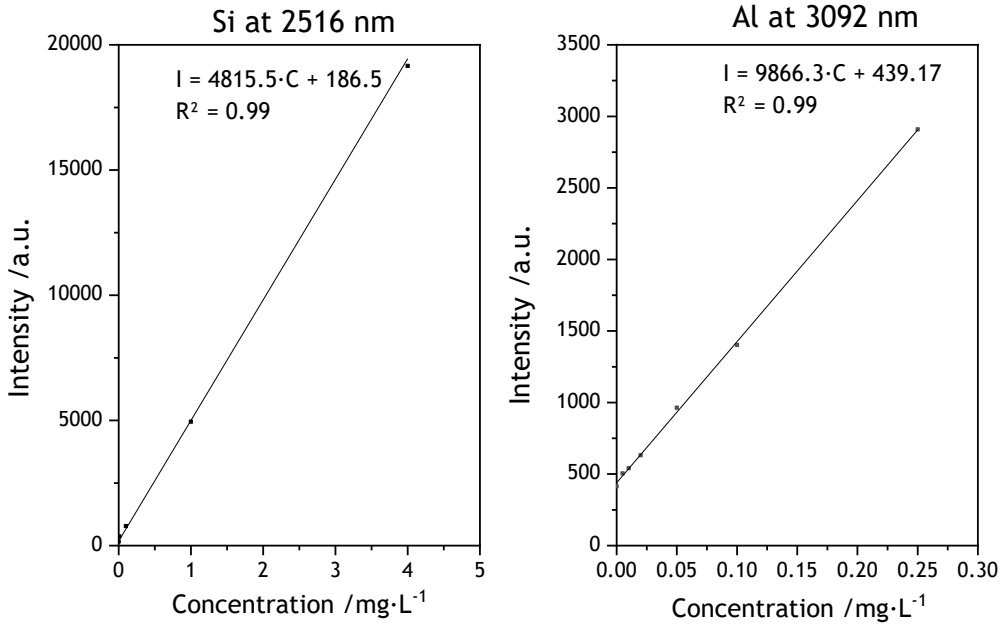

Figure c.1. Calibration curve obtained for Si and Al at 2516 nm and 3092 nm, respectively.

c.2. FTIR

Figure c.2 shows the FTIR spectra obtained for template-free formulation assay produced with NETmix for different drying equipment. That result demonstrates that the equipment used in this step does not considerably affect the vibrational bonds created.

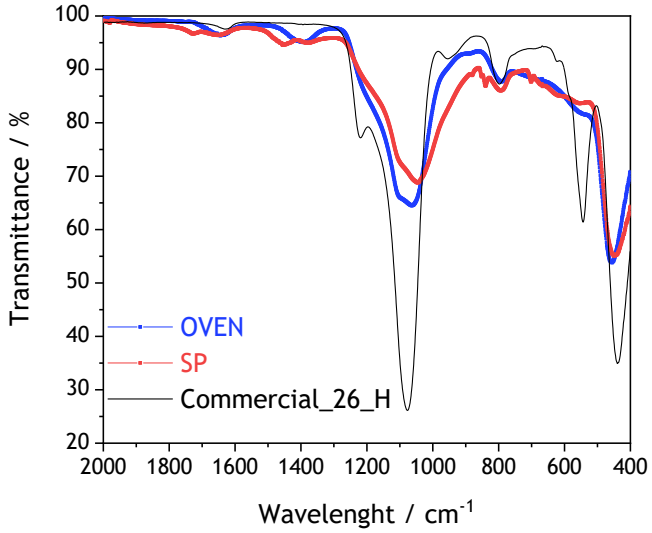

Figure c.2. FTIR spectra obtained for template-free formulation assay produced with NETmix for different drying equipment: oven and SP.

Figure c.3 compares the FTIR spectra obtained for the reactants used in each formulation and the commercial reference. That was an important initial analysis to understand the origin of each peak. Note that only TEOS was not evaluated since it was dangerous to dry it, since the oven does not have air suction.

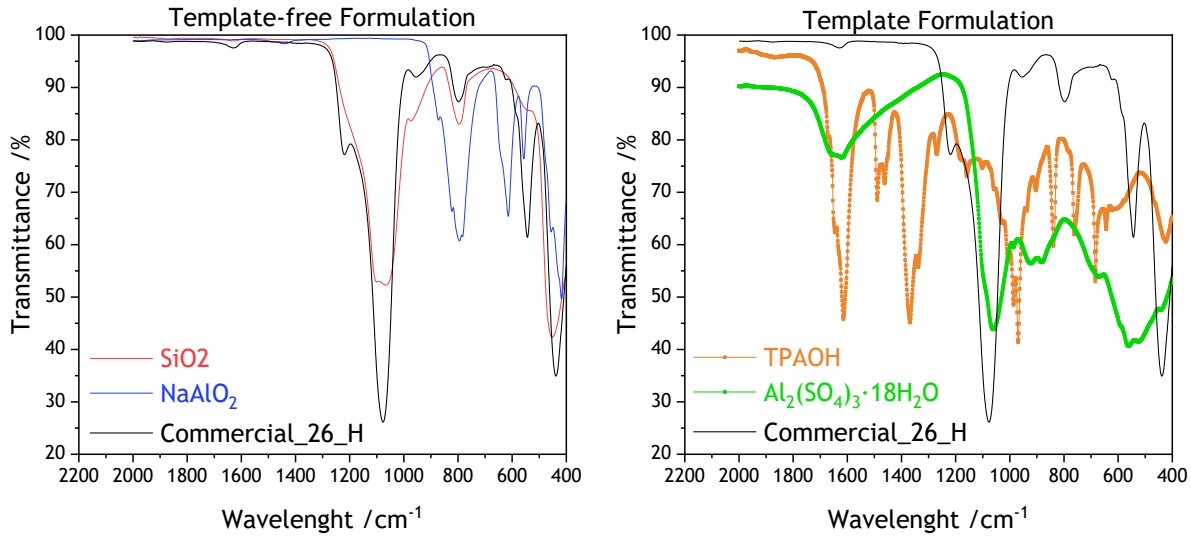

Figure c.3. FTIR spectra obtained for the reactants of each formulation and the commercial reference. On the left side for template-free and on the right side for template formulation.

c.3. SEM and EDS

Figure c.4 presents the EDS spectra obtained for the commercial reference and for the produced samples with the qualitative analysis of the Si/Al ratio.

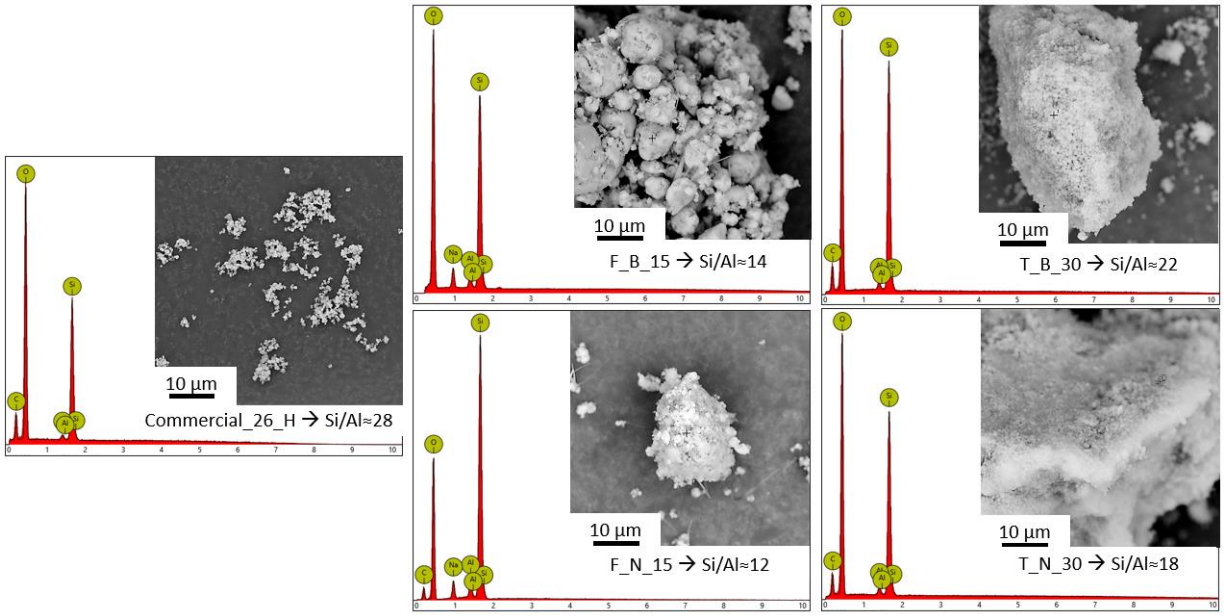

Figure c.4. EDS spectra obtained for the commercial reference and for the produced samples: F_B_15, F_N_15, T_B_30 and T_N_30 with the qualitative analysis of the Si/Al ratio.

Figure c.5 shows the SEM images obtained for samples produced by template-free formulation with NETmix, for different drying methods (oven and SP) and washing steps.

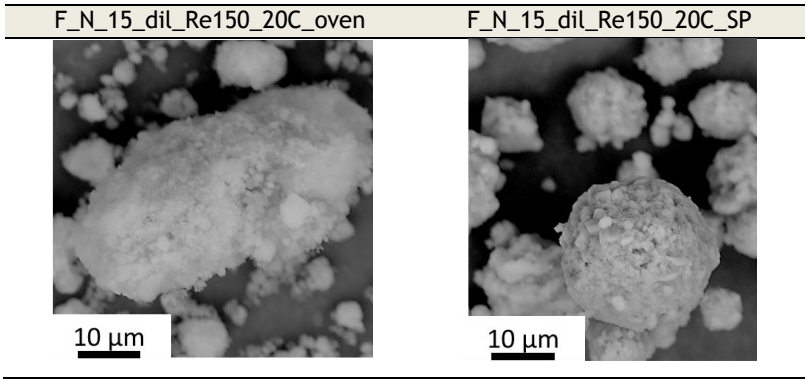

Figure c.5. SEM images obtained for samples produced by template-free formulation with NETmix and for different drying methods, in the oven and in the SP.

It was visible that SP particles were spherical and oven particles were not structured defined, as expected. Nevertheless, the individual particle shape does not appear to be different by each drying method, but should be confirmed by high-resolution SEM.

c.4. Nitrogen Isotherms

Figure c.6 shows the isotherms obtained for each template-free assays.

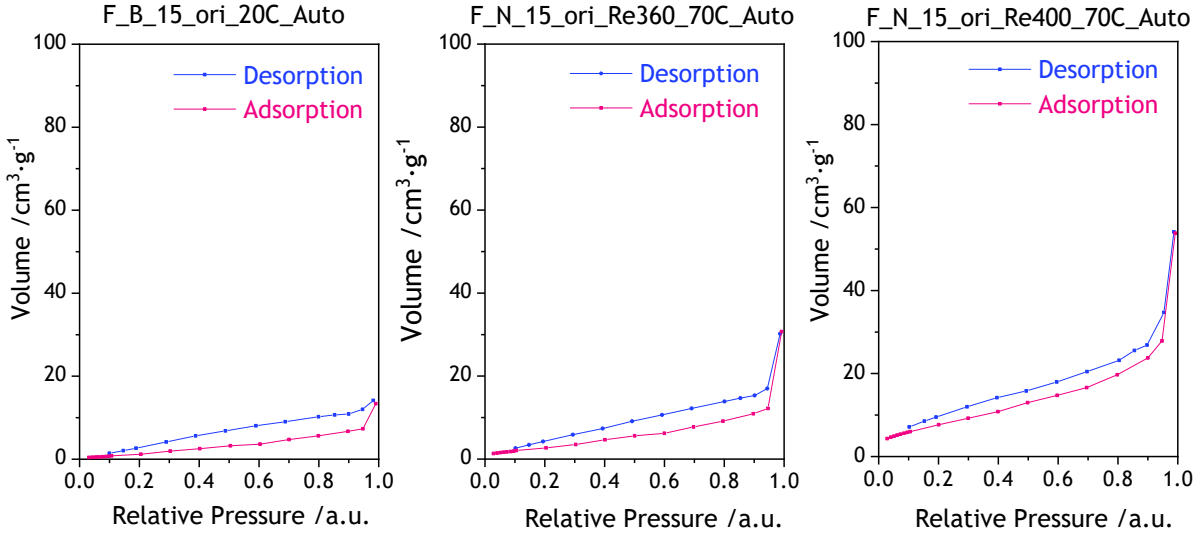

Figure c.6. Isotherms for adsorption and desorption of nitrogen for template-free assays.

Figure c.7 presents the parameters S_{BET}, $S_{\neq micro}$, V_{pores_total} and V_{micro} of each calcinated sample.

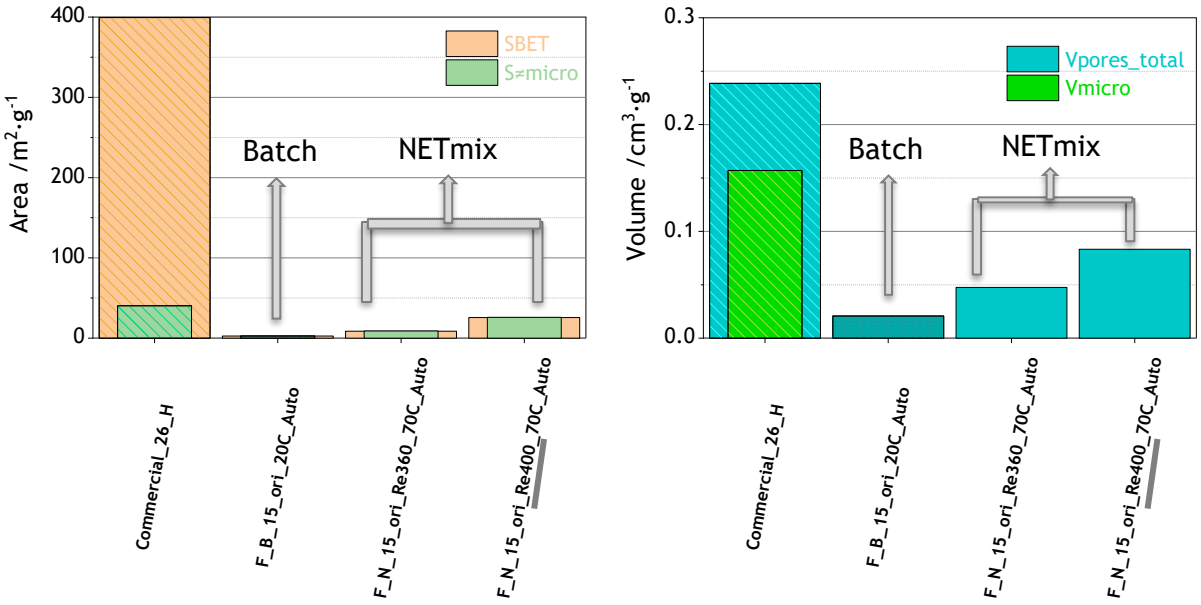

Figure c.7. Representation of S_{BET}, $S_{\neq micro}$, V_{pores_total} and V_{micro} for template-free calcinated assays and commercial reference.

The isotherms obtained for each experimental with template assay are presented in Figure c.8 to Figure c.10, divided by its pore classification: microporous, MICRO-mesoporous and micro-mesoporous, respectively.

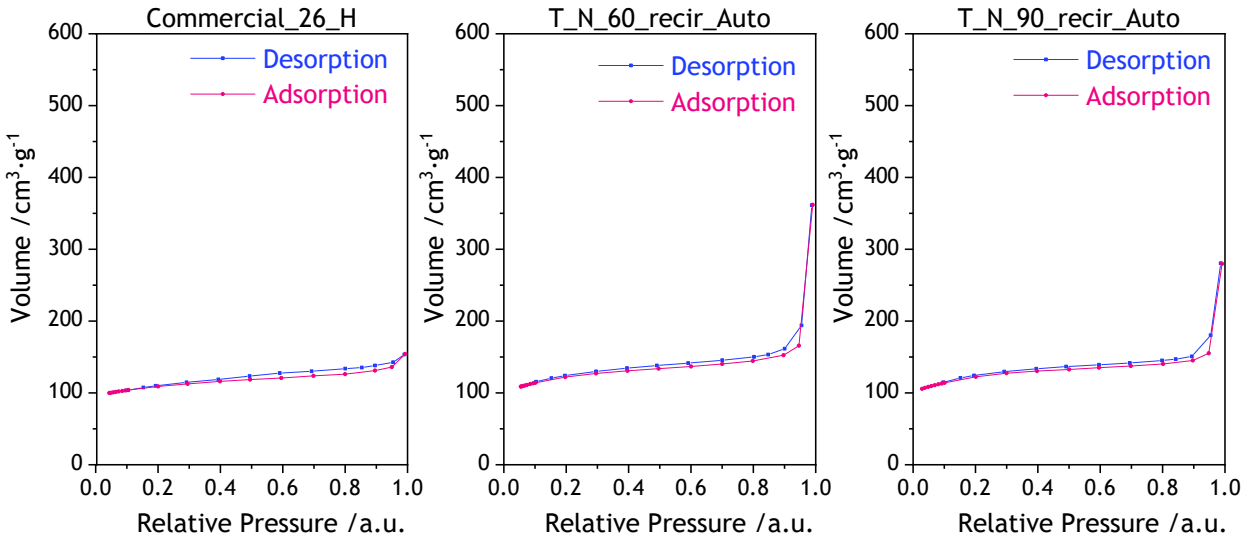

Figure c.8. Isotherms for adsorption and desorption of nitrogen for assays produced with template, classified by having microporous.

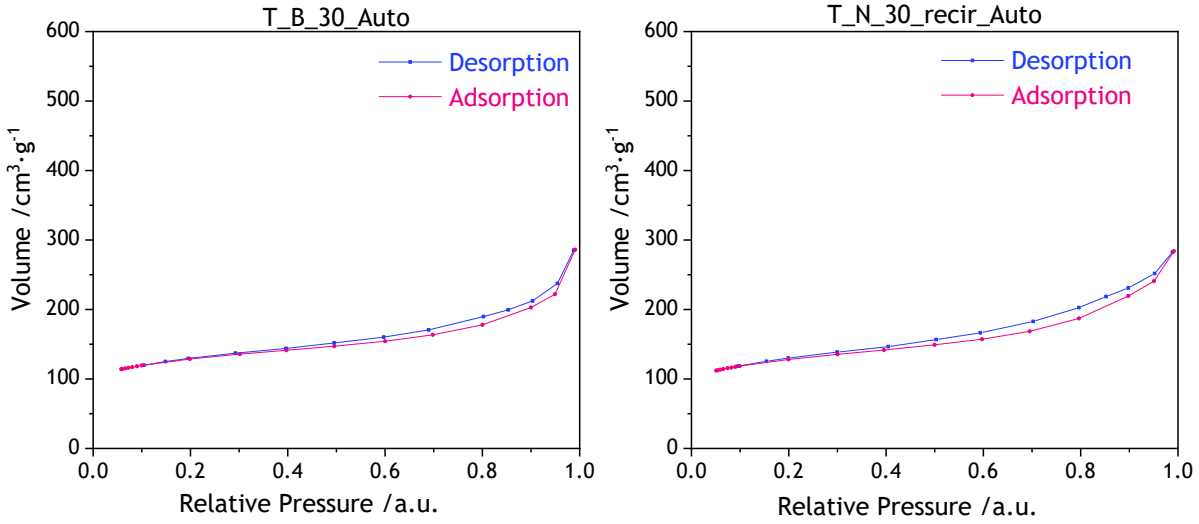

Figure c.9. Isotherms for adsorption and desorption of nitrogen for assays with template, classified by having MICRO-mesoporous.

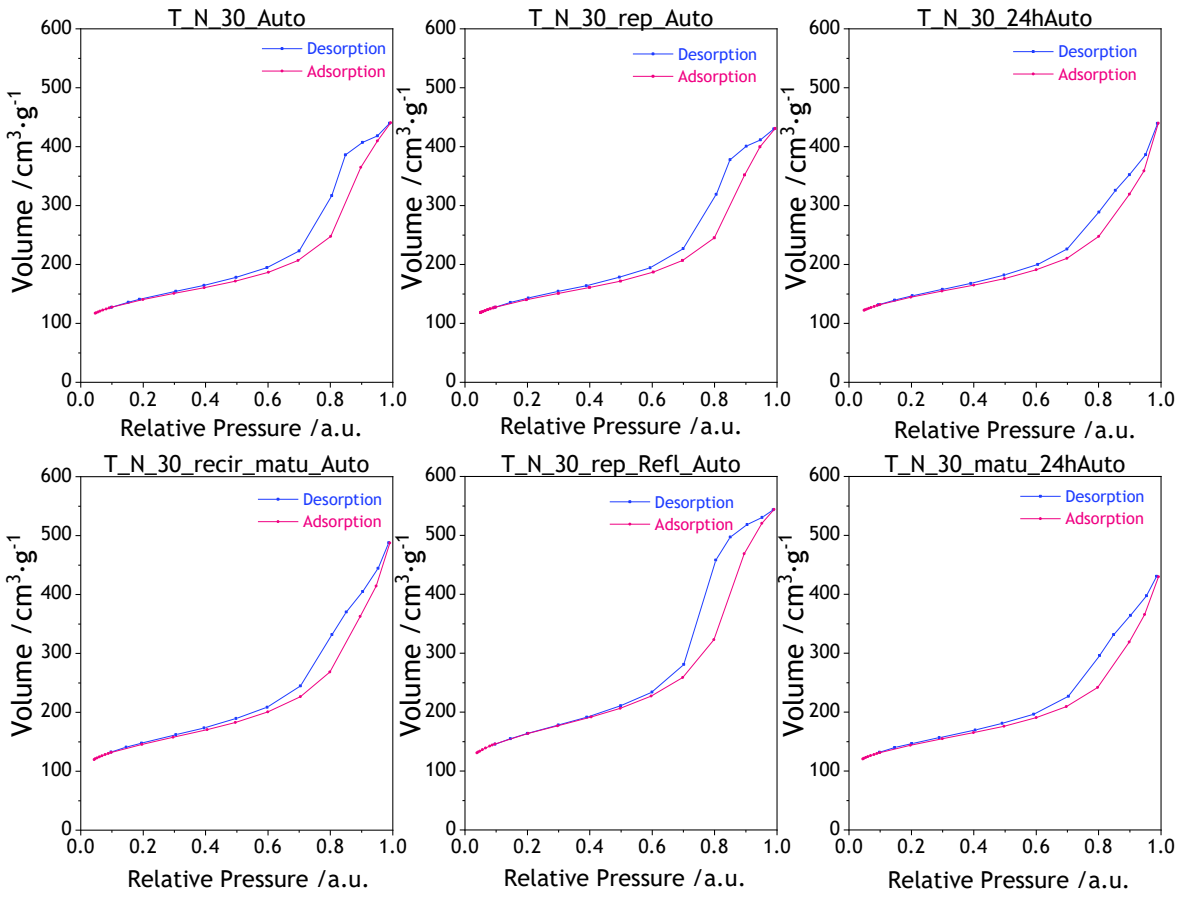

Figure c.10. Isotherms for adsorption and desorption of nitrogen for assays with template, classified by having micro-mesoporous.

Figure c.11 presents the parameters S_{BET}, $S_{\neq micro}$, V_{pores_total} and V_{micro} of each calcinated sample.

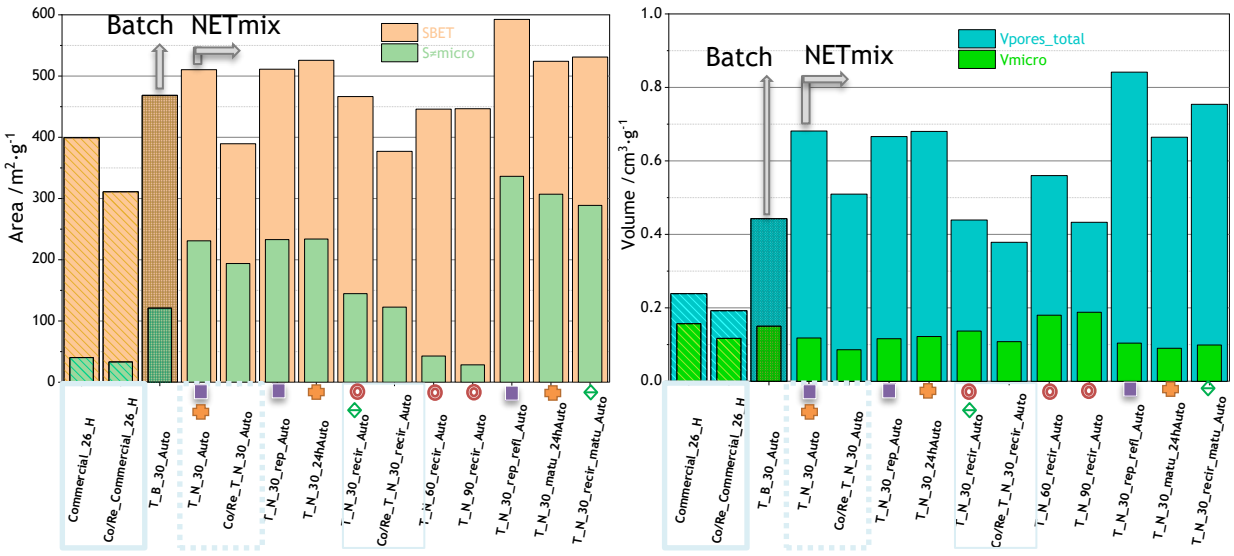

Figure c.11. Representation of S_{BET}, $S_{\neq micro}$, V_{pores_total} and V_{micro} for calcinated assays produced with template formulations and for the commercial reference, where the areas are in $m^2 \cdot g^{-1}$ and the volumes in $cm^3 \cdot g^{-1}$.

The assays are grouped by comparison characteristics: purple square assemble the repetition experiment; orange cross identifies the assays of only 24 h in autoclave; red circles are the different ratios assays; green rhombus the assays with recirculation and blue rectangles are the impregnated samples.

c.5. FTS

Figure c.12 presents the products distribution for all tested assays.

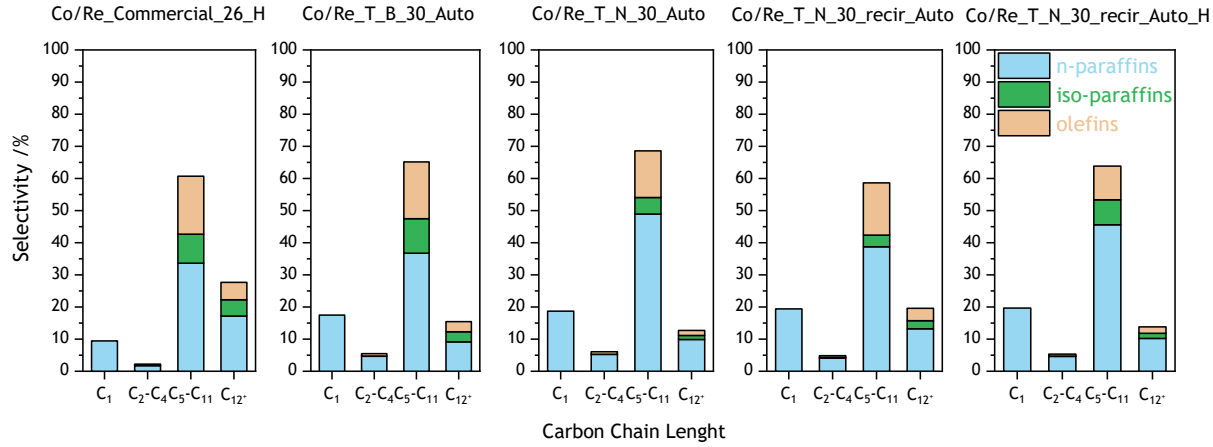

Figure c.12. Products distribution for the different carbon length chain and for the different structures, obtained for all tested assays.